Integrated Approach and Analysis of Reliability, Robustness, Resilience and Infrastructure Applications

Shuoqi Wang

A dissertation
submitted in partial fulfillment of the
requirements for the degree of

Doctor of Philosophy

University of Washington

2017

Reading Committee:

Kailash C. Kapur, Chair

Dorothy A. Reed, Chair

Zelda B. Zabinsky

Program Authorized to Offer Degree:
Industrial and Systems Engineering

University of Washington

Abstract

Integrated Approach and Analysis of Reliability, Robustness, Resilience and Infrastructure Applications

Shuoqi Wang

Co-Chairs of the Supervisory Committee:
Dr. Kailash C. Kapur
Industrial and Systems Engineering

Dr. Dorothy A. Reed
Civil and Environmental Engineering

A rising number of man-made and natural disasters have occurred since the beginning of the 21st century in the United States. Improving the quality of civil infrastructure in an increasingly hazardous environment has become a top priority. One of the predominant reasons that hurricanes and earthquakes become community disasters is the failure of civil infrastructure systems, also known as "lifelines", on which communities rely. An integrated approach is presented here to model the reliability, robustness, and resilience through the use of system-based models of performance. The models are based on empirical evidence of the ability of the underlying structural systems to provide essential infrastructure services to the community. The reliability and robustness are modeled through fragility functions, which are used to represent the probability of failure of a structure or lifeline system conditional upon a hazard or set of hazards. Traditional analyses of infrastructure performance have relied upon evaluating the effect of one hazard or demand variable such as wind speed or peak storm surge on the loss of structural capacity. This investigation suggests that multivariate distributions of the demand variables of wind speed, storm surge, and rainfall are important for the analysis of infrastructure performance. The resilience of a structure or lifeline system is characterized in part by an inoperability function that is modeled as the mechanical analog

of the single-degree-of-freedom (SDOF) system. Interdependency is assessed first through previously derived input-output models of recovery to storm hazards and then significantly expanded. The combined fragility and resilience model framework derived here allows for the implementation of numerical simulations to predict system performance for various demand levels.

TABLE OF CONTENTS

LIST OF FIGURES

LIST OF TABLES

LIST OF SYMBOLS

H Loading or demand variable for a given hazard

$Q(t)$ Quality function over time t of a given infrastructure system

RES Resilience metric of a given infrastructure system

$RS(t)$ Restoration function of power delivery at time t

T Rainfall

V Wind speed

W Storm Surge

$X(t)$ Infrastructure system inoperability over time t

$\Im$ Damage state variable

$\ddot{X}$ Second derivative of X

$\dot{X}$ First derivative of X

$\mathbf{A}$ Interdependency matrix

$\mathbf{F}$ Interdependent infrastructure system fragility vector

$\mathbf{X}$ Interdependent infrastructure system inoperability vector

$\mathcal{F}(\bullet)$ Fragility function for a given damage state

ω natural frequency of a single-degree-of-freedom system in (rad/s)

STAIFI_n Normalized STAIFI by the annual SAIFI

ζ damping ratio of a single-degree-of-freedom system

a_{ij} Influence of lifeline j inoperability on lifeline i inoperability

c damping factor of a single-degree-of-freedom system

k stiffness of a single-degree-of-freedom system

m mass of a object

AIC Akaike Information Criterion

CAIDI Customer Average Interruption Duration Index

CAIFI Customer Average Interruption Frequency Index

SAIDI System Average Interruption Duration Index

SAIFI System Average Interruption Frequency Index

STAIFI SAIFI for storm events

ACKNOWLEDGMENTS

First, I would like to express sincere gratitude to my advisors Dr. Kailash C. Kapur and Dr. Dorothy A. Reed for their continuous support. It is their encouragement, patience and knowledge that guided me through the entire Ph.D. study. I would also like to thank the committee members, Dr. Zelda Zabinsky and Dr. Ramulu Mamidala for their advice.

I am grateful to Dr. Cheng Zheng (University of Wisconsin, Milwaukee) for his input on regression analysis, and to Dr. Carol Friedland and Carol Massarra (Louisiana State University) for their collaboration on collecting and analyzing hazard GIS data. To all the staff of the Department of Industrial and Systems Engineering, and Civil and Environmental Engineering at the University of Washington, thank you for all the assistance over the years, without which this would not have been possible.

Lastly, I want to thank my parents, grandparents, and my uncle's family for their unconditional love and understanding.

DEDICATION

To my parents

Wenlong Wang and Jiduan Du

Chapter 1
INTRODUCTION

1.1 Motivation

Globalization, climate change and the growing population of the earth are by-products of efforts to raise living standards world-wide. Consequently, enormous burdens have been placed on the infrastructure services on which modern society depends. These systems are not only aging but are also vulnerable to disruptions [1]. As populations become more dependent upon properly functioning infrastructures in their daily lives, the reliability of these systems becomes crucial. Unfortunately, a rising number of disruptive events have occurred since the beginning of the 21st century such as terrorist attacks and extreme natural hazard events. Figure 1.1 shows the total number of terrorist attacks each year on infrastructure in the United States that resulted in property damage from 1970 to 2015 [2]. It can be seen that the number of events in recent years has been in the thousands. Figure 1.2 shows the number of natural disaster events that occurred each year in the United States for the same time span [3]. The trend in natural disasters has been an overall increase since the 1990s. In the face of these unfortunate trends, improving the *quality* of civil infrastructure in an increasing hazardous environment has become a top priority for the United States.

As a concept, *quality* has evolved over time, and there are numerous ways to evaluate it for a product or system. For example, Aikens [4] gave an operational definition of *quality* as a two-dimensional gap measure, i.e. the gap between (1) expectation and actual outcome, and (2) losses and benefits, from both the stakeholder and customer point of view. Many other terms have also been introduced into the quality framework, such as “maintainability”, “availability”, “safety”, and “system effectiveness” e.g. [5]. In the context of manufacturing,

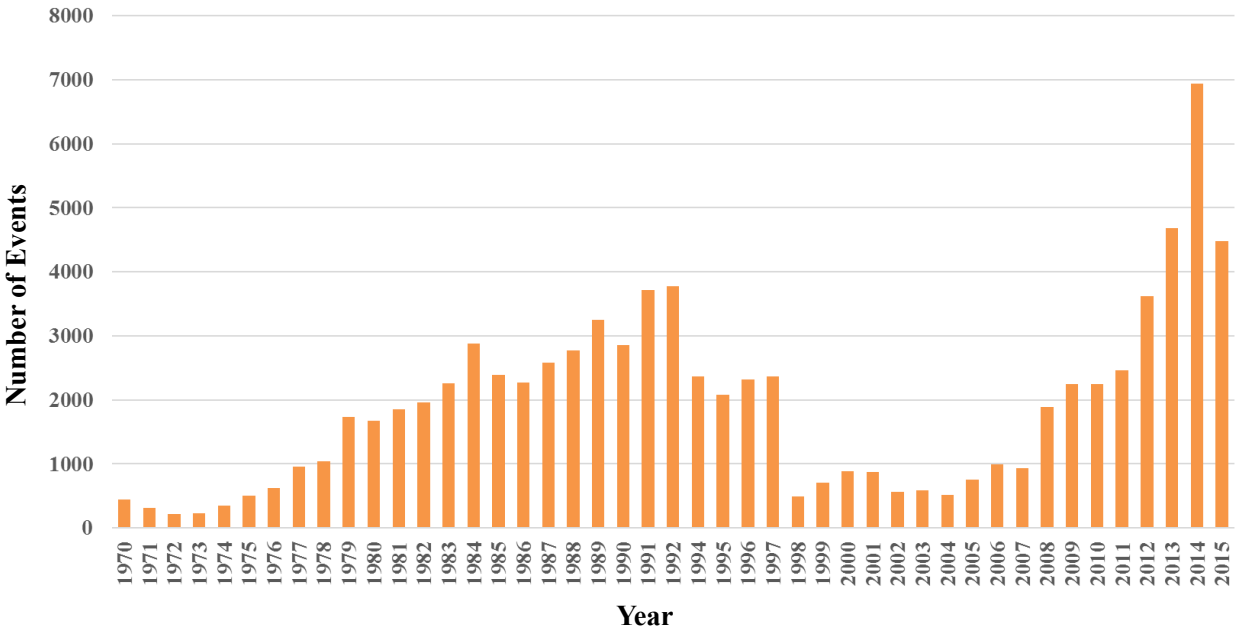

Figure 1.1: Number of terrorist attacks on infrastructures which resulted in property damage each year in the United States [2].

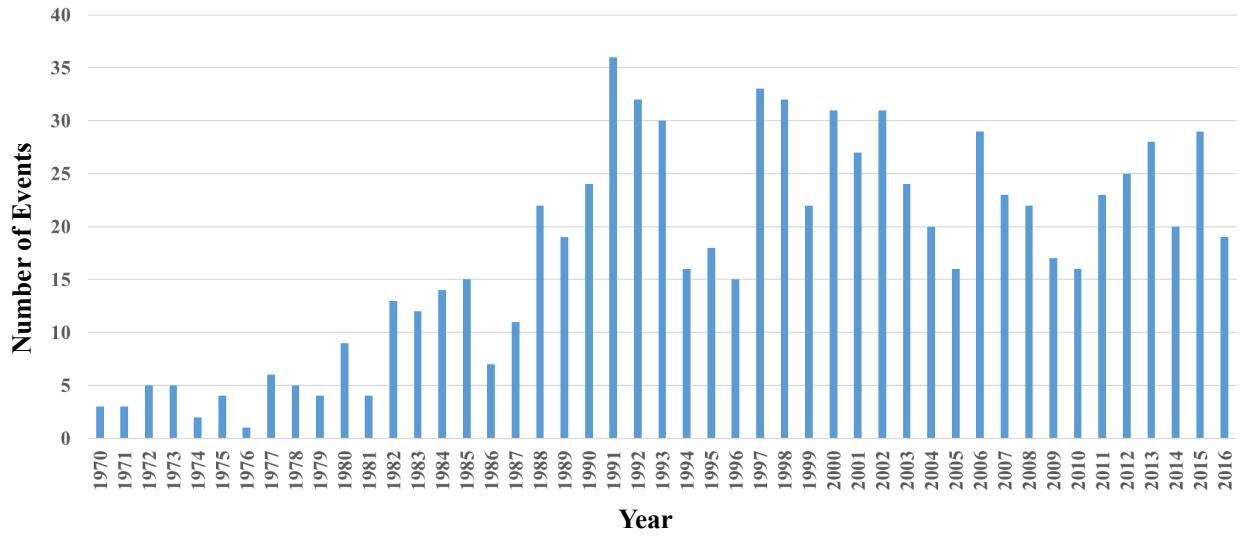

Figure 1.2: Number of natural disasters occurred each year in the United States [3].

eight dimensions or components of quality were introduced by Garvin [6] and expounded by Montgomery [7] as "(1)performance, (2)reliability, (3)durability, (4)serviceability, (5)aesthetics, (6)features, (7)perceived quality, and (8)conformance to standards". Montgomery also pointed out that the meaning of *quality* originally described as "fitness for use" had changed to being "inversely proportional to variability" [7]. The latter definition shows that the emphasis was changed from the perspective of the manufacturer to the customer.

In the context of the industrial and civil engineering disciplines, one of the important properties of *quality* is *reliability*. *Reliability* is defined as "the *probability* that an item will perform its required function under given conditions for a stated period of time" e.g. [5]. The reliability of the physical underpinnings of the infrastructure can be evaluated and used to identify its physical quality. Building codes rely on component reliability calculations, and these are assumed to enable acceptable building reliability. In recent years, performance-level requirements at the building structural level have been developed to provide a more consistent overall building reliability [8]. However, the reliability metric, with associated uncertainty measures, in and of itself, is not adequate to completely characterize the dimensions of quality because it does not consider the behavior of the system explicitly when damaged by disruptive events. Post-event investigations in the US for weather related extreme events have shown that while individual buildings often fare well in storms, the same cannot be said for infrastructure systems.

Civil infrastructure is defined here as "a system of systems of networked interdependent lifelines" as shown in Figure 1.3, derived from McDaniels et al. [9] and Reed et al. [10]. "Lifelines" are defined by Reed et al. [10] as "the networks that provide for the proper functioning of modern society". In Figure 1.3 each node represents a subsystem of the set of systems that comprise the civil infrastructure. All of the interactions are not shown in the figure in order to maintain clarity, but the systems may be thought of as being linked and dependent upon one another. In the context of civil infrastructure, *resilience* and *robustness* are also important metrics for evaluating quality because they incorporate the damage incurred during disruptive events, and the amount of time and effort required for

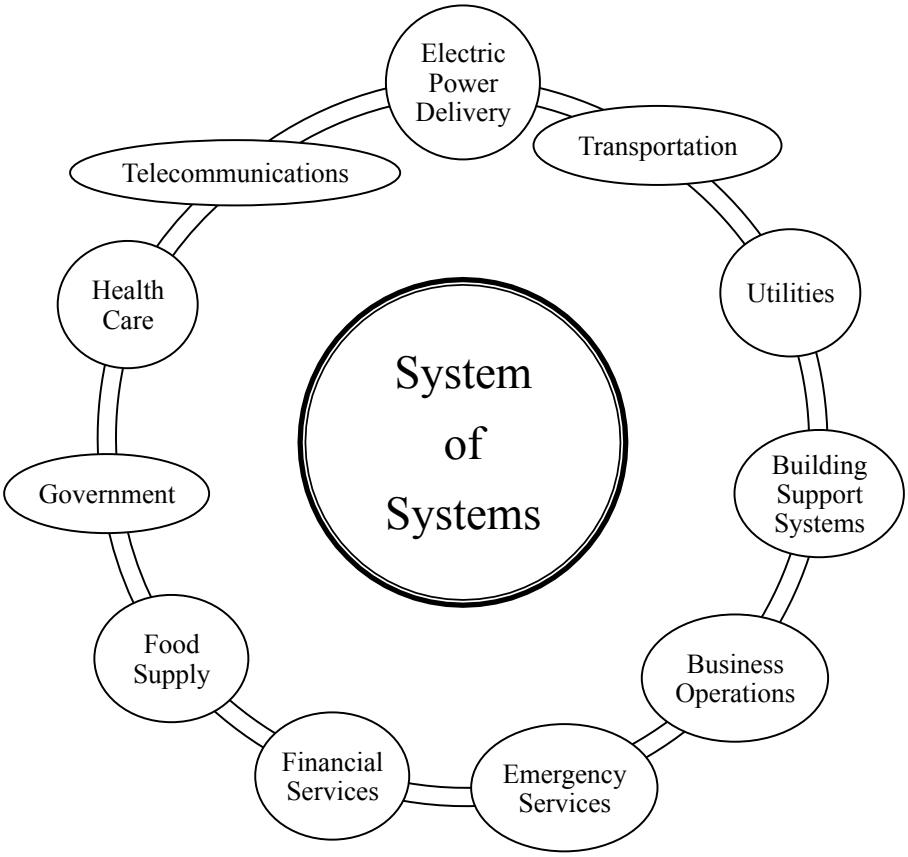

Figure 1.3: System of systems description of civil infrastructure.

complete recovery. It is noted that in some instances, the system may not recover completely, but attain a new state, or new "normal".

Robustness as described by Taguchi [11], is "a state where the sensitivity of a system to factors causing variability is at the minimum level." Within the context of civil engineering, when the sensitivity or vulnerability of a physical entity, such as a bridge, to extreme loadings is low, the capacity of that bridge is said to be *robust*. In some situations, the term *fragility* of a component is used to describe its *vulnerability*. *Resilience* is defined here as "the ability of a system to maintain its level of performance under internal or external disturbances and to restore its lost function due to the disturbance using a minimum amount of *time*". The three metrics of *robustness*, *reliability* and *resilience* may overlap in some ways, but when

combined, they provide a better characterization of the quality of a physical system than each one alone. The central concept of this dissertation is that when combined, the three provide the necessary and sufficient characterization of the quality of civil infrastructure over its lifetime. Ultimately these metrics will result in improved designs that adequately support society. The three combined also provide essential background to predict the performance of a system when subjected to disruptions so that resources may be properly allocated to reduce service outages.

1.2 Research objectives

The primary objective is to develop a comprehensive method of characterizing the quality of civil infrastructure systems using reliability, robustness and resilience metrics. In order to evaluate these metrics, the behavior of the infrastructure systems must be described in sufficient detail to capture the physical and functional aspects required for services. The disruptions to which these systems may be subjected will be limited to natural hazards for which there is adequate data for verification and calibration. After the systems have been described, the implementation of the three metrics of reliability, robustness and resilience to characterize their quality will be considered. The effect of the spatial and temporal scales of the hazards on infrastructure systems will be investigated. It is noted that all three metrics involve uncertainty in subjective and objective ways, and the degree to which the uncertainty affects decision-making is important, but it is beyond the scope of this work.

1.3 Outline of chapters

Chapter 2 starts with the definition of the civil infrastructure employed in this dissertation. It will then provide a review of methods used to date to describe the infrastructure behavior. This dissertation will focus on the electric power delivery system for particular evaluation because most other lifelines depend on electric power to function, and the power system is frequently repaired and restored first after a disruption.

Chapter 3 employs new methodologies developed by the writer for combined reliability,

robustness and resilience metrics as applied to power delivery and some of its dependent lifelines. Fragility functions are defined as conditional probability functions that are used in structural and civil engineering relating capacity and demands. Although introduced as part of the reliability and resilience methods derived in this chapter, the expansion of fragilities using geospatial characterization will be presented in Chapter 4.

Chapter 4 develops new methods for characterizing fragility functions for single and multiple hazards. The methods are derived and calibrated using in-situ damage and hazard data.

Chapter 5 introduces extended input-output models for assessing interdependencies between various lifeline systems.

Chapter 6 illustrates the use of the combined fragility and resilience model framework to predict system performance over time under various demand levels.

Chapter 7 summarizes the work and lays groundwork for future investigations.

Chapter 2
LITERATURE REVIEW

Quality can be evaluated at various spatial scales, such as a component, network, system or system of systems. In this thesis, the "system of systems" refers to the "civil infrastructure comprised of eleven interconnected subsystems". These are delineated in Figure 1.3 and described in Section 2.1. A review of methods to assess the reliability, robustness and resilience of these systems is then provided.

2.1 Civil infrastructure systems

2.1.1 Overview of eleven system of systems

Civil infrastructure is regarded as the foundation upon which modern society depends. It has been well-established that the existing infrastructure systems in the US are aging and in need of a major overhaul [1]. The eleven subsystems discussed here were derived by Chang et al. [12], and based upon Rinaldi et al. [13], for modeling of the post-event interdependent critical infrastructures failures observed in the US and Canada. The eleven systems, shown as nodes in Figure 1.3, are defined as follows:

1. Electric power delivery, with subsystems distribution, transmission, and generation;

2. Telecommunications, with subsystems of cable, cellular, Internet, landlines and media;

3. Transportation, with subsystems of air travel, roadways, mass transit, rail, port facilities;

4. Utilities, with subsystems water supply, sewage treatment, sanitation, oil and natural gas delivery;

5. Building support, with subsystems HVAC, elevators;

6. Business, with subsystems computer systems, hotels, gaming, manufacturing, retail, restaurants;

7. Emergency Services, with subsystems 911, ambulance, fire, police, and shelters;

8. Financial systems, with subsystems ATM, banks, credit cards and stock exchanges;

9. Food supply, with subsystems distribution, storage, preparation, and production;

10. Government, with subsystems of offices and services; and

11. Health care, with subsystems of hospitals and public health.

This organization reflects the general categories of the critical infrastructure as derived by the US federal government e.g. [12]. In the government formulation, the infrastructure systems are defined through "emergency support functions" that the agencies and offices of the US government deem necessary following a major disruption. In [12], a matching of the various departments and agencies for primary or secondary support of infrastructure was undertaken. For example, for the energy sector of the United States, The Department of Energy is the primary support agency, with secondary support provided by the Departments of Agriculture, Commerce, Defense, including the Army Corps of Engineers, Homeland Security, Interior and Labor. The division of the physical infrastructure into critical sectors is based on the need to manage response and recovery efforts after natural disasters in an organized manner.

Due to the large scale of the built environment, the infrastructure can be modeled locally at the community level, at the state level, and nationally. Many systems are international in nature, such as the energy flow across the US-Canadian border. Geospatial software such as ArcGIS [14] and Google Earth [15] have made the physical modeling of many large

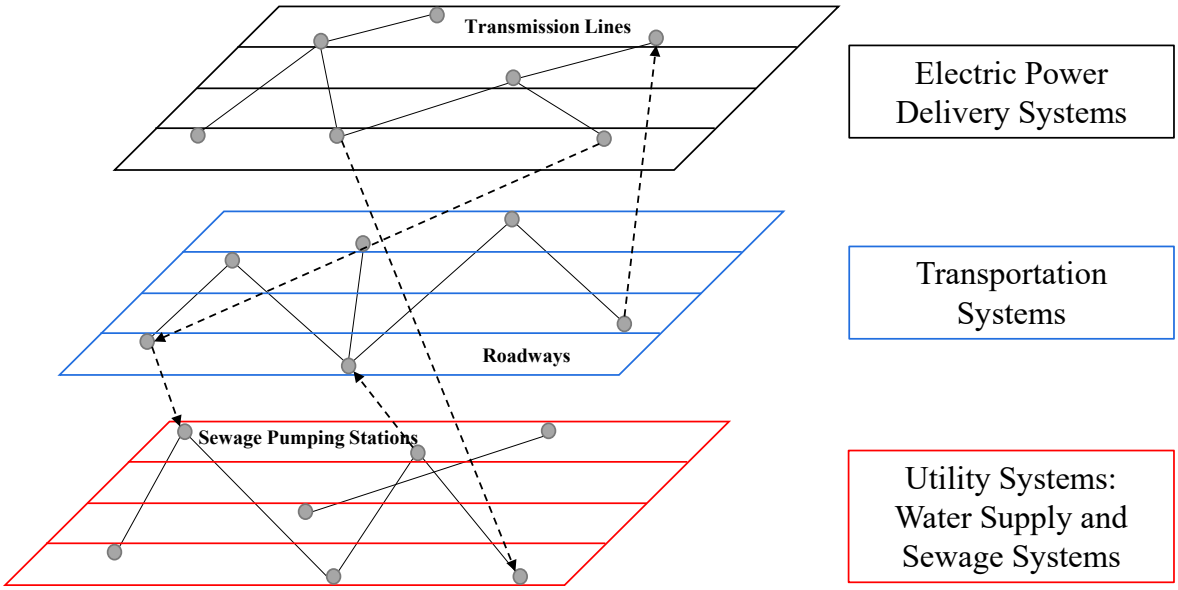

Figure 2.1: Geospatial overlay of Electric Power Delivery, Transportation, and Utility Systems.

scale systems easier in recent years. Figure 2.1 illustrates the geospatial overlay of three of the eleven infrastructure systems. It can be seen that the co-location of many system components represents a physical dependence among the systems. In particular, the electric power delivery system has been identified as the core system upon which most other systems depend to function normally e.g. [10]. For this reason, it will be the focus system of this thesis investigation.

2.1.2 Electric power delivery system

Historically, the power system is the first to be repaired after an extreme event as the loss of power disrupts many other sectors. Figure 2.2 provides a schematic of the typical US power delivery system [16]. Staring in the left hand top corner of the diagram, energy is generated by dams (hydro), coal plants or other means, and is transmitted at high voltage across long

distances to substations where the voltage is dropped to distribution levels. Transmission towers tend to be large steel lattice frames. The power is then "fed" to businesses and neighborhoods through a series of poles, lines, feeders and possibly other substations. It is noted that the physical system of generation, transmission and distribution of power affects the *functionality* of the power system.

The reliability of the constituent elements of the power delivery system has been addressed through structural design guides such as [17–20]. That is, the structural *reliability* of the individual poles, towers, cables and substations of the system are not the same as the *reliability* of the electrical service provided by the system. In a manner similar to the "beam by beam" reliability analysis of a building, the reliability of the physical network may be estimated through combinations of the reliabilities of the constituent members. The complexity of the individual connections, as well as the overhead or underground locations of lines, makes physical reliability assessment of the system very challenging. For this reason, outages of service areas or localities have been used to characterize the performance of the power delivery system. The configuration of power distribution systems is usually classified into three categories, i.e. radial, ring, and network systems [21]. Service interruptions may occur when even a single pole fails. Therefore, in this thesis, the *service provided* will be referred to as the *quality* or *operability* of the system, because the term "serviceability" in the structural engineering literature refers to the non-safety related performance of structural components. An example of a "serviceability" requirement is "deflections of floor beams must not exceed allowable limits for unfactored ten-year loads" whereas "safety analysis of floor beams requires that the beam capacity must not be exceeded over a 700 year return period for specified combined overloads".

2.2 Reliability

The introduction of reliability concepts to engineering disciplines can be dated back to the 1930s [22]. The demand for manufactured products in particular provided the impetus to ensure quality products balanced with costs. A reliability-based approach to product

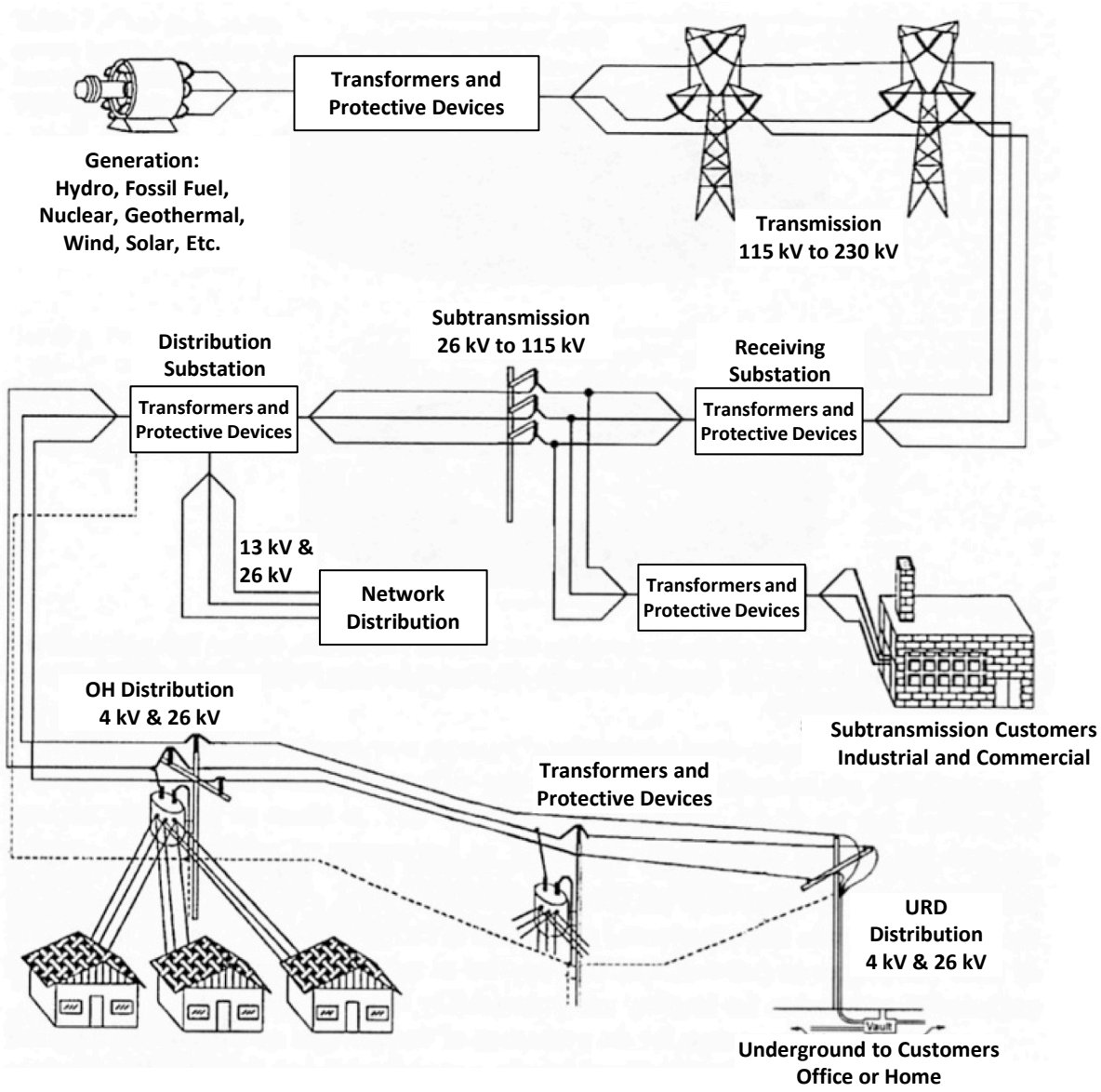

Figure 2.2: Schematic of the typical US power delivery system [16].

design and fabrication resulted from these considerations. Deterministic approaches were implemented first, with probability assessments becoming more popular in the 1940s [5, 23]. For example, Birolini [5] argued that the expectation of an item's quality was no longer solely about being free of defects or systematic failures when it was put into operation, but should also include the ability to perform within specified limits for a specified life cycle.

Reliability is traditionally defined as "the probability that, when operating under stated environmental conditions, a system will perform its intended function adequately for a specified interval of time" [24]. This definition is quantitative; qualitatively, reliability can also mean the ability of an item to remain functional [5]. Since the uncertainty of the item's ability to remain functional can be characterized through probability, the quantitative rather than qualitative definition has been implemented broadly. *Reliability* is a general concept that can be applied freely to various subjects with necessary adjustments: *function*, *performance* and *lifetime* are concepts that will be discipline-specific.

In structural engineering, reliability approaches have been employed to characterize building and bridge component designs as early as 1947 [25]. Data required to fit probability distributions to loading demands and material capacities were not widely available until the late 1970s. Probability based load resistance factor design or LRFD was formally introduced in the 1980s e.g. [26, 27] for material-specific application, i.e. concrete or steel. Timber design has only recently adopted LRFD principles e.g. [28]. The components of the electric power delivery system are designed using reliability-based principles, but as mentioned previously, the connected network system must employ other metrics to assess the delivery of electric power. In most settings, a line of connected towers and poles is a series or weakest link system with a radial or ring configuration. Structural redundancy in delivery is provided through overlapping series-based systems. Electrical engineers employ reliability metrics that describe the service provided to customers i.e. metrics that reflect the travel of electricity through a physical network. Because the delivery and *quality* of service depends upon the physical *reliability* of the poles, towers and other equipment, the service metrics implicitly reflect the physical reliability of the system.

The Institute of Electrical and Electronics Engineers (IEEE) has prepared guidelines regarding the measurement of customer-based reliability in [29]. Per the IEEE guidelines, the "customer" is defined as "a metered electrical service point for which an active bill account is established at a specific location". An *interruption* is "the total loss of electric power on one or more normally energized conductors to one or more customers connected to the distribution portion of the delivery system". A *sustained interruption* is defined as "any interruption that lasts more than five minutes". In the US, utilities and companies that provide power must report annual performance metrics to the appropriate state agencies who regulate them, such as public utility commissions. The commissions regulate the cost of power to customers; that is, rate increases are usually approved at the state level. Unfortunately, the IEEE performance metrics do not include prolonged disruptions due to extreme hazard events, although some states require recovery updates based upon customer service at regular intervals, e.g. New York State [30].

The IEEE employs several reliability indices. The System Average Interruption Frequency Index (SAIFI) measures how often the average customer experiences a sustained interruption over a year; that is, it is measured in units of "number of interruptions per year". It is defined by

$$\begin{aligned}\textbf{SAIFI[interruptions/year]} &= \textbf{System Average Interruption Frequency Index} \\ &= \frac{\sum \textbf{Customers affected by each interruption}}{\textbf{Total number of customers served}}.\end{aligned} \tag{2.1}$$

The System Average Interruption Duration Index (SAIDI) measures the total duration of the interruption for the average customer per year as given by

$$\begin{aligned}\textbf{SAIDI[hours/year]} &= \textbf{System Average Interruption Duration Index} \\ &= \frac{\sum \textbf{Customer hours off for each interruption}}{\textbf{Total number of customers served}}.\end{aligned} \tag{2.2}$$

Two other metrics can be derived from SAIDI and SAIFI. The Customer Average Inter-

ruption Duration Index (CAIDI) measures the average time required to restore service:

$$\textbf{CAIDI} = \frac{\sum \textbf{Total customer hours of interruption}}{\textbf{Total number of customers interrupted}}. \tag{2.3}$$

The Customer Average Interruption Frequency Index (CAIFI) measures the average frequency of sustained interruptions of customers experiencing sustained interruptions:

$$\textbf{CAIFI} = \frac{\sum \textbf{Total number of customer interruptions}}{\textbf{Total number of customers interrupted}}. \tag{2.4}$$

Values for SAIFI are typically on the order of 1.5 to 3.0 interruptions per year. SAIFI for storm events is denoted as STAIFI (Storm Average Interruption Frequency Index), as follows [31]:

$$\textbf{STAIFI[interruptions/year]} = \frac{\sum_{initial}^{final} \textbf{Customers affected by each interruption}}{\textbf{Total number of customers served}}. \tag{2.5}$$

Frequently, STAIFI is normalized by the annual SAIFI to compare system performance over a storm event and denoted as STAIFI_n:

$$\textbf{STAIFI}_n = \frac{\textbf{STAIFI[interruptions/year]}}{\textbf{SAIFI[interruptions/year]}}. \tag{2.6}$$

STAIDI_n is defined in a similar manner. STAIFI and STAIDI are best fit by lognormal probability distributions [32]. In this context, the metrics are comparable to strength or capacity metrics as used in structural design. For winter storms in the Pacific Northwest region, Reed and Cook [33] found that linear relationships applied between STAIFI_n and STAIDI_n, respectively, with the square of the maximum 5-second wind gust speeds. Analyses of data for hurricanes have not been as successful as for winter storms; that is, the STAIFI_n data are not best fit with the gust ratio squared at the county or parish level. In Chapter 3, STAIFI is related to newer inoperability metrics, which indicate that these commonly kept statistics may be relevant in evaluating newer models.

Researchers have found that annual SAIDI and SAIFI values are best fit by lognormal distributions [34, 35]. Using post-event in-situ outage duration data for hurricanes [36] and

winter storms [37], the probability distribution of outage durations in hours for particular utilities such as Duke Power were fit. Davidson [36] found that outage durations for utilities for several hurricanes were remarkably similar. Reed [35] compiled several outage data sets for hurricanes and winter storms and found them to be similar. A Gamma distribution was found to be appropriate for the data sets relating the duration of outages to various delivery systems after specific storms. However, the distribution was implicitly based upon storm data such as peak wind speeds so its use in prediction for future storms was limited.

Power delivery outages after earthquakes have been studied extensively e.g. the Applied Technology Council (ATC) [38], Schiff [39], Werner and Taylor [40], Dueñas-Osorio [41]. The structural damage to delivery systems in earthquakes is primarily due to substation failures rather than towers or poles. Therefore, the focus has been on substation dynamic analysis. Also, in the US, the number of outage events for storms is far greater than for seismic events so the focus has been on storm-related outages. The influence of the loading demand placed on the system components will be explored in terms of the robustness in the next section as well as in Chapters 3 and 4.

2.3 Robustness

Robustness as a concept in industrial engineering applications emerged in Japan after World War II. Taguchi developed a general methodology known as "robust design" in order to ensure the high quality of manufactured products with limited resources [11]. Founded based upon the theory of statistical experimental design, "robust design" addressed two emerging issues, (1) how to reduce the variation in products with minimum cost and (2) how to reduce the sensitivity of products to different manufacturing and customer environments [42].

Originally, quality was measured by the number of defective items out of a set of items. That is, the underlying process was binary: an item was perfect or defective. Figure 2.3 shows a block diagram of a simple manufacturing process. The box representing the "Product/Process" receives "signals" from the manufacturer or customer and converts them into "Responses". During this process, there are control factors that the manufacturer is able to

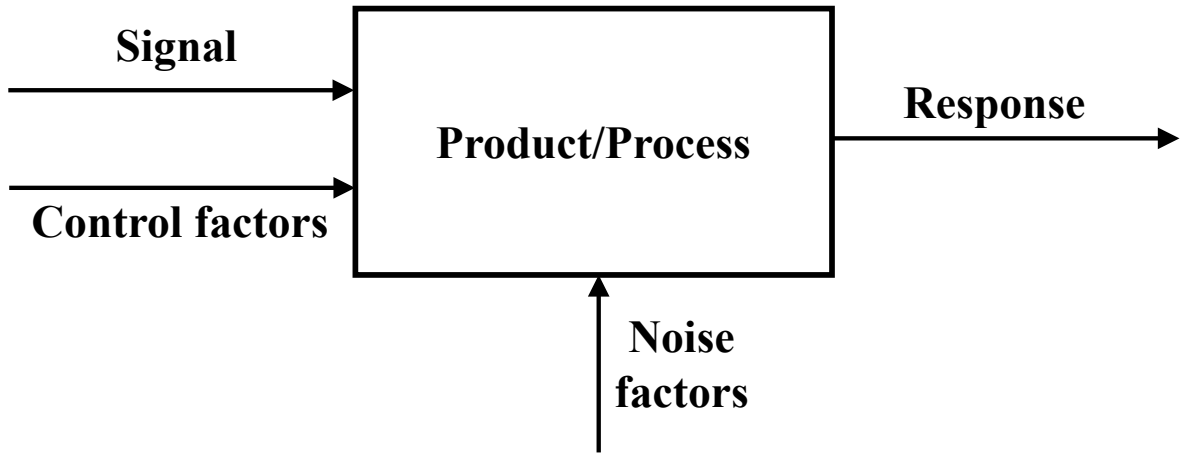

Figure 2.3: Block diagram of a manufacturing process.

adjust, as well as noise factors that are unpredictable and cannot be managed. The presence of noise factors causes the response to deviate from its intended target. Therefore, most manufacturing processes have a set of predetermined tolerances for the factors and responses, and the product that generates a response within the given tolerance is considered acceptable. That is, the tolerance limit is a boundary which divides working products from defective ones. However, customers do not treat all "qualified" products equally.

A study of Sony television customers showed that customers always preferred the product that gave a response that corresponded to a target value [42]. As the deviation from the target increased, customer satisfaction decreased. Manufacturers concluded that merely identifying defective products was not sufficient for customer satisfaction. In order to deliver products that met the target as closely as possible, many companies sought to tighten the tolerance limits, which resulted in the purchase of higher quality raw materials and equipment. Such actions increased both the production and maintenance costs dramatically. To ensure the competitiveness in the manufacturing process, Taguchi developed the concept of robust design [42].

In this approach, *robustness* is defined as the state where the technology, product or

process performance is minimally sensitive to factors causing variability in either the manufacturing or user's environment and aging at the lowest unit manufacturing cost [11]. Sensitivity and variability are the two main issues addressed by this definition. Robustness emphasizes target performance with minimal sensitivity. It may contribute to reliability but it is a broader concept.

Taguchi [23] suggested that the design process of a product consists of three phases, system design, parameter design and tolerance design. Control factors and noise factors exist in each of the three phases. The objective of robust design is to set control factors to appropriate levels so that the process is insensitive to noise factors. The sensitivity to noise factors is measured by the signal to noise (S/N) ratio, and Taguchi believed that it was the only good measure of robustness in the engineering disciplines [11]. The S/N ratio emphasizes the sensitivity to noise, rather than just a deviation from a target mean. The historical development of the Taguchi-based robust design methodology is provided in [11, 42, 43]. In addition, Hasenkamp et al. [44] and Arvidsson and Gremyr [45] have provided detailed reviews of robust design methodologies currently in practice. Phadke [42] argued that the most cost-effective approach to improve *reliability* is to find appropriate continuous quality characteristics and reduce their sensitivity to all noise factors, that is, to improve *robustness*.

In the field of civil engineering infrastructure, the notion of *robustness* has a slightly different meaning, as the opposite of *vulnerability*. That is, a system is robust physically if it maintains its integrity when demands are applied. In the case of electric power delivery, a system is robust if small changes in the delivery system due to applied loadings (demand) do not significantly change the overall functionality or quality. It is more closely related to the notion of *fragility* which is a conditional probability of failure of a system given the level of the applied loading, which will be discussed in greater detail in Chapters 3 and 4. Robustness is also related to resilience in the civil engineering literature and it will be discussed in section 2.4 below.

2.4 Resilience

Within engineering, the term "resilience" was originally used to describe the mechanical behavior of materials. In this context, the resilience of a material was a measure of the amount of energy that can be absorbed under elastic loading conditions and which was released when the loads are removed [46]. In the context of environmental science and engineering, Holling [47] defined resilience as a "measure of the persistence of systems and of their ability to absorb change and disturbance and still maintain the same relationship between populations or state variables." In Holling's terms, "stability" was the "ability to return to an equilibrium state after a temporary disturbance". The concept of returning to an "equilibrium state" post-disturbance has been incorporated into some definitions of resilience. It is noted that a uniform definition of the term does not exist across disciplines, and the usage varies. Examples from various disciplines include the following:

- *Resilience in safety:* System safety is a major area where resilience has been studied. Hollnagel [48] defined "resilience" as "the intrinsic ability of a system to adjust its functioning prior to, during or following changes and disturbances, so that it can sustain required operations under both expected and unexpected conditions". Sheridan [49] suggested that resilience engineering presupposes that human errors and machine failures will likely occur, and a more useful effort should be placed on means to anticipate disturbances and be able to recover and restore the system to the original state or, if need be, some acceptable state that is different but still safe.

- *Community resilience:* Bruneau [50] defined "community seismic resilience" as "... the ability of social units (e.g. organizations, communities) to mitigate hazards, contain the effects of disasters when they occur, and carry out recovery activities in ways that minimize social disruption and mitigate the effect of future disasters".

- *Resilience in civil engineering:* In the context of civil engineering, resilience is usually expressed mechanistically as the ability to "bounce back" after a major disturbance

[51]. Similarly, infrastructure resilience is the ability to reduce the magnitude and/or duration of disruptive events [52].

- *Enterprise resilience:* "Enterprise resilience" is the "ability and capacity to withstand systemic discontinuities and adapt to a new risk environment". A resilient organization effectively aligns its strategy, operations, management systems, governance structure, and decision-support capabilities so that it can uncover and adjust to continually changing risks, endure disruptions to its primary earnings drivers, and create advantages over less adaptive competitors [53].

- *Operational resilience:* "Operational resilience" is a organization's "ability to adapt to risk that affects its core operational capacities". It is a emergent property of effective operational risk management, supported and enabled by activities such as security and business continuity. As a subset of enterprise resilience, *operational resilience* focuses on the organization's ability to manage operational risk, whereas enterprise resilience encompasses additional areas of risk such as business risk and credit risk [54].

- *Network resilience:* Resilience in networks is the "ability of an entity to tolerate, endure and automatically recover from challenges under the conditions of the network, coordinated attacks and traffic anomalies" [55].

- *Healthcare resilience:* In healthcare, resilience is the "process of negotiating, managing and adapting to significant sources of stress or trauma" [56].

In the civil engineering field, Bruneau et al. [50] defined the seismic resilience of a community as having the four properties of robustness, redundancy, rapidity and resourcefulness within technical, organizational, social and economic dimensions. These terms are shown on a plot of quality $Q(t)$ of a system over time t in Figure 2.4. In this formulation 100% quality means that a system is completely functional; zero percent is a completely non-functional

system. This entire plot has been used to represent the resilience of a system over time after a disruption.

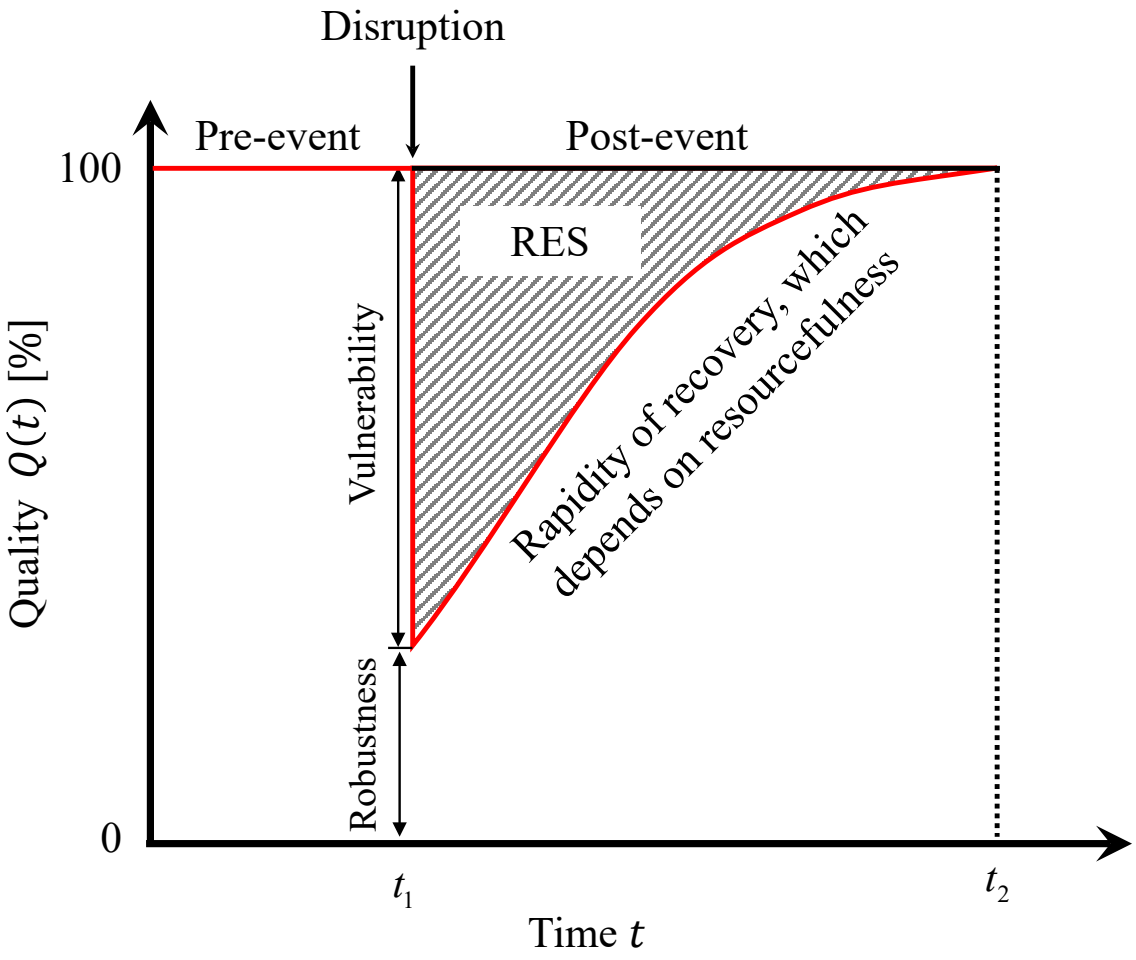

Figure 2.4: Quality $Q(t)$ of a system over time t (after Bruneau et al. [50]).

The *response* and *recovery* of infrastructure following extreme hazard events has been a focus of studies in the emergency management field. Following the devastating effects of several earthquakes on infrastructure in California, such as San Fernando and Loma Prieta, the Applied Technology Council (ATC) conducted an investigation into the recovery and response of major lifelines following seismic events in the US [38]. One of the basic questions

was whether to use technical or non-technical methods to improve resilience. That is, was it better to spend resources preparing communities by improving the structural capacity of the built environment or would resources be better spent on assisting communities to recover from damaged systems and system outages? Because damage and recovery data were not widely available at the time, ATC implemented subjective probability assessment of experts, using a Delphi approach, of whether physical infrastructure would withstand minor, moderate and major earthquakes with damage [57]. Although this investigation was the beginning of an entirely new way of modeling the safety and resilience of an entire community, the assessments made were much harsher than has proven to be the case; that is, predictions that power outages in the Puget Sound region would last for over one month for a magnitude 6.8 earthquake did not prove to be true for the Nisqually event of 2001, as power was restored within 36 hours [34]. However, the report provided the impetus for the research community and practitioners in engineering and social science to work together to develop models of *response* and *recovery* using probabilistic methods. This report was a precursor to the Bruneau et al. [50] report. In this thesis, the terms of *response* and *recovery* are part of the resilience characterization. The concept of using multiple properties to characterize resilience of the infrastructure will be significantly expanded in Chapter 3.

2.5 Infrastructure Network and Interdependencies

Civil infrastructure is defined as "a system of systems of networked interdependent lifelines" as shown in Figure 1.3. Networked models require dependency relationships so introducing the network approach to infrastructure systems in this section will focus on interdependency modeling. The interdependencies of the infrastructure network did not draw much attention until the 1990s when the President's Commission on Critical Infrastructure Protection (PCCIP) was established by President Clinton in 1996 [58]. As stated in the report presented by the PCCIP in 1997 [59], "the rapid proliferation and integration of telecommunications and computer systems have connected infrastructures to one another in a complex network of interdependence". Since then, an increasing number of studies on infrastructure interde-

pendencies have been conducted by both public and private entities.

Built on the PCCIP report, Rinaldi et al. [13] introduced the four types of interdependencies, i.e. physical, cyber, geographic, and logical interdependency, and discussed the framework of modeling interdependencies through agent-based simulation. The taxonomy of interdependencies defined by Rinaldi et al. [13] was adopted widely by later studies, e.g. [60–62]. Also based on this taxonomy, the eleven lifeline systems discussed in this thesis (as shown in Figure 1.3) were derived by Chang et al. [12] for modeling of the post-event interdependent critical infrastructure failures observed in the US and Canada.

Besides using agent-based approaches and simulation tools, e.g. [61, 62], current methods for assessing infrastructure interdependencies also include time-series cross-correlation functions, e.g. [41, 63], and input-output models, e.g. [64–67].

Dueñas-Osorio and Kwasinski [41] introduced the use of cross-correlation function (CCF) to evaluate the coupling strength among interconnected lifeline systems. Time series data from electric power delivery and telecommunication service restoration after the 2010 Chile Earthquake were used as a test case in [41] to illustrate the application of cross-correlation function to calculate the interdependency between the two lifelines. Krishnamurthy et al. [63] continued the effort by studying power and telecommunication lifeline interdependencies after the 2011 Japan Earthquake using CCF, and the results were compared with that from Chile Earthquake. It is noted that the use of CCF requires the input to be stationary or at least weakly stationary, which is not usually the case for lifeline restoration data. In [41, 63], differencing was used to remove some of the nonstationary. Therefore, although the CCF method provides insight for lifeline interdependencies, quality of the input data needs to be improved to meet the stationarity assumption.

Input-output models are another approach of studying interdependency among different infrastructure systems. Originally introduced as a economy model by Leontief [68, 69], input-output models are used to assess interdependencies among different economy sectors, i.e. goods and services. Haimes and Jiang [66] developed the inoperability input-output model (IIM) as an extension of the economy input-output model for study of infrastructure

interdependencies. The modeling of interdependencies using IIM after terrorist attacks (e.g. high-altitude electromagnetic pulse) was presented in [64, 70]. Reed et al. [10] extended the input-output modeling to hurricane data and derived a proof-of-concept approach to evaluating interdependency metrics using physical damage data (e.g. electrical power outage) rather than economic data. This approaches differs from CCF as it enables the prediction of physical damage through the use of interdependency coefficients.

In summary, although the application of a networked paradigm to infrastructure modeling has been undertaken it remains challenging even though computational methods have greatly expanded in recent years. Unfortunately, finely discretized data sets of infrastructure are not available for public examination due to security concerns. The degree to which the subsystems should be discretized remains an open question. The thrust of this thesis is to build models at spatial scales, such as communities, cities, counties and states, that can be used to predict the performance of infrastructure during and after extreme events.

2.6 Overlap among the three methods

The concepts of Figure 2.4 may be applied to any infrastructure system subjected to any type of hazard loading. In the resilience function $Q(t)$, the vulnerability represents the initial damage. The response and recovery are functions of the resourcefulness of a community, as resources are needed to repair and restore physically damaged components. The area above the $Q(t)$ curve, denoted as RES, has been suggested as a combined *resilience* metric [50, 71]. *Redundancy* metrics can be applied to the engineering system to denote multiple sources of capacity, or repair teams; or it may describe the multiplicity of organizations that work together to repair and restore infrastructure systems. In Chapter 3, mathematical models will be derived and calibrated using in-situ post-event data for power and other systems to illustrate the importance of using more than one single metric – reliability, robustness or resilience – to capture the behavior of infrastructure, and ultimately, communities subject to extreme hazards.

Chapter 3

COMBINED RELIABILITY, ROBUSTNESS, AND RESILIENCE METHODS AS APPLIED TO POWER DELIVERY AND OTHER SYSTEMS

The development of the spatial methods and field data for several hurricanes and earthquakes have made the expansion of the reliability, robustness and resilience models possible. In this chapter the resilience paradigm will be presented and applied to a set of hurricane and earthquake data sets. It will be shown that progression in geo-statistical modeling has provided support for these advances. Methodologies presented in this chapter have been discussed in [72].

3.1 Mathematical models

Quality models for resilience over time may be formulated in distinct phases: pre-event, during event and post-event. Pre-event models are assumed to describe functioning at a status quo; typically $Q(t) = 100\%$. Mathematical models have been proposed for the other sections of the resilience curve in Figure 2.4. These models are presented in this section. It is noted that the $Q(t)$ data to be modeled may be in the form of time series of outages for a given region, such as a community, parish, county or state. The data may also be in the form of a damage index, such as the length of a damaged line segment divided by the total length of that segment, for a specific region. Both data types represent the damage to the ability of the system to deliver specified services such as power. Further discussion of the data distinctions will be delayed until the data fits are provided in section 3.2.

Post-event restoration of power delivery has been modeled by a simple exponential function e.g. Chang [73] as given by

$$RS(t) = 1 - e^{-bct}, \tag{3.1}$$

where t is time in days, b is a constant which characterizes how rapidly the process is restored, and c is a scaling factor to compare restoration curves with different time frames. For power delivery, outage data are divided by the total number of outages to determine $RS(t)$. That is, $RS(0) = 0\%$ and $RS(t)$ approaches 100% restoration as time increases. Therefore, it differs from both SAIDI and quality $Q(t)$ metrics because they are estimated relative to the entire number of customers, not the number of outages.

A formulation for $Q(t)$ similar to that of Equation 3.1 is given by

$$Q(t) = 1 - q_0 e^{-q_1 t}, \tag{3.2}$$

where q_0 and q_1 are constants derived from the data.

The parameter q_0 has been labeled as the *vulnerability*, which in this context is represented as being additive with the robustness to unity. The exponent q_1 is often called the rapidity parameter as it governs how rapidly the $Q(t)$ function is restored to full capacity. The total amount of time d required for 100% of the outages to be restored in Equation 3.1 was introduced in section 2.1; it is typically evaluated for a system for several storms, and fit with a probability distribution [36]. This approach of linking probability to restoration times has been implemented by FEMA [74] to build limited predictive models for restoration times of structural components for seismic events. It is noted that the duration at which 50% restoration occurs is considered an important restoration metric for emergency managers.

The resilience metric RES can be defined in terms of $Q(t)$ as follows:

$$RES = 1 - \frac{\int_{t_1}^{t_2} Q(t)dt}{t_2 - t_1}, \tag{3.3}$$

where t_1 and t_2 are the endpoints of the time interval under consideration. RES is the area above the $Q(t)$ curve. Minimization of this area has been suggested as a design strategy, although the means to do this physically is not straightforward.

Cimellaro et al. [75] discussed three types of functionality recovery curves, that is for functionality post-event: linear, exponential and trigonometric as illustrated in Figure 3.1. The type of functionality recovery post-event was assumed to be a property of the underlying structural capacity. Zobel [76] investigated an approximation of the *linear* formulation of system recovery, without identifying the demand variable, as a graphical means for decision-making by managers post-event. However, the linear formulation has not been apparent in post-event in-situ engineering systems: the exponential model has been observed most commonly for engineering data sets. It was shown by Cimellaro et al. [75] that $Q(t)$ in

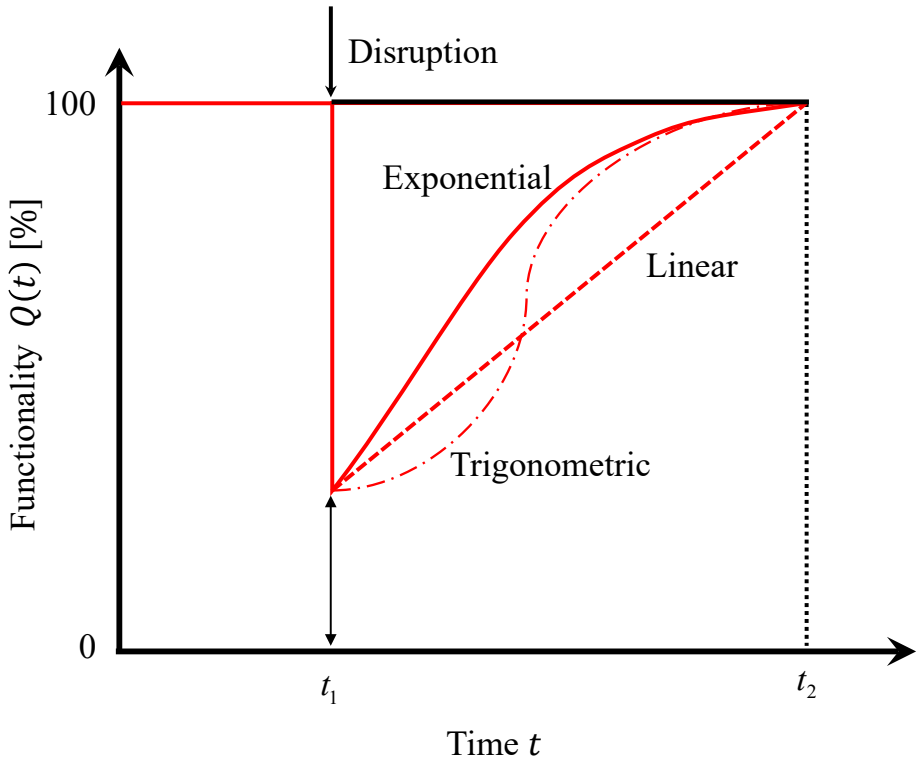

Figure 3.1: Functionality recovery curves in linear, exponential and trigonometric format.

exponential form was related to the solution of the single-degree-of-freedom (SDOF) free vibration mechanical model; however, the model was not actually fitted or explored. In this thesis, in order to facilitate fitting the SDOF model, it is best to define *inoperability* $X(t)$ as

follows:

$$X(t) = 1 - Q(t). \tag{3.4}$$

The conversion of $Q(t)$ to $X(t)$ is illustrated in Figure 3.2.

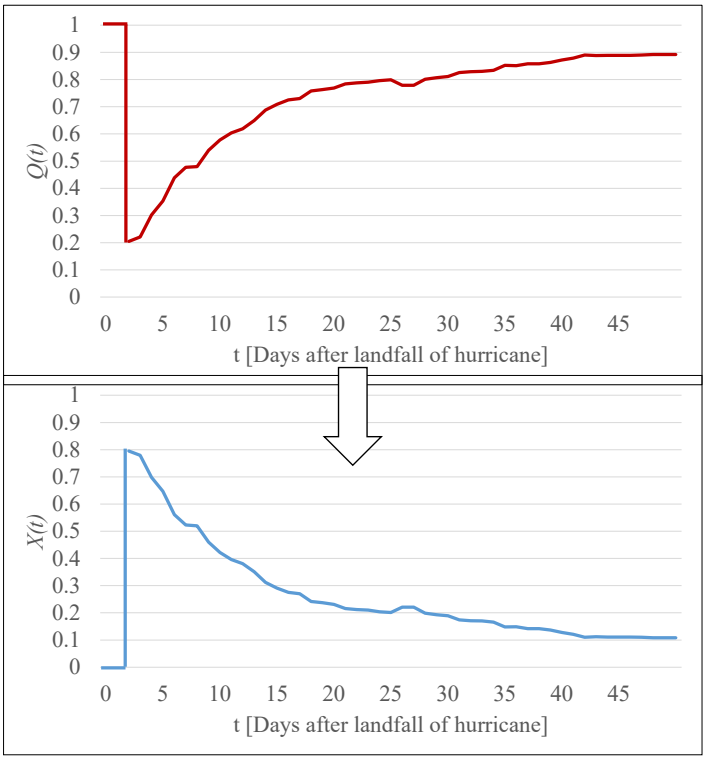

Figure 3.2: $X(t)$ function as related to $Q(t)$.

For most lifeline systems, $X(t)$ can be directly determined from post-event data as follows:

$$X(t) = \frac{\text{Number of customer outages at time } t}{\text{Total number of customers served}}. \tag{3.5}$$

Therefore, when $X(t)$ is zero, the lifeline is fully operational. For $X(t) = 1$, the entire system is "inoperable", or not functioning. The same type of metric is appropriate for other lifelines, such as transit. For transit, "riders" would replace "customers". The total number of riders during a "normal" day would be used in the denominator. Another interpretation

is to use the damage index, that is, damage per length of line; that is, whether complete or partial recovery of a transit line or train is operating, e.g. Zimmerman et al. [77].

It is noted that the maximum $X(t)$ (number of customer outages at time t divided by the total number of customers) approximates STAIFI, as follows:

$$STAIFI \approx X_{max}. \tag{3.6}$$

In addition, the area underneath the $X(t)$ curve represents the resiliency parameter RES. Because a smaller value of RES represents a more resilient system, it is appropriate to seek a functional characterization of $X(t)$ in order to identify properties of the system best suited to reduce this area.

3.1.1 Modeling inoperability $X(t)$ as the free vibration of a critically damped or overdamped single-degree-of-freedom system

The equation of motion of the the free vibration of a single-degree-of-freedom system (SDOF) illustrated in Figure 3.3 is

$$m\ddot{X} + c\dot{X} + kX = 0 \quad \text{or} \quad \ddot{X} + 2\zeta\omega\dot{X} + \omega^2 X = 0, \tag{3.7}$$

for

- $\ddot{X}$ = second derivative of X with respect to time t;
- $\dot{X}$ = first derivative of X with respect to time t;
- m = mass;
- c = damping factor;
- k = stiffness;
- $\omega = \sqrt{\frac{k}{m}}$ = natural frequency in (rad/s);

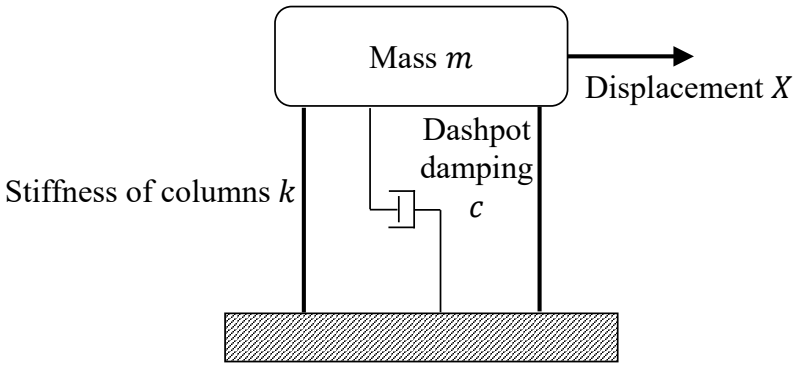

Figure 3.3: Illustration of a single-degree-of-freedom (SDOF) system.

- $\zeta = \frac{c}{2\sqrt{mk}} = \frac{c}{2m\omega}$ = damping ratio

To recover without oscillations, the SDOF system needs to be in overdamped or critically damped condition where $c^2 - 4mk \geq 0$.

When $c^2 - 4mk > 0$, the system is overdamped and the general solution to Eq. 3.7 is

$$X(t) = \frac{(\alpha+\beta)X_0 + \dot{X}_0}{2\beta} e^{-(\alpha-\beta)t} + \frac{(\beta-\alpha)X_0 - \dot{X}_0}{2\beta} e^{-(\alpha+\beta)t}, \tag{3.8}$$

where $\alpha = \omega\zeta$, $\beta = \omega\sqrt{\zeta^2 - 1}$, $X(t=0) = X_0$ and $\dot{X}(t=0) = \dot{X}_0$.

3.1.2 Fitting the SDOF parameters to $X(t)$

In order to determine the two parameters ω and ζ, it is advantageous to convert the derivatives of Equation 3.7 into finite differences and use linear regression. Unfortunately, it was found that in order to obtain a good fit over the entire range of time t, it was necessary to use a nonlinear fitting procedure. This difficulty is attributed to the small sample sizes for some of the data sets. For the nonlinear fitting, the least-square method was used to estimate ω and ζ. That is, if $\{x_{t_i}, i = 1, \ldots, n\}$ denotes the actual power outage data obtained from power companies or government agencies, then $X(t = t_i) = x_{t_i}$ (the fraction of customer without power at time t_i). Define $\mathbf{r}$ as the residual vector:

$$\mathbf{r} = \begin{pmatrix} r_1 \\ r_2 \\ \vdots \\ r_n \end{pmatrix} = \begin{pmatrix} x_{t_1} - X(t_1) \\ x_{t_2} - X(t_2) \\ \vdots \\ x_{t_n} - X(t_n) \end{pmatrix}. \tag{3.9}$$

Mathematically, in order to find the best fit parameters, the least-square fitting method attempts to minimize the sum of squares of the components of $\mathbf{r}$ [78]:

$$\begin{aligned} \underset{\omega,\zeta}{\text{minimize}} \quad & r_1^2 + r_2^2 + \cdots + r_n^2 \\ & = \sum_{i=1}^{n} \left[x_{t_i} - \left(\frac{(\alpha+\beta)X_0 + \dot{X}_0}{2\beta} e^{-(\alpha-\beta)t_i} + \frac{(\beta-\alpha)X_0 - \dot{X}_0}{2\beta} e^{-(\alpha+\beta)t_i} \right) \right]^2. \end{aligned} \tag{3.10}$$

The optimization was done using the method described by Levenberg [79] and Marquardt [80]. The Levenberg-Marquardt method combines the gradient descent method and the Gauss-Newton method. It acts more like gradient descent method when the parameters are far from optimal value, and more like Gauss-Newton method when the parameters are close to the optimal value [81]. Given $X_0 = X(t = 0)$, the parameters being estimated are $\dot{X}_0$, ω and ζ.

The initial values of $\dot{X}_0$, ω and ζ are required to begin the least-square fitting process. The choice of initial values are crucial since Levenberg-Marquardt method is iterative and may not converge to global minimum. A poor estimate of initial values may lead to convergence to local minimum. Karnopp and Fisher discussed a simple method for estimating ω and ζ of a overdamped systems [82]. Given the curve of a overdamped system in free motion, this method was proved accurate to estimate the parameters. Although a function curve is not available before data fitting, applying this method to the raw time series data points is still a suitable choice for obtaining initial values of ω and ζ. Detailed discussion and proofs of the method can be found in [82].

Figure 3.4 shows the key points on the curve needed for the method. I is the inflection point where $\frac{d^2X}{dt^2} = 0$; A, B are two points at large values of t. A summary of the estimating process is given in the following steps:

1. A tangent line to $X(t)$ is drawn through I and the value T is determined by the intercept of this tangent line on x-axis;

2. Select two points A and B as far as to the right as the data are meaningful;

3.
$$\omega_1 = \frac{1}{\Delta t} \ln \frac{X_A}{X_B}; \tag{3.11}$$

4.
$$\zeta = \frac{T\omega_1}{2\sqrt{T\omega_1 - 1}}; \tag{3.12}$$

5.
$$\omega = \frac{2\zeta}{T}. \tag{3.13}$$

For data used in this thesis, point I is set at $X(t = 0)$. The choices of points A and B are limited by Equations 3.11 and 3.12 which require $X_A > 0$, $X_B > 0$ and $T\omega_1 > 1$. Assuming a tangent line through data point at $X(t = 0)$ intercept x-axis at t_T, the subsequent two points where the t values are greater than t_T can be chosen as A and B. If there are no eligible A and B points, the initial values for such cases will be set to $\omega = 1$ and $\zeta = 1.1$.

The total variation in $X(t)$ denoted by R^2 as explained by the model can be written as

$$R^2 = \frac{\sum_{i=1}^{n} \left[X(t_i) - \hat{X}(t_i)\right]^2}{\sum_{i=1}^{n} \left[X(t_i) - \bar{X}\right]^2}, \tag{3.14}$$

where $\bar{X} = \frac{\sum_{i=1}^{n} x_{t_i}}{n}$.

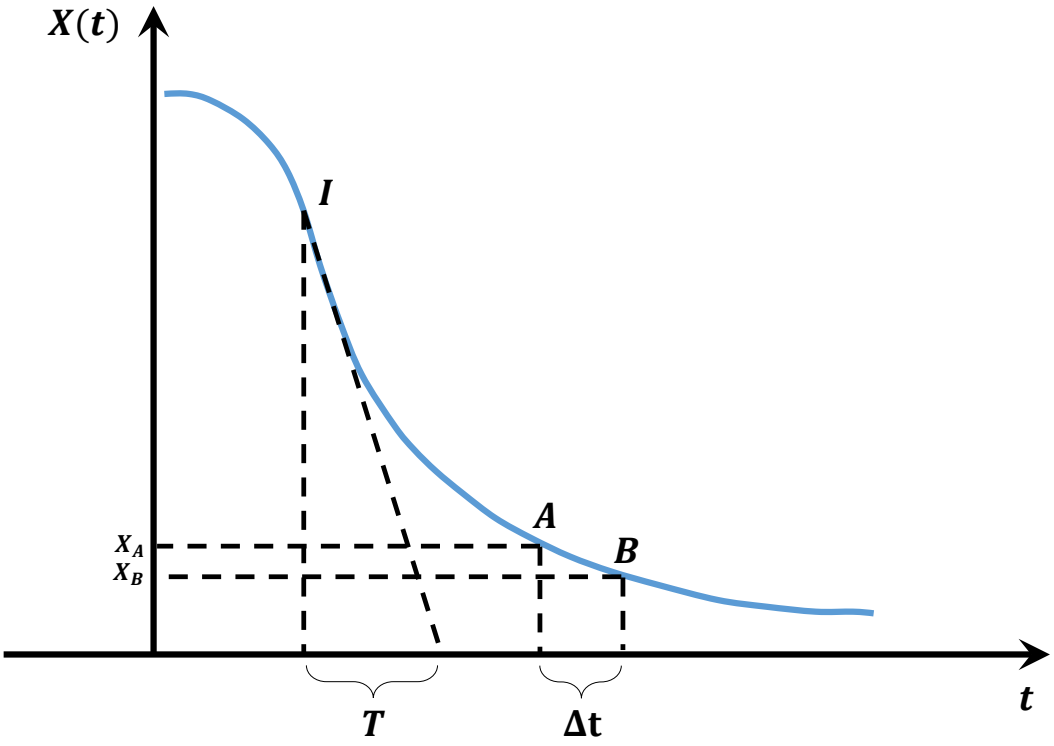

Figure 3.4: Illustration of function $X(t)$ initial values estimating method (after [82]).

3.2 Applications

The reliability, robustness and resilience of hurricane or earthquake-induced outage data are modeled using the methods described in section 3.1. Before presenting the results, the data sets are discussed.

3.2.1 Data description

3.2.1.1 Hurricane events in US

The electric power grid in the US is more vulnerable to storm events, such as hurricanes and winter storms, than seismic events. Each year during the hurricane season in the US,

Table 3.1: Characteristics of the selected hurricanes [83].

Hurricane	First landfall in US			Total Damage in the US (Billion $)
	Date	Location	Wind Speed (mph)	
Charley	19:45 UTC, Aug 13, 2004	Southwest coast of Florida near Cayo Costa	150 (Category 4)	15.1 (as of 2011)
Frances	04:30 UTC, Sep 5, 2004	Southern end of Hutchinson Island, Florida	104 (Category 2)	9 (as of 2004)
Ivan	06:50 UTC, Sep 16, 2004	West of Gulf Shores, Alabama	121 (Category 3)	14.2 (as of 2004)
Katrina	22:30 UTC, Aug 25, 2005	Border of Miami-Dade County and Broward County, Florida	81 (Category 1)	108 (as of 2011)
Rita	07:40 UTC, Sep 24, 2005	Southwestern Louisiana just west of Johnson's Bayou and east of Sabine Pass	115 (Category 3)	12 (as of 2011)
Wilma	10:30 UTC, Oct 24, 2005	Southwestern Florida near Cape Romano	121 (Category 3)	20.6 (as of 2006)
Gustav	15:00 UTC, Sep 1, 2008	Cocodrie, Louisiana	104 (Category 2)	4.3 (as of 2009)
Ike	07:00 UTC, Sep 13, 2008	North end of Galveston Island, Texas	109 (Category 2)	24.9 (as of 2010)
Isaac	00:00 UTC, Aug 29, 2012	Along the coast of Louisiana at Southwest Pass on the mouth of the Mississippi River	81 (Category 1)	2.4 (as of 2013)
Sandy	23:30 UTC, Oct 29, 2012	Brigantine, New Jersey	81 (Category 1)	$\geq$50 (as of 2013)

significant power outages occur near the Gulf of Mexico region. To maintain national security and collect information regarding emergency situations on US electric energy supply systems, the Department of Energy (DOE) requires electric utilities to file incident and disruption reports when certain criteria are met, such as loss of electric service of greater than 50,000 customers for one hour or more [84]. Power outage data collected through this channel are usually at the state level and published by DOE as situation reports [85] following major hurricanes. More detailed power outage data, that is at county/parish or city level, are often not public out of security concerns. Power outage data of ten hurricanes were extracted from DOE situation reports, and examined in this section. The selected ten major hurricanes span from 2004 to 2012, and each of them has resulted in damage costs of billions of dollars in the US. Characteristics of each selected hurricane are listed in Table 3.1 with information gathered from National Oceanic and Atmospheric Administration's (NOAA) tropical cyclone reports [83]. Additional GIS and infrastructure related data for Hurricane Isaac and Sandy can be found in [86, 87]. The time series power outage restoration data collected from DOE

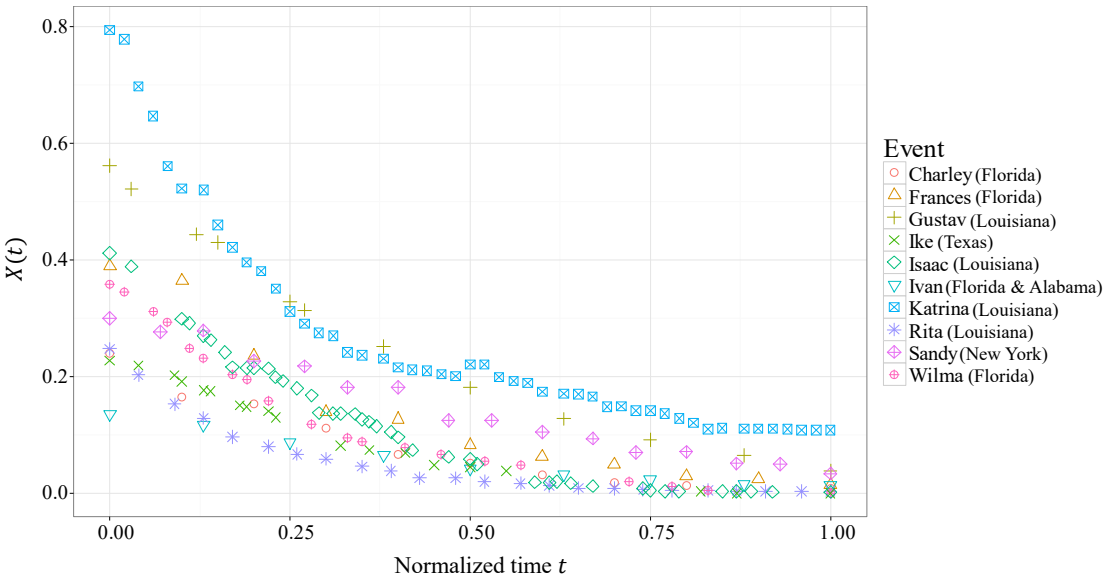

Figure 3.5: Electric power outage data after major hurricane events in the US.

for the ten selected hurricanes are shown in Figure 3.5 on a normalized time scale. The outage data are from the state(s) which sustained longest outage (the name of the state is given in the legend). It can be seen that although there is scatter, the restoration processes follow a similar exponential decay. Power outage data at the parish/county level were obtained from LPSC for Hurricane Gustav, Ike and Isaac in spreadsheet format, as shown in Figure 3.6 [88]. The highest resolution of power outage data were obtained from New York State Department of Public Service (NYDPS) for Hurricane Sandy at the "locality" level. The term "locality" is similar to "neighborhood" and its boundaries are defined by utility providers such as Consolidated Edison who supplies electric power to Manhattan. Figure 3.7 shows the boundaries of some localities of lower Manhattan in New York City.

Governor's Office of Homeland Security and Emergency Preparedness
LPSC Office: Phone: (225) 922-2487

Email: lpsc.outage@la.gov
ELECTRIC UTILITIES OUTAGE REPORT
LOUISIANA PUBLIC SERVICE COMMISSION
HURRICANES GUSTAV & IKE
DATE: September 12, 2008 TIME: 1800 HRS

Up to 21 days
Up to 10 days
Up to 5 days

Parish	Utility	# of Customers Out of Service	Total # of Customers	% of Customers Out
ACADIA	Entergy Gulf States	4	6,394	0.06%
	SLEMCO	544	12,386	4.39%
	CLECO	0	7,423	0.00%
ACADIA TOTAL		548	26,203	2.09%
ALLEN	Beauregard	0	5,178	0.00%
	Entergy Louisiana	0	135	0.00%
	Jefferson Davis	0	383	0.00%
	CLECO	0	6,258	0.00%
ALLEN TOTAL		0	11,954	0.00%
ASCENSION	Entergy Gulf States	4,682	33,168	14.12%
	DEMCO	1,815	11,731	15.47%
ASCENSION TOTAL		6,497	44,899	14.47%
ASSUMPTION	Entergy Louisiana	3,190	10,422	30.61%
	SLECA	0	927	0.00%
ASSUMPTION TOTAL		3,190	11,349	28.11%

Figure 3.6: Screen capture of power outage reports obtained from LPSC for Hurricane Gustav and Ike.

Figure 3.7: Example of some localities in lower Manhattan, New York City.

3.2.1.2 2011 Japan Earthquake

A magnitude 9.0 earthquake occurred on March 11, 2011 near the northeast coast of Honshu, Japan. The strong ground shaking and the following tsunami caused significant damage to lifelines, such as electric power delivery and water supply systems [89]. Figure 3.8 shows the ground motion and shaking intensities of the 2011 Japan Earthquake produced by U.S. Geological Survey (USGS) [90].

The number of customers without electric power and water supply for each prefecture (prefectures form the first level of jurisdiction and administrative division of Japan) after the 2011 Japan earthquake was obtained from Nojima and Kato [91]. The data were then converted to $X(t)$ using the total number of customers within each prefecture as shown in

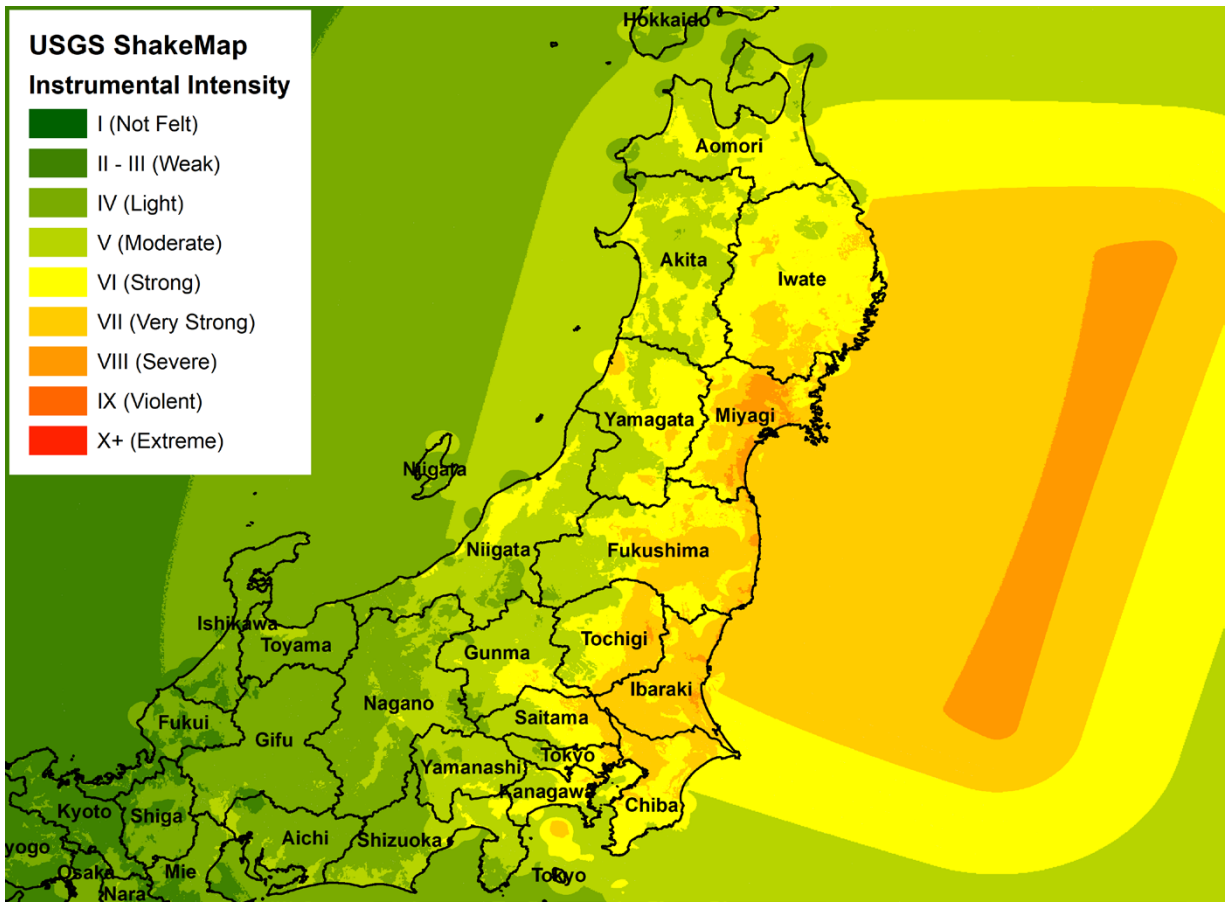

Figure 3.8: USGS ShakeMap of 2011 Japan Earthquake [90].

Equation 3.5. The electric power and water service recovery process $X(t)$ for 14 prefectures are shown in Figure 3.9 and 3.10. As indicated by Nojima and Kato [91], four events occurred during the earthquake disaster:

1. Main shock of magnitude 9.0 on March 11, 14:46, off the Pacific Coast of Tohoku;
2. Aftershock No.1 of magnitude 7.7 on March 11, 15:15, off Ibaraki Prefecture;
3. Aftershock No.2 of magnitude 7.1 on April 7, 23:32, off Miyagi Prefecture;
4. Induced earthquake of magnitude 7.0 on April 11, 17:16, Nakadori, Fukushima Prefecture.

It can be seen from Figure 3.9 and 3.10 that the electric power and water services of most prefectures were affected by the main shock, therefore, the restoration data from $t = 0$ to $t = 27$ are used to fit the SDOF model.

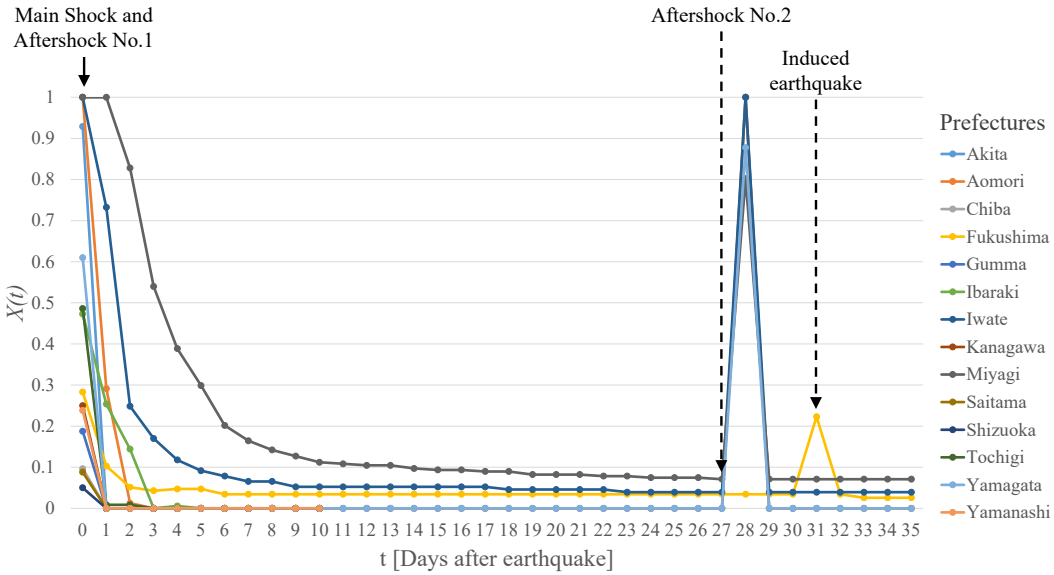

Figure 3.9: Electric power recovery after 2011 Japan Earthquake.

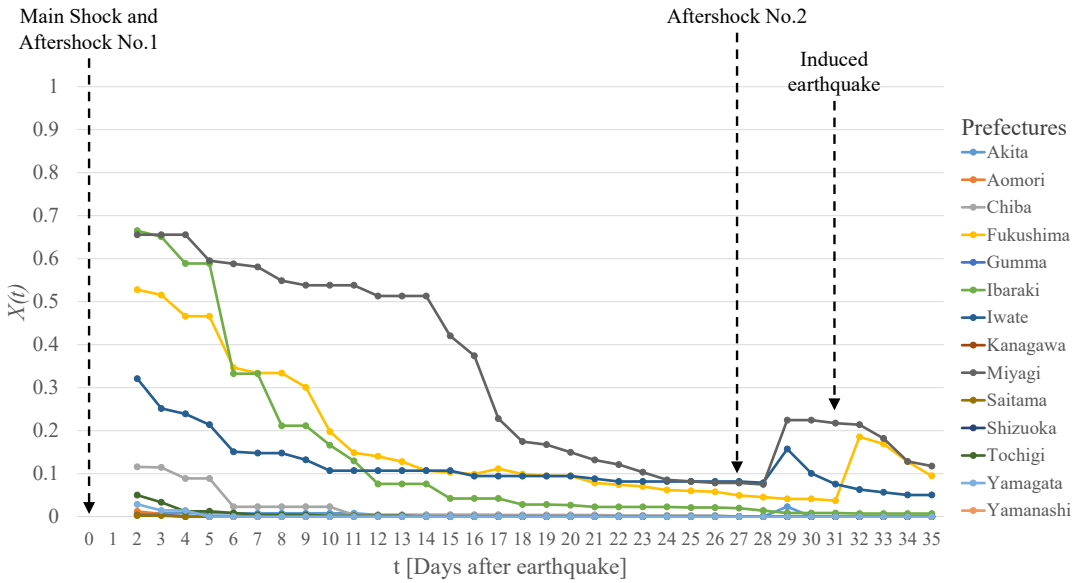

Figure 3.10: Water supply recovery after 2011 Japan Earthquake.

3.2.1.3 2010 Chile Earthquake

A magnitude 8.8 earthquake occurred in central Chile on February 27, 2010 at 3:34 AM local time (06:34 UTC). Figure 3.11 shows the ground motion and shaking intensities of the 2010 Chile Earthquake produced by USGS [92]. The earthquake caused direct damage to lifeline systems, such as power delivery, telecommunication, water service, and gas systems [41]. The fraction of customers with electric power and telecommunication service (including mobile and fixed phones) were extracted from [41] for Region VII (Maule) and VIII (Bio-Bio) (equivalent to $Q(t)$). The data were then converted to $X(t)$ as shown in Figure 3.12 and 3.13. Similar to prefectures, regions are also Chile's first-level administrative division.

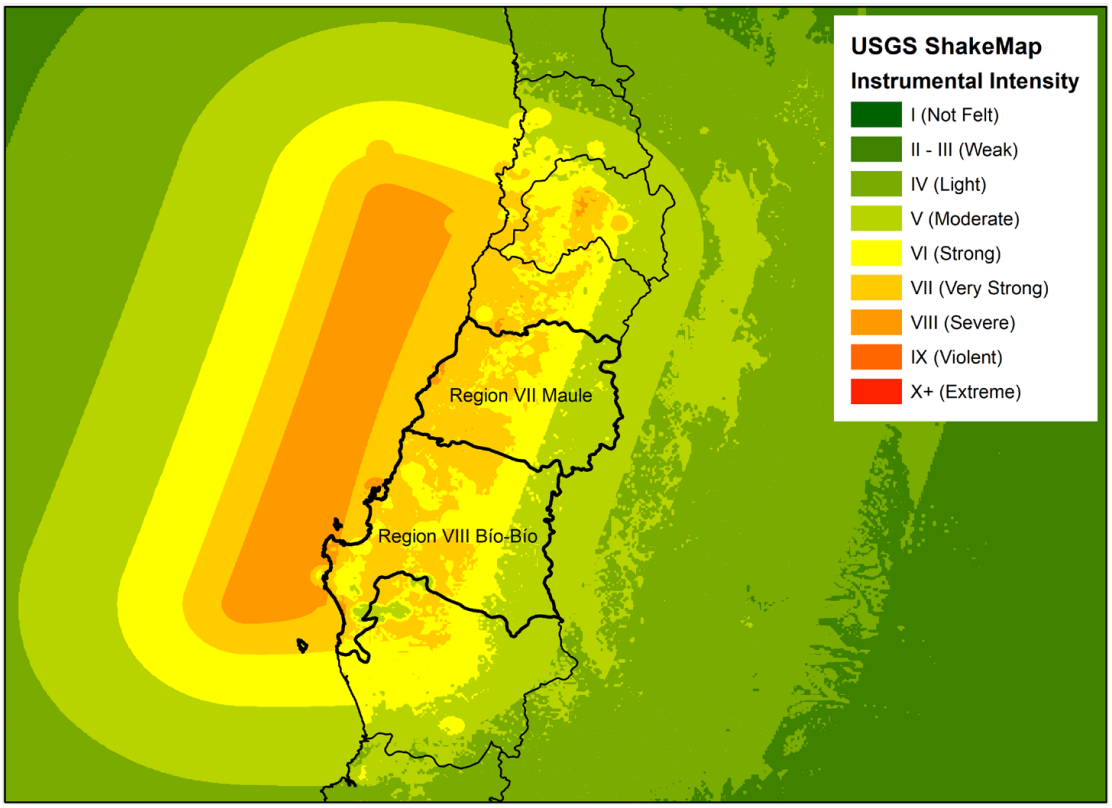

Figure 3.11: USGS ShakeMap of 2010 Chile Earthquake [92].

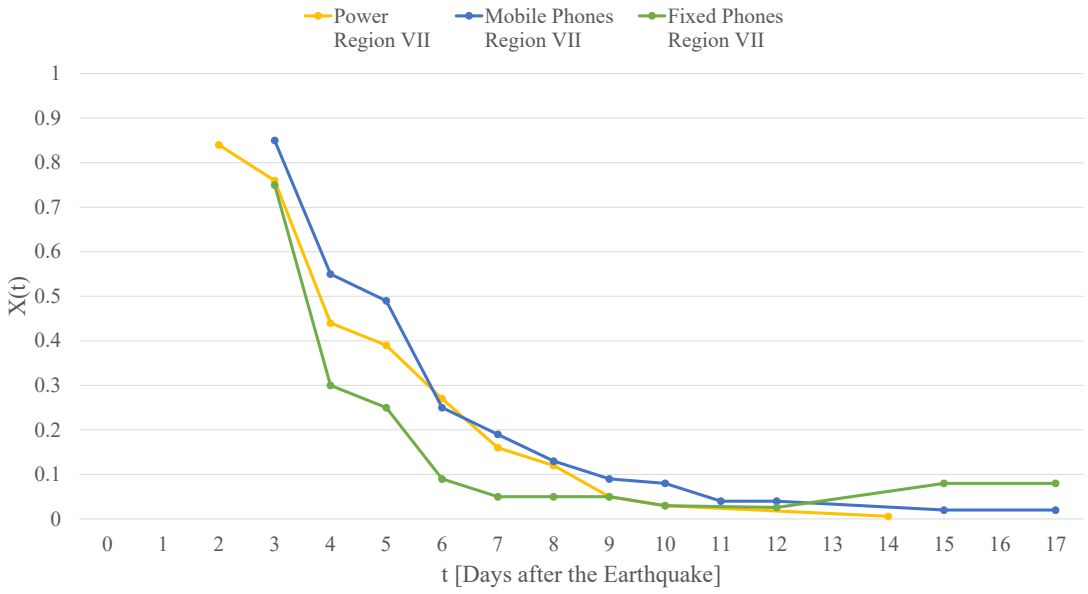

Figure 3.12: Electric power and telecommunication service recovery for Region VII after 2010 Chile Earthquake.

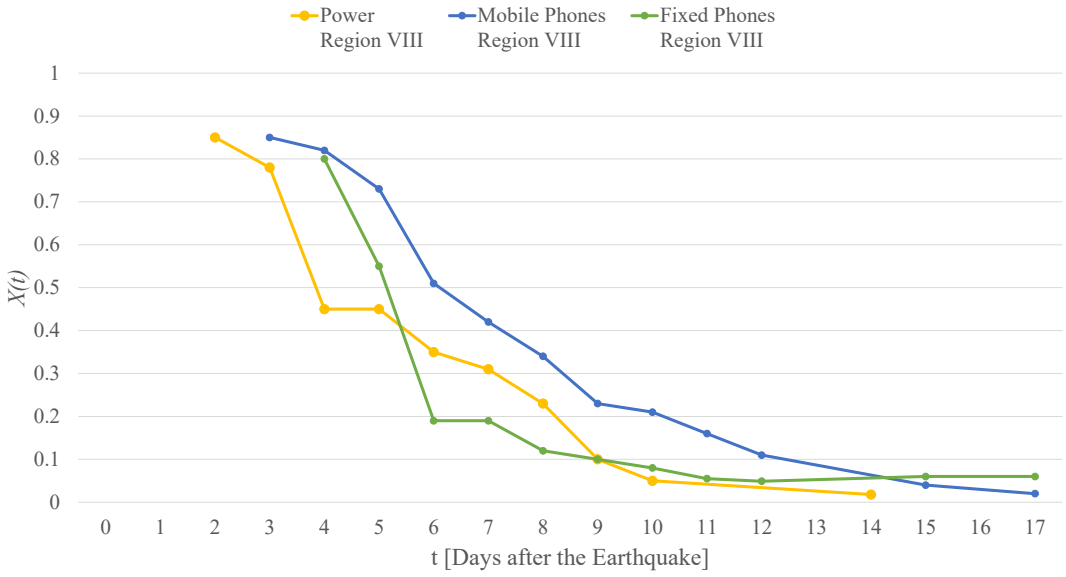

Figure 3.13: Electric power and telecommunication service recovery for Region VIII after 2010 Chile Earthquake.

3.2.2 Model fitting results

It can be seen from the restoration figures presented in the last section, maximum power outage does not always occur at $t = 0$ after earthquake or hurricane landfall due to various reasons such as data availability and timing of the report. However, the mathematical models given in Equations 3.1, 3.2 and 3.8 assume that the maximum power outage is sustained at time $t = 0$. Therefore, the outage data for the selected hurricanes and earthquakes are modified such that for each event, the time $t = 0$ corresponds to the maximum or peak power outage.

3.2.2.1 Electric power delivery system

The Levenberg-Marquardt method was used for fitting of the data to restoration function $RS(t)$ (as defined in Equation 3.1). The fitted parameter values are given in Table 3.2 for the selected hurricanes (scaling factor c is fixed at 1). The goodness of fit parameter R^2 (as defined in Equation 3.14) varied from 0.929 to 0.998 for each event. It is noted that the parameter b varied mainly because the storm intensity differed. Although this formulation provides some insight, it is limited in its ability to predict future behavior. Figure 3.14 shows the fitted restoration curves $RS(t)$ versus the outage data for the hurricanes.

Converting the data into $Q(t)$ and using Equation 3.2 provided more insight than the restoration function $RS(t)$ as the q_0 value reflects the system *robustness*. The fitted parameter q_1 values are found in Table 3.3. The RES for each data set is evaluated using Equation 3.3 and the results are shown in Table 3.3. It is noted that larger RES value indicates longer outages, and greater damage to the system overall. Figure 3.15 shows the fitted restoration curves $Q(t)$ versus the outage data for the hurricanes.

Table 3.2: Least-square fitting results for selected hurricane events using restoration function $RS(t)$.

Hurricane Event	State	b	R^2	No. of Observations
Charley	Florida	0.302	0.979	10
Frances	Florida	0.286	0.965	11
Gustav	Louisiana	0.276	0.994	12
Ike	Texas	0.125	0.957	19
Isaac	Louisiana	0.447	0.979	42
Ivan	Florida and Alabama combined	0.264	0.977	9
Katrina	Louisiana	0.061	0.929	49
Rita	Louisiana	0.218	0.998	24
Sandy	New York	0.225	0.959	16
Wilma	Florida	0.201	0.991	20

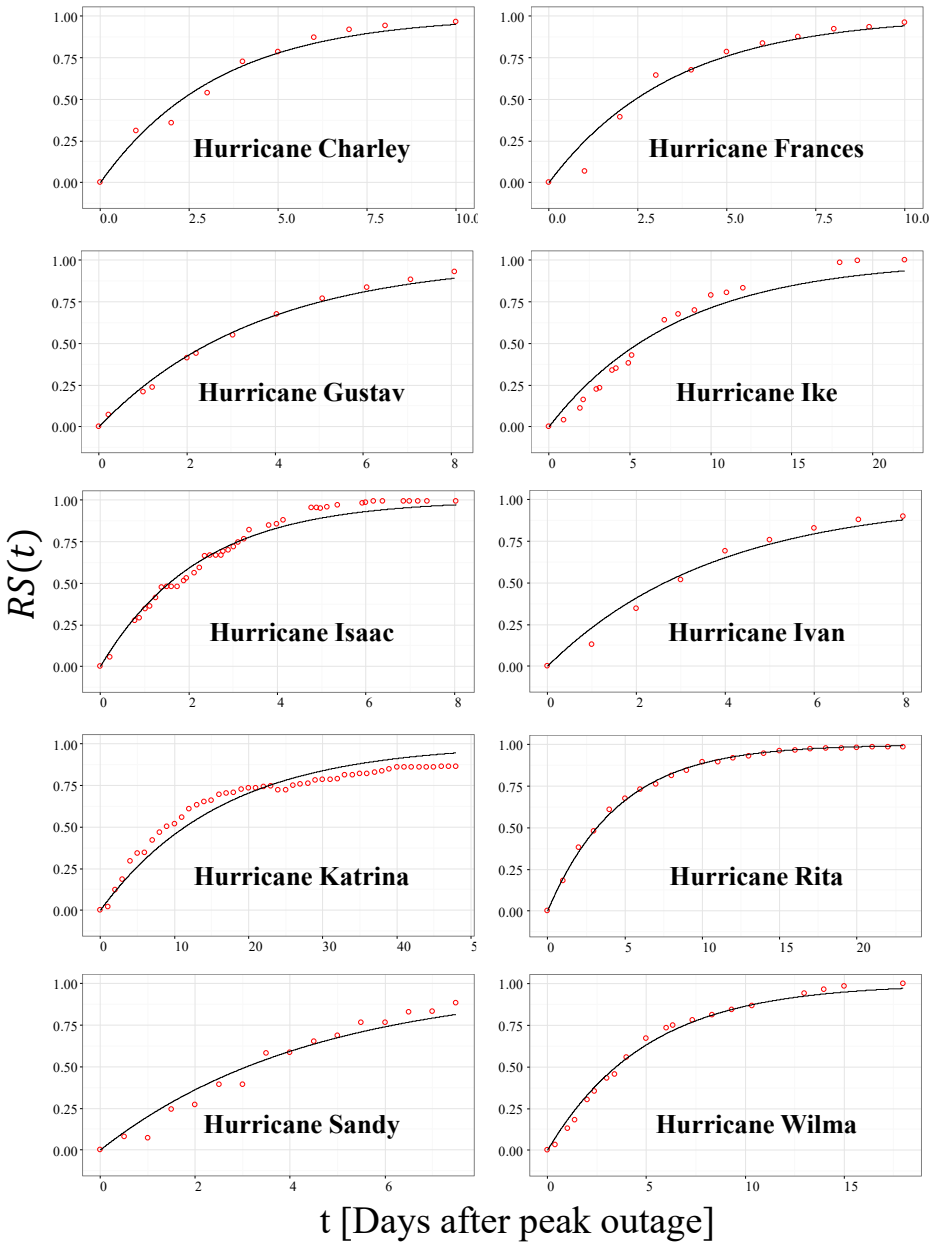

Figure 3.14: Fitted restoration function $RS(t)$ curves for selected hurricane events.

Table 3.3: Least-square fitting results for selected hurricane events using function $Q(t)$.

Hurricane Event	q_0	q_1	R^2	RES
Katrina	0.795	0.061	0.929	0.271
Gustav	0.562	0.276	0.994	0.250
Sandy	0.300	0.225	0.959	0.157
Frances	0.390	0.286	0.965	0.151
Isaac	0.412	0.447	0.979	0.112
Wilma	0.358	0.201	0.991	0.103
Charley	0.240	0.302	0.979	0.087
Ike	0.229	0.125	0.957	0.081
Ivan	0.135	0.264	0.977	0.065
Rita	0.248	0.218	0.998	0.055

Deriving $X(t)$ from the $Q(t)$ data allows for a more focused analysis. Plotting the $X(t)$ values versus time in Figure 3.5 for several hurricanes illustrates the exponential decay behavior of the system. It can be seen that the restoration for storms takes a similar form despite the differences in storm characteristics or locations. Fitting the SDOF model to several hurricanes using the methodology described in Equations 3.7 to 3.14 yields the results in Table 3.4. Results for selected storms are shown in Figure 3.16.

Table 3.4: Least-square fitting results for selected hurricane events using SDOF model $X(t)$.

Hurricane Event	Duration (Days)	ω	ζ	R^2	X_0	$\dot{X}_0$	RES
Katrina†	49	0.249	2	0.900	0.795	0	0.271
Gustav	9	0.440	1.0001	0.999	0.562	-0.122	0.250
Sandy	8	0.566	1.172	0.989	0.300	0	0.157
Frances	11	0.739	1.255	0.986	0.390	0	0.151
Isaac	9	0.695	1.0001	0.990	0.412	-0.141	0.112
Wilma	19	0.650	1.595	0.998	0.358	-0.012	0.103
Charley	11	0.174	1.0001	0.985	0.240	-0.042	0.087
Ike	23	0.298	1.044	0.996	0.228	0	0.081
Ivan	9	0.675	1.225	0.999	0.135	0	0.065
Rita†	24	0.879	2	0.995	0.248	0	0.055

† Note: Results for Katrina and Rita showed irregularities, and parameters were re-estimated by limiting ζ value in the range of $(1, 2]$.

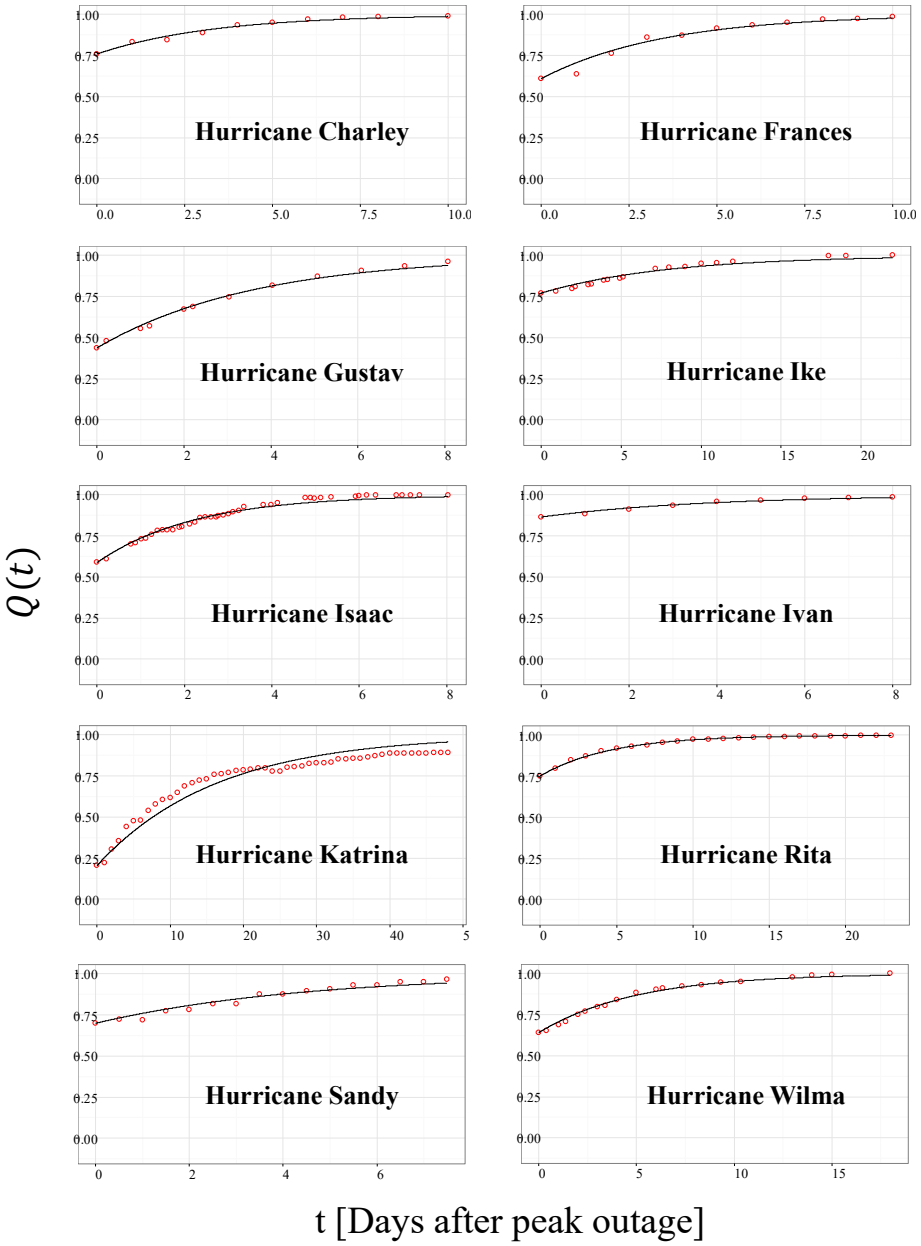

Figure 3.15: Fitted function $Q(t)$ curves for selected hurricane events.

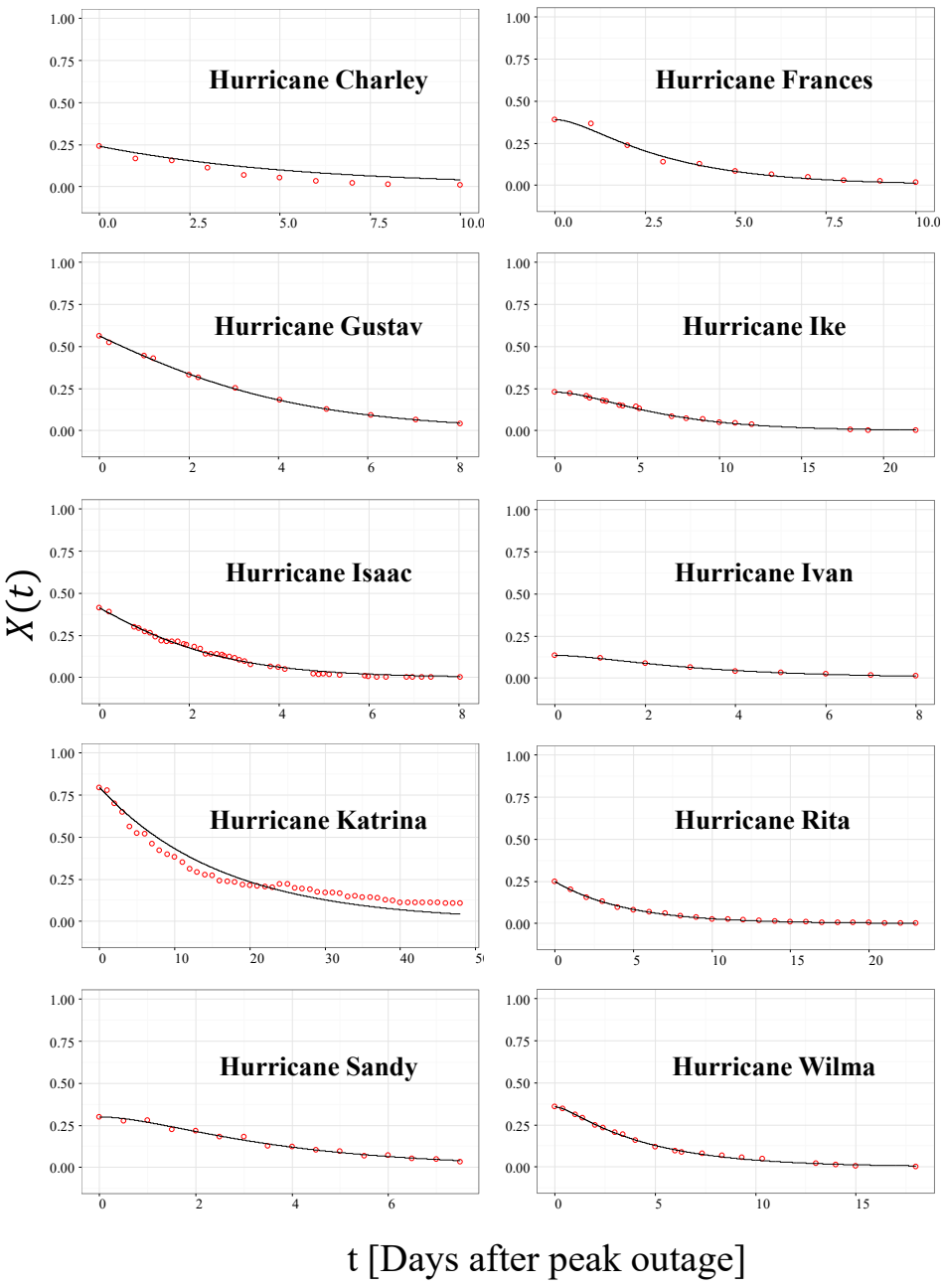

Figure 3.16: Fitted SDOF model $X(t)$ curves for selected hurricane events.

As a comparison to the ω and ζ values estimated from the state level outage data, Table 3.5 shows the fitted SDOF model parameters for power outage data at parish level in Louisiana State after Hurricane Isaac, and only the parishes with peak outage greater than 10% were included. LPSC provided the time series power outage data in approximately half hour intervals for 11 days from August 28 to September 7, 2012. To reduce the fluctuations, daily average power outage was calculated and used for fitting the SDOF model. Table 3.6 shows the fitted SDOF model parameters for power outage data at locality level in Manhattan, New York City after Hurricane Sandy. Similarly, only the localities with peak outage greater than 10% were included. NYDPS also provided the time series power outage data in half hour intervals, and daily average power outage was used for fitting the SDOF model.

From Table 3.4, 3.5 and 3.6, it can be seen that greater initial damage X_0 usually leads to greater RES value, which indicates a less resilient system. The parameter ω and ζ represent the stiffness and rapidity of the system respectively. The rapidity ζ is approaching 1 in most cases as the spatial resolution moves from state to parish, then to locality level. The SDOF model is critically damped when $\zeta = 1$, and the system obtains the highest recovery speed. The stiffness ω, on the other hand, represents the robustness of the system under disruption. The larger parameter ω indicates a more robust system, which has lower RES values given the same level of initial damage X_0 and parameter ζ.

The dataset for electric power recovery after 2011 Japan Earthquake has previously been shown in Figure 3.9. Services in many prefectures were fully restored after just one day. The least square fitting result for the 2011 Japan Earthquake dataset using the SDOF model is listed in Table 3.7 and only the prefectures with peak outage greater than 10% are included. The fitted curves are plotted and displayed in Figure 3.17.

The dataset for electric power recovery after 2010 Chile Earthquake includes data for two regions, i.e. Region VII and VIII. The least square fitting results for the 2010 Chile Earthquake dataset using the SDOF model are listed in Table 3.8. The fitted curves are plotted and displayed in Figure 3.18.

Table 3.5: Least-square fitting results of each parish in Louisiana State for Hurricane Isaac using SDOF model $X(t)$.

Parish	ω	ζ	R^2	X_0	$\dot{X}_0$	RES
Plaquemines	0.320	1.0001	0.912	0.950	0	0.701
Saint John the Baptist	0.501	1.0001	0.921	0.961	0	0.487
Jefferson	0.606	1.0001	0.957	0.813	0	0.384
Orleans	0.697	1.0001	0.978	0.840	0	0.380
Saint Bernard	0.590	1.0001	0.972	0.888	0	0.366
Saint Charles	0.668	1.0001	0.965	0.773	0	0.353
Saint James	0.718	1.0001	0.964	0.873	0	0.322
Lafourche	0.798	1.0001	0.990	0.729	0	0.287
Tangipahoa	1.183	1.0001	0.9996	0.749	0	0.202
East Feliciana	1.331	1.0001	0.995	0.736	0	0.178
Iberville	1.419	1.0001	0.992	0.714	0	0.173
Terrebonne	1.072	1.0001	0.9994	0.635	-0.503	0.172
Livingston	1.004	1.0001	0.994	0.618	-0.134	0.171
Saint Tammany	1.612	1.0001	0.999	0.676	0	0.155
West Feliciana	1.421	1.0001	0.993	0.689	0	0.155
Saint Helena	1.105	1.0001	0.985	0.52	0	0.146
Ascension	2.395	1.273	0.9999	0.496	0	0.115
East Baton Rouge	0.425	1.0001	0.998	0.434	-0.187	0.110
Pointe Coupee	2.197	1.129	0.9996	0.479	0	0.103
Washington	1.949	1.0001	0.9996	0.559	0	0.099
Assumption	1.478	1.0001	0.987	0.330	0	0.084
West Baton Rouge	1.536	1.0001	0.998	0.34	0	0.077
Caldwell	3.071	1.0001	0.9999	0.196	-0.092	0.023
East Carroll	1.044	1.0001	0.999	0.154	-0.163	0.019

Table 3.6: Least-square fitting results of each locality in Manhattan for Hurricane Sandy using SDOF model $X(t)$.

Locality	No. of Obs	ω	ζ	R^2	X_0	$\dot{X}_0$	RES
Greeley Square	10	0.503	1.0001	0.809	1	0	0.474
Park Place	10	0.481	1.0001	0.805	0.9999	0	0.381
Greenwich	10	0.490	1.0001	0.816	0.9997	0	0.194
Fulton	25	0.419	1.0001	0.907	0.999	0	0.172
City Hall	20	0.575	1.0001	0.858	0.998	0	0.168
Bowling Green	24	0.430	1.0001	0.911	0.972	0	0.160
Kips Bay	22	0.477	1.0001	0.880	0.996	0	0.150
Sheridan Square	16	0.514	1.0001	0.864	0.812	0	0.122
Cooper Square	28	0.620	1.0001	0.901	0.744	0	0.096
Madison Square	16	0.653	1.0001	0.904	0.763	0	0.096
Cortlandt	17	1.281	1.529	0.932	0.924	0	0.094
Chelsea	24	0.627	1.0001	0.911	0.754	0	0.087
Canal	24	0.549	1.0001	0.890	0.199	0	0.026

Table 3.7: Least-square fitting result for 2011 Japan Earthquake electric power dataset using SDOF model $X(t)$.

Prefecture	ω	ζ	R^2	X_0	$\dot{X}_0$
Akita	4.128	1.0001	0.999	0.929	-4.762
Aomori	2.507	1.0001	0.999	1.000	0
Fukushima	0.082	8.236	0.996	0.283	-0.328
Gumma	4.130	1.0001	0.999	0.188	-0.962
Ibaraki	1.160	1.0001	0.986	0.473	-0.202
Iwate	1.344	1.271	0.946	1	0
Kanagawa	4.131	1.0001	0.999	0.250	-1.281
Miyagi	0.580	1.375	0.944	1	0
Tochigi	3.671	2.743	0.999	0.486	-9.093
Yamagata	4.127	1.0001	0.999	0.610	-3.126
Yamanashi	4.129	1.0001	0.999	0.238	-1.221

Table 3.8: Least-square fitting result for 2010 Chile Earthquake electric power dataset using SDOF model.

Region	ω	ζ	R^2	X_0	$\dot{X}_0$
Region VII	0.702	1.132	0.985	0.840	0
Region VIII	0.320	1.0001	0.958	0.850	-0.178

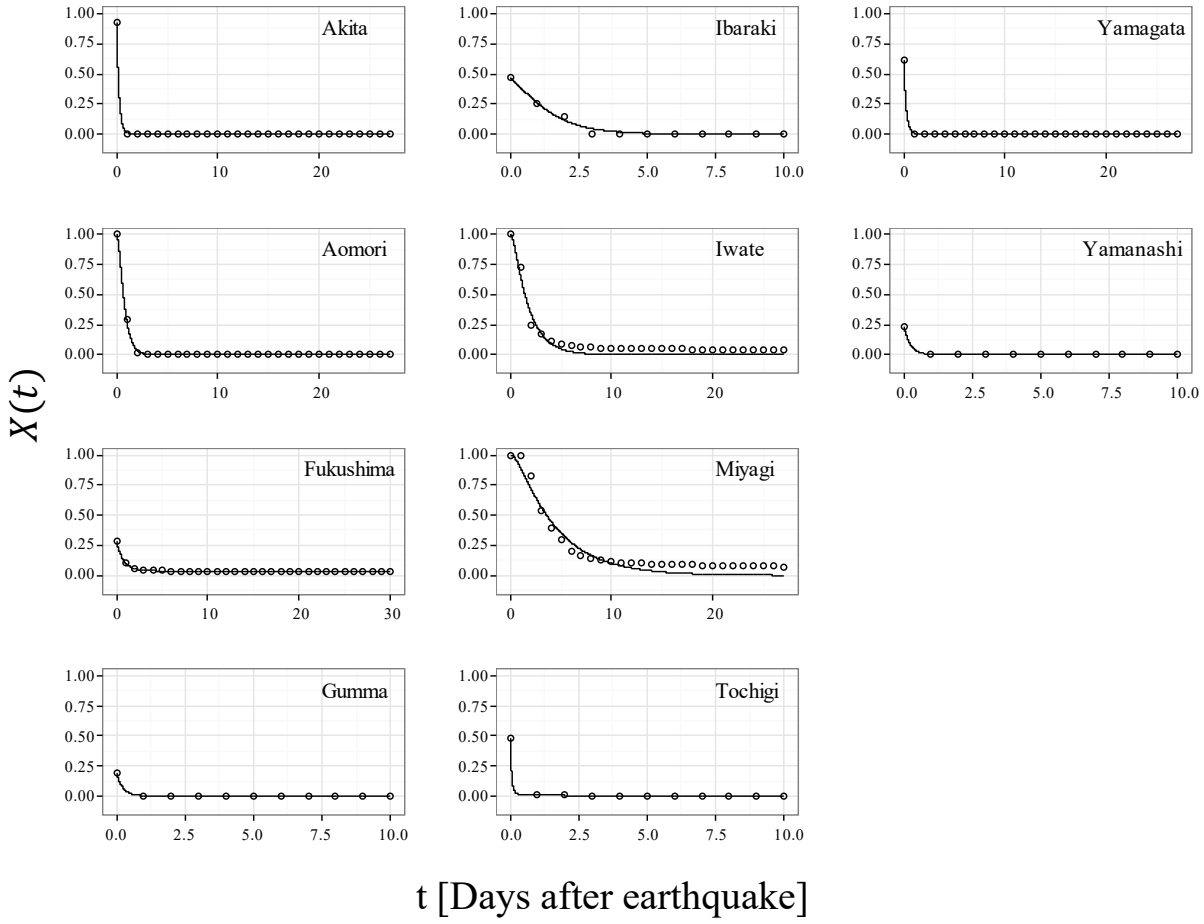

Figure 3.17: Fitted electric power recovery curve $X(t)$ of each prefecture for the 2011 Japan Earthquake.

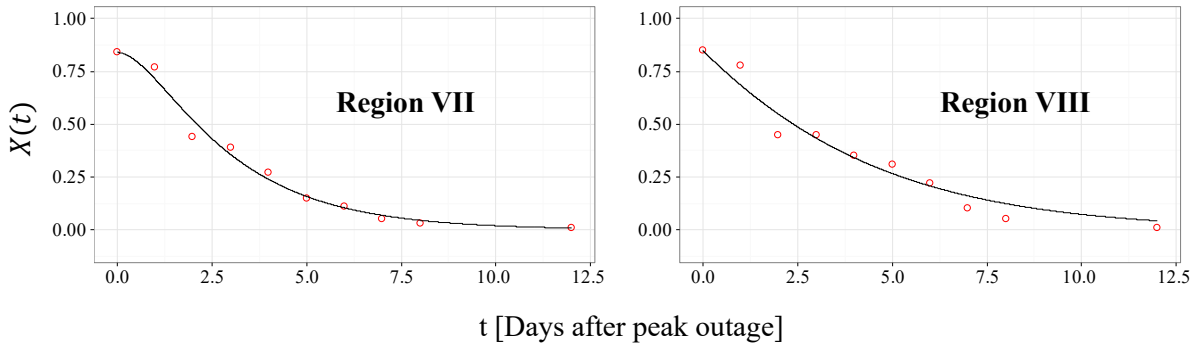

Figure 3.18: Fitted electric power service recovery curve $X(t)$ of each region for the 2010 Chile Earthquake.

3.2.2.2 Other infrastructure systems

The SDOF model was also applied to telecommunications and water services. Table 3.9 shows the fitted SDOF model parameters for the water service recovery after 2011 Japan Earthquake and only the prefectures with peak outages greater than 10% are included.

Table 3.9: Least-square fitting result for 2011 Japan Earthquake water dataset using SDOF model.

Prefecture	ω	ζ	R^2	X_0	$\dot{X}_0$
Chiba	0.495	1.009	0.955	0.116	0
Fukushima	0.336	1.582	0.970	0.528	0
Ibaraki	0.350	1.039	0.984	0.665	0
Iwate	0.061	2.485	0.982	0.321	-0.063
Miyagi	0.126	1.0001	0.910	0.656	0

The least square fitting result for the mobile phone recovery after 2010 Chile Earthquake

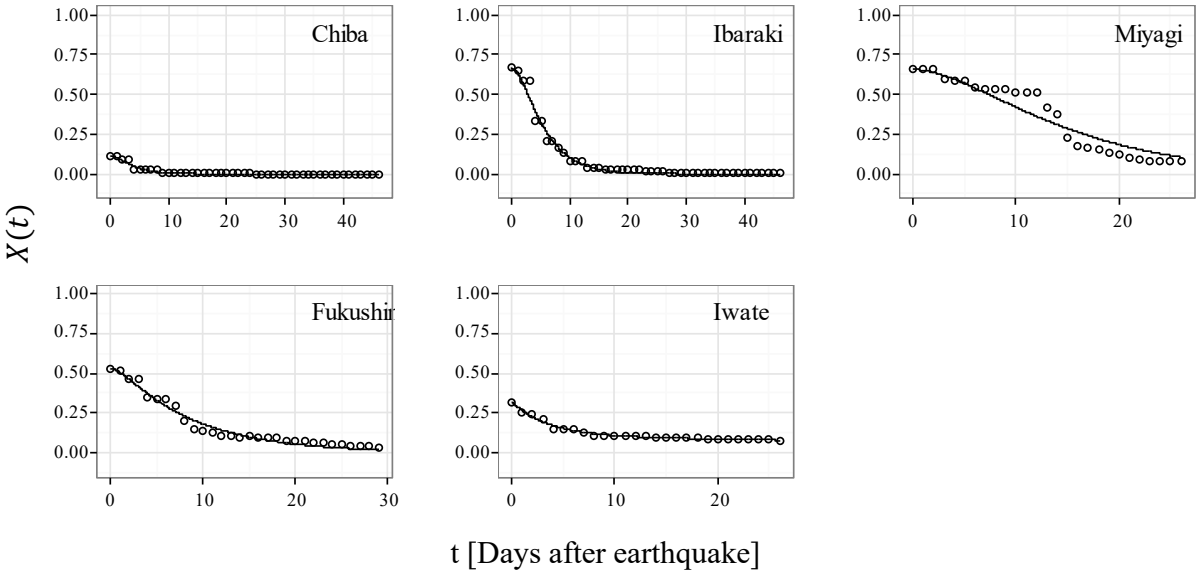

Figure 3.19: Fitted water service recovery curve $X(t)$ of each prefecture for the 2011 Japan Earthquake.

using SDOF model is listed in Table 3.10. The fitted curves are plotted and displayed in Figure 3.20.

Table 3.10: Least-square fitting result for 2010 Chile Earthquake mobile phone dataset using SDOF model.

Region	ω	ζ	R^2	X_0	$\dot{X}_0$
Region VII	0.350	1.0001	0.987	0.850	-0.302
Region VIII	0.423	1.040	0.993	0.850	0

The least square fitting result for the fixed phone recovery after 2010 Chile Earthquake using SDOF model is listed in Table 3.11. The fitted curves are plotted and displayed in Figure 3.21.

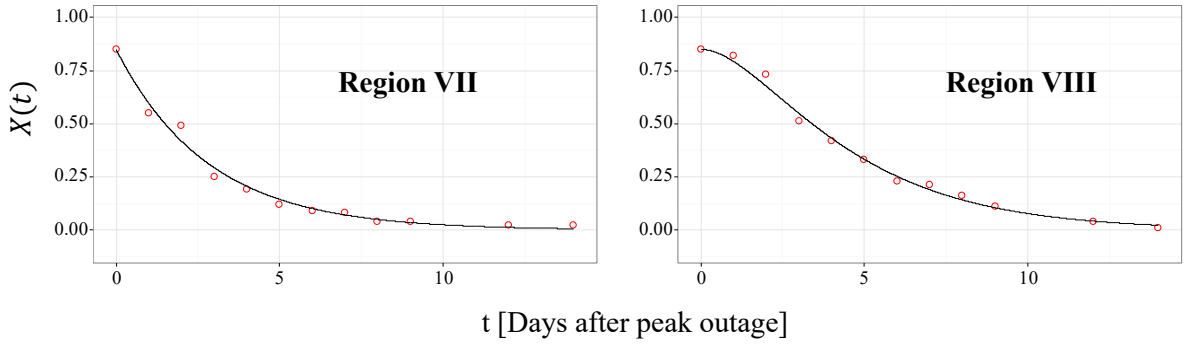

Figure 3.20: Fitted mobile phone service recovery curve $X(t)$ of each region for the 2010 Chile Earthquake.

Table 3.11: Least-square fitting result for 2010 Chile Earthquake fixed phone dataset using SDOF model.

Region	ω	ζ	R^2	X_0	$\dot{X}_0$
Region VII	2.643	3.065	0.961	0.750	-4.392
Region VIII	2.236	2.258	0.957	0.8	0

3.3 Discussion

The application of mathematical models to data for various regions employs geographical data implicitly; that is, the data sets are derived at certain scales. In investigating the input-output models, it became apparent that geospatial analysis to identify fragilities could be extended using hazard records and simulations. The representation of the hazard demand at the same scale as the infrastructure capacity or operability is possible with improved measurements provided post-event by geoscientists. The geospatial modeling also has implications for network model construction. The derivation of fragilities is explored in the next chapter.

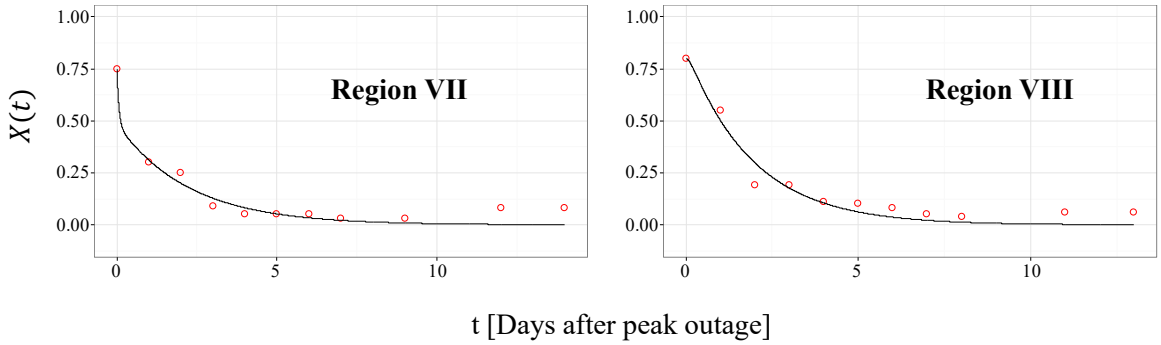

Figure 3.21: Fitted fixed phone service recovery curve $X(t)$ of each region for the 2010 Chile Earthquake.

3.4 Summary

Mathematical models of infrastructure behavior using reliability, robustness and resilience metrics were derived and applied to in-situ post-event power delivery and other infrastructure damage data. The models provide predictive capabilities for typical US distribution and transmission systems, and these predictions are helpful to decision makers such as public officials and emergency managers, as well as infrastructure operators.

Chapter 4

FRAGILITY MODELS

4.1 Overview of fragility models

Fragility curves are used extensively in seismic risk analysis to provide assessment and prediction of damage of certain structures, e.g. bridges, buildings, highways. Gardoni et al. [93] defined fragility as the conditional probability of attaining or exceeding a specified damage state for a given set of input variables. In earthquake engineering, the input variables are usually measure of ground motion intensity. Park et al. [34] used fragility curves to assess the performance of an urban electric utility distribution system for the 2001 Nisqually earthquake. Kaynia et al. [94] classified the methodology of developing fragility curves in seismic engineering into four groups, i.e. empirical curves, expert opinion-based curves, analytical curves, and hybrid curves. Among them, empirical curves and analytical curves are widely used and discussed in the literatures. Empirical fragility curves relies on data collected from actual events, therefore limiting the application of the curves. Analytical curves use numerical simulation methods to generate loading conditions and can cover a wider range compared to empirical curves, which is limited by the available data points, but simulation results cannot always represent the actual events.

Traditionally, a lognormal distribution function is assumed to derive an empirical fragility curve. Damage data from the disruptive event, e.g. a earthquake, must be obtained to establish the relationship between input variables and damage state. Let $F(\bullet)$ denote the fragility curve for a given damage state, and H be the loading variable. Then $F(H)$ is the probability of reaching or exceeding the given damage state when the loading equals to H.

Using lognormal distribution function, the form of fragility function is given by:

$$P(\text{reaching or exceeding a damage state}|H) = F(H) = \Phi\left[\frac{\ln\left(\frac{H}{c_F}\right)}{\sigma_F}\right], \qquad (4.1)$$

where $\Phi(\bullet)$ is the standard normal distribution; $c_{\mathcal{F}}$ and $\sigma_{\mathcal{F}}$ are the median and log-standard deviation of the fragility curves, which can be estimated using maximum likelihood method [95].

Many representations of structural fragilities of the form in Equation 4.1 exist for different types of building constructions, e.g. [8, 96–98]. One of the disadvantages of using the lognormal approach for modeling fragilities is the inability to capture the influence of more than one hazard simultaneously. Some investigators have tried to circumvent this problem by implementing hazard parameters that incorporate more than one variable. For example, for seismic fragilities, the Japanese Meteorological Agency (JMA) intensity scale or the instrumental Modified Mercalli Index [I_{mm}] have been used [34]. The integrated kinetic energy [IKE] metric created by Powell and Reinhold [99] includes a combination of different aspects of the wind and storm surge potential, but it is challenging to use in predictions. For example, two IKE data points are presently available from RMS HWind [100] on a daily basis for storms; however, the time scale is too long for use in estimating the level of structural damage required for fragility models. Due to the limitations of the lognormal approach described in Equation 4.1, research in the use of logit transformations for seismic and wind hazards has been undertaken, e.g. [34, 101–103]. These research investigations were focused on individual hazards or damaged structures, such as bridges, and the use of empirical data was limited. In the next section, the modeling of fragilities through logit transformations is presented before application to post-event in-situ analysis for lifeline system is presented. The methodologies and results presented in this chapter have been discussed in [104].

4.2 Logit transformation and logistic regression models

4.2.1 Structural damage due to single hazard

Logistic regression can also be used to develop fragility curves as presented in [34] and it is better suited for constructing fragilities for two or more loadings. An example of fragility curve generated by logistic regression is shown in Figure 4.1. The curve gives the maximum fraction of customers without power for a specified wind speed for Hurricane Isaac in Louisiana State. The fragility curve takes the form of logistic response function:

$$P(\text{reaching or equal to a damage state}|H) = F(H) = \frac{\exp(\beta_0 + \beta_1 H)}{1 + \exp(\beta_0 + \beta_1 H)} = \pi(H), \quad (4.2)$$

where β_0 and β_1 are parameters of the logistic regression model. The logit transformation of F is given by:

$$y(H) = \ln\left[\frac{F(H)}{1 - F(H)}\right] = \beta_0 + \beta_1 H. \quad (4.3)$$

In the example shown in Figure 4.1, the loading H is the maximum H*Wind speed, and the damage state is a binary variable defined as,

$$\Im = \begin{cases} 1 & 100\% \text{ of customers without power} \\ 0 & 0\% \text{ of customers without power,} \end{cases} \quad (4.4)$$

with a probability mass function,

$$\begin{cases} P(\Im = 1) = \pi \\ P(\Im = 0) = 1 - \pi. \end{cases} \quad (4.5)$$

The maximum fraction of customers without power is used here as a simple estimation of π.

Analytical method of constructing fragility curves is discussed in [105, 106]. Monte Carlo simulation is often used to develop analytical fragility curves. Since the damage state of system after disruptive events relates to the system reliability, Gardoni et al. [93] proposed an approach of using reliability analysis, especially the stress-strength interference theory to construct fragility curves, which links the concept of reliability and fragility.

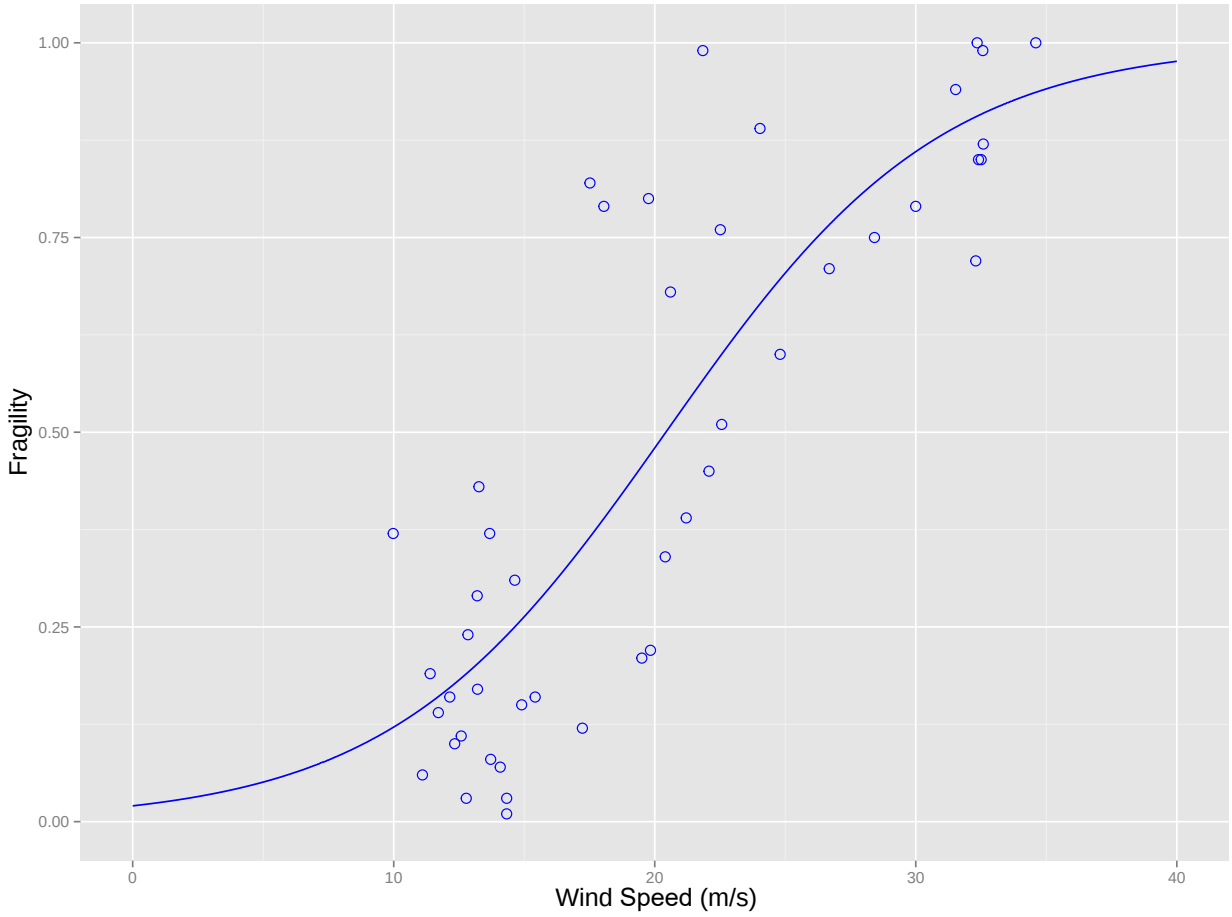

Figure 4.1: Fragility curve of electrical power delivery for Hurricane Isaac's maximum wind speed for each parish (derived from H*Wind data [100]).

Equation 4.3 is for one hazard variable H only. When using this format, typically, the parameter β_0 is referred to as the "intercept" and β_1 as the "coefficient". The ratio of π to $(1-\pi)$ is sometimes referred to as the "odds ratio". The advantage to using the logit model is that the function F is transformed to a linear function y, which is easier to fit to actual data. It is noted that for the two parameter F, the β_0 parameter dictates the placement along the hazard variable axis, whereas the β_1 parameter controls the slope of the so-called "S" curve. Logistic transformation and regression models for fragilities have been used successfully in the earthquake community for evaluating fragilities of buildings, bridges and lifeline systems for single hazard metrics, e.g. [34, 103]. Lallemant et al. [107] note that lognormal and logit transformation models result in very similar curves but that logistic regression has the advantage of being easy to understand in that the estimated model coefficients represent the log of the odds ratio of damage due to a unit increase in the independent variable.

4.2.2 Structural damage due to multiple hazards

Distinct hazards generated simultaneously from a single event (e.g. hurricane) cause single and joint hazard damage and failure to structures and infrastructure. Modeling the effects of multiple hazards requires representation of hazard and hazard-structure interactions, as well as the cascading nature of hazard-induced damage [108, 109]. The interaction of multiple hazards is widely believed to cause damage conditions that differ from the aggregation of single-hazard damage [110, 111]. Therefore, statistical methods, which represent system-level response, are appropriate to represent infrastructure response to a range of multiple hazard conditions.

Equation 4.3 can be modified to include the influence of more than one hazard. Hazards may be considered separately as given in equation 4.6

$$\text{Linear model} : y = \beta_0 + \beta_1 H_1 + \ldots + \beta_m H_m \tag{4.6}$$

Here "y" represents the dependent variable of fragility; H_i represents the hazard variables;

and β_i are the fitted coefficients.

The linear model shown in equation 4.6 has been applied by Koutsourelakis [102] for geotechnical systems subject to earthquake hazards, where the hazard variables were the peak ground acceleration, and the root-mean-square intensity and the Arias intensity, which were calculated based upon the ground acceleration time history. The structure was modeled simplistically as located on a rigid foundation atop a deep sand deposit. It was concluded that including all three seismic hazard parameters provided a superior representation of the fragility function.

Gehl et al. [112] developed fragility functions with uncorrelated and correlated seismic intensity metrics for buildings. A simple unreinforced masonry structure was used in numerical simulations to provide examples of fragility functions. In each formulation, two intensity metrics were used for the two damage states of "yield" and "collapse" respectively. The use of two hazard parameters was found to be superior to a single-value hazard based fragility function.

In the companion papers [113, 114], fragility functions for aging highway bridge networks were modeled using both seismic loading variables and material deterioration effects as hazards. The material deterioration parameters were based on data derived from instrumented bridges and included surface chloride concentration, chloride diffusion coefficient and corrosion rate. The highway bridge network was modeled with bridges represented as nodes and roads represented as the connecting links. In [114], a fully parameterized fragility function with seven independent variables was derived. Only one of these variables was a seismic hazard intensity measure. Monte Carlo simulations were used to derive the fragilities employed for the bridges and highway networks.

Kameshwar and Padgett [113] derived fragility functions for bridges located in Charleston, South Carolina, subject to earthquake and hurricane hazards, respectively. Comparisons between earthquake and hurricane fragilities were made on the basis of numerical simulations. The models provided insight into the relative influence of each hazard parameter upon bridge risk.

Mardfekri and Gardoni [115] developed a probabilistic framework for the structural performance of offshore wind turbines subject to both wind and seismic loadings. The hazard data were modeled using extreme value seismic and wind load probability distributions at specific site locations. Annual probabilities of being in any specified damage state for the wind turbine at any particular location using the total probability rule were evaluated.

In all cases, fragilities were derived from numerical simulations. For network fragilities, the component fragilities of networks were determined and combined according to a network modeling approach. The ability of logistic models to characterize system response has been demonstrated, but the application of logistic models has been mostly for seismic hazards and the influence of material aging and deterioration of concrete bridges. Although correlations between seismic parameters were discussed by Koutsourelakis [102], interactions among the hazard variables were not directly modeled logistically; that is, products of hazard variables were not directly employed in the models.

Equation 4.7 provides the so-called interaction terms; it contains the linear model of equation 4.6 combined with a weighted sum of hazard product terms such as "$H_j H_k$":

$$\text{Interaction model} : y = \beta_0 + \beta_1 H_1 + \beta_2 H_2 + \ldots + \beta_m H_m + \sum_{1 \le j \ne k \le m}^{m} \beta_{jk} H_j H_k \qquad (4.7)$$

It is noted that the more hazard parameters considered, the more data are required for appropriate fitting; however, it is also anticipated that as data collections amass online each year, the data required for model fitting will be readily available in the near future. In the next section, interaction models will be presented for the hurricane hazards of storm surge, wind speed and rainfall using post-event in-situ hazard and damage data.

4.3 Application to electric power system for multiple hazards

Electric power is generated, transmitted and then fed through distribution network systems to buildings and other structural systems. Voltage drops occur at substations. Industrial or commercial facilities may have their own substations. Distribution lines may be located

underground or overhead. For seismic loadings, substations are the most vulnerable structural components of the system [116]. For hurricanes, the towers and poles that comprise the lines feeding power to facilities are more vulnerable than the substations, especially in heavily wooded regions. If substations fail in hurricanes or other storms, it is due to flooding caused by excessive rainfall or storm surge, or through damaging wind-borne debris. Design guides and standards are available for the various structural components of the power grid, e.g. [17–20]. These guides may be implemented at a component level to assess the structural fragility as a "stand-alone" element of the network itself.

Seismic-based fragilities for the electric power delivery system have been investigated in greater detail than for wind-induced failures. In particular, the FEMA-based Multi-hazard Loss Estimation Methodology HAZUS-MH program [74] provides users with loss estimates based upon five possible structural damage states for generation facilities, substations and distribution circuits subject to seismic hazards. The hazards are characterized by peak ground acceleration. It is noted that HAZUS runs on ArcGIS software platforms, so geocoding of the hazard data has been undertaken.

Park et al. [34] investigated the failure of an urban power delivery system through the use of the geographical information system (GIS) based power distribution grid overlaid with actual seismic intensities for the Nisqually earthquake of 2001. A thorough analysis of damage due to earthquake hazards in the region, yielded a lifeline fragility based upon the damage index, defined as the "length of a line damaged relative to the total length of a power line". It is noted that substation damage was not significant for the Nisqually earthquake. It was found that the damage index was equivalent to the total number of customer outages divided by the total number of customers at the neighborhood or county level. The importance of this result is that the number of outages is associated with the distribution system, which affects customers directly, and usually power companies supply these data for every earthquake or storm. In the US, the power grid is more vulnerable to storm events, whether these are winter storms or hurricanes, than earthquakes. Indeed, almost every hurricane season in the US produces remarkable outages in the Gulf of Mexico

region. Recent Atlantic storms such as Sandy have wreaked havoc on the power grid in the northeastern US [117].

Formulations of the lifeline fragilities have been modified in recent years to characterize the loss of service through a fragility function, as opposed to a structural variable. In the case of electric power delivery, the "damage" variable of interest as used in this investigation was the inoperability $X(t)$, or inability to provide service. The maximum fraction of customers without power at time t, is denoted by X_{max}, where $X_{max} = \max\{X(t), \text{for all } t\}$. In this section, the results of logit models described in equations 4.3, 4.6 and 4.7 fit to data collected for Hurricane Isaac and Sandy will be provided as a proof of concept in the approach. First, the data employed in the analysis are described and the limitations and caveats discussed. Then the model results are presented.

4.3.1 Data used for the fragility analysis

4.3.1.1 Hurricane Isaac

Hurricane Isaac made first landfall at Southwest Pass in Louisiana on August 29, 2012 at 00:00 UTC with maximum sustained winds of 36 m/s (70 kt) [118]. According to Berg [118], the storm center moved back over water and then made second landfall west of Port Fourchon, Louisiana, later on August 29, 2012 at 08:00 UTC. The meteorological data of wind speed, inundation levels due to storm surge, and rainfall were cataloged for locations within the State of Louisiana. The description and sources of data are presented in Table 4.1.

There are limitations regarding the collected data. First, all of the hazards are uncertain random variables. Second, the geo-coded power grid was not available for overlay due to security reasons, so the damage data consisted of power delivery data per parish (county) obtained in spreadsheet format from the Louisiana Public Service Commission (LPSC) [121]. These data are not exact representations of damage, but close approximations, as noted previously. The LPSC provided outage time series data per parish as well as per utility or

Table 4.1: Hazard Data Employed in the Isaac Analysis.

Data	Description	Source
Wind Speed [m/s]	H*Wind: Maximum sustained wind speed swaths for Hurricane Isaac for the State of Louisiana.	RMS HWind† [100]
Inundation due to Storm Surge [m]	Depth of water above local land elevation as determined for storm surge using hindcasting.	Coastal Emergency Risks Assessment (CERA) [119]
Rainfall [mm]	Observed daily precipitation for the duration of the storm.	National Weather Service, Advanced Hydrologic Predictive Service [120]
† Note: The Hurricane Research Division of the National Oceanic & Atmospheric Administration produced surface wind analysis of tropical cyclones from 1993 - 2013 as part of the H*Wind Project. In 2014 this activity was transferred to RMS HWind, a US private sector firm. The images and data sets formerly available on the Hurricane Research Division website are now publicly available on the RMS HWind website.		

company at approximately half hour intervals from August 28 to September 7, 2012. The $X(t)$ function per parish, from which the peak X_{max} values were derived, has been studied in detail, e.g. [10, 32]. The X_{max} data were geo-coded and then overlaid with hazard data using ArcGIS software [14]. Figure 4.2 illustrates the ratio of peak customer outages to the total number of customers X_{max} per parish (county) in the State of Louisiana for Isaac. It

can be seen that the percentages vary widely over the range of zero to one hundred. Figure 4.3 shows a map of the peak outages per parish. Although outage, wind speed and rainfall data were available for 64 parishes, only 20 were affected by storm surge. Therefore, the data set for the fragilities focused on the 20 parishes affected by all three hazards.

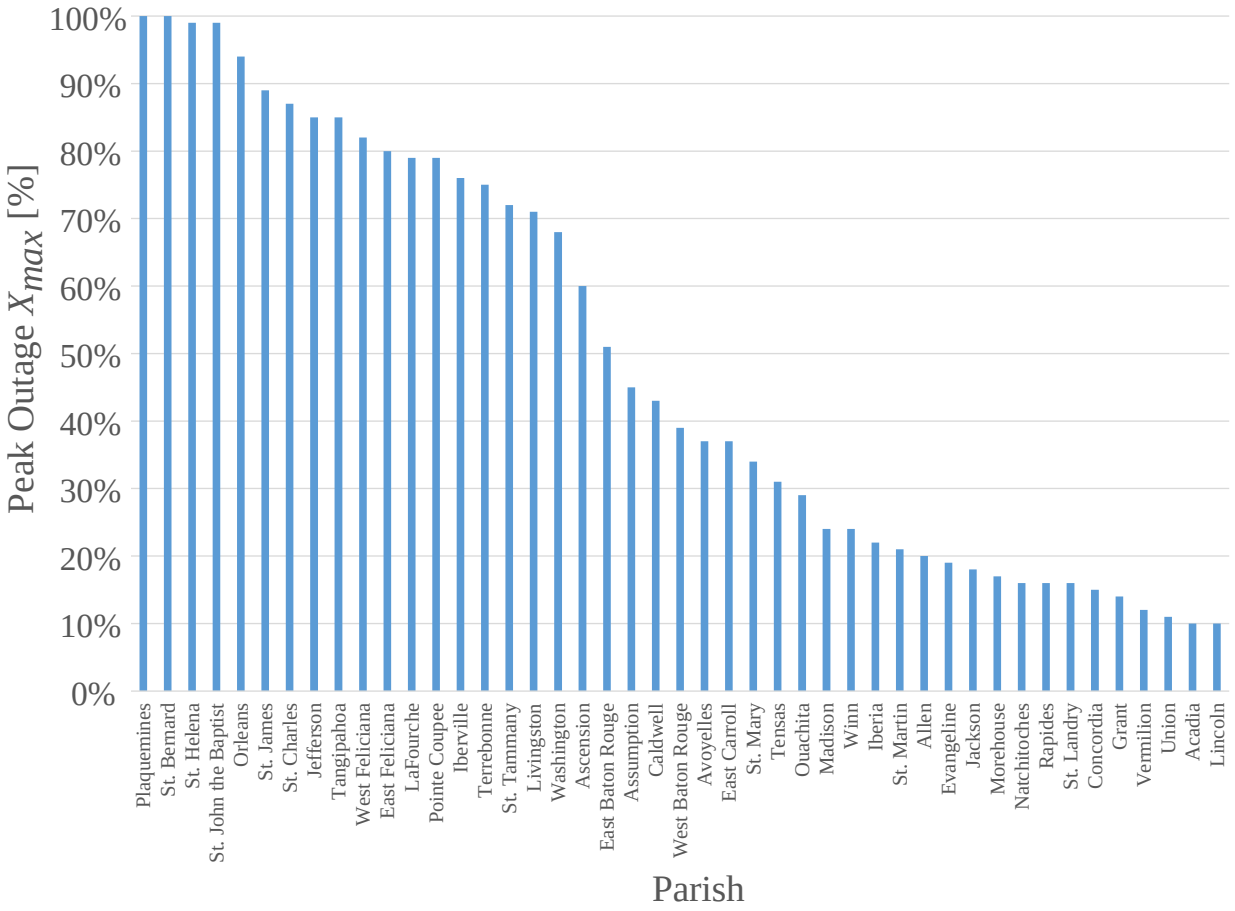

Figure 4.2: Peak outages X_{max} in percent per parish (county) in the State of Louisiana for Isaac (parishes with X_{max} less than 10% are not displayed).

4.3.1.2 Hurricane Sandy

Hurricane Sandy made landfall near Brigantine, New Jersey, to the northeast of Atlantic City, on October 29, 2012 at approximately 23:30 UTC [122]. It was categorized as a post-

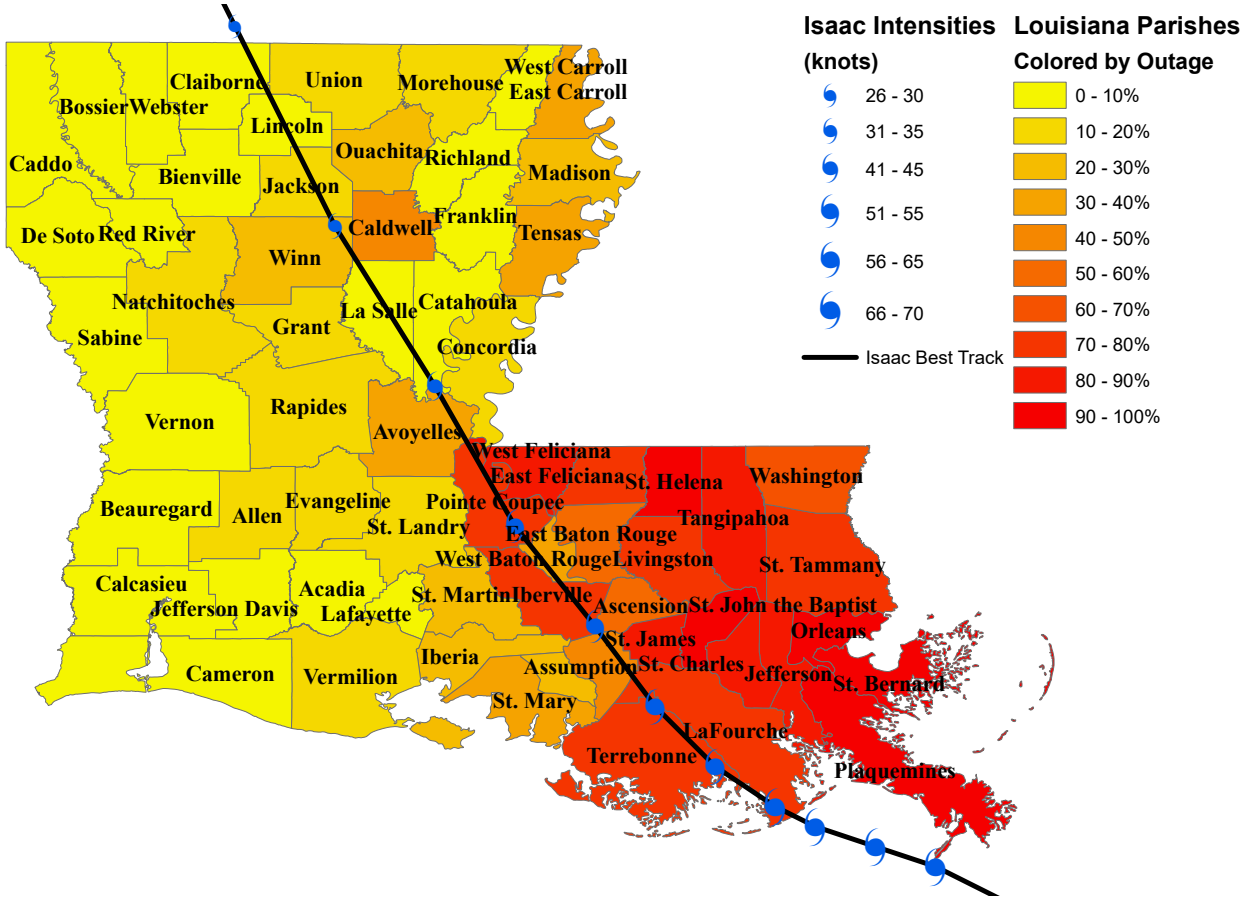

Figure 4.3: Map of peak power outages per parish in the State of Louisiana for Isaac overlaid with Hurricane Isaac Best Track
(Source: Parish boundary data provided by PennWell MAPSearch; Isaac Best Track and Intensities data provided by National Hurricane Center of National Oceanic and Atmospheric Administration (NOAA)).

tropical cyclone with an estimated intensity of 36 m/s [70 kt] and a minimum pressure of 945 mb [122]. The specifics of the hazard data are given in Table 4.2.

The limitations regarding the Isaac data also apply for Hurricane Sandy: all hazards are uncertain random variables and outage data were collected by Consolidated Edison (ConEd) employees and reported to the New York State Public Service Commission (NYSPSC). Specifically, NYSPSC provided electric power outage time series data per locality at approximately half hour intervals from October 29 to November 29, 2012 (some localities had

Table 4.2: Hazard Data Employed in the Sandy Analysis.

Data	Description	Source
Wind Speed [m/s]	H*Wind: Maximum sustained wind speed swaths for Hurricane Sandy for the New York City.	RMS HWind† [100]
Storm Surge Inundation [m]	Water surface elevation above local ground interpolated using High Water Marks (HWMs) and Storm Surge Sensor data from the United States Geological Survey (USGS)	Federal Emergency Management Agency (FEMA) Modeling Task Force (MOTF) [123]
Rainfall [mm]	Observed daily precipitation for the duration of the storm.	National Weather Service, Advanced Hydrologic Predictive Service [120]
† Note: The Hurricane Research Division of the National Oceanic & Atmospheric Administration produced surface wind analysis of tropical cyclones from 1993 - 2013 as part of the H*Wind Project. In 2014 this activity was transferred to RMS HWind, a US private sector firm. The images and data sets formerly available on the Hurricane Research Division website are now publicly available on the RMS HWind website.		

longer or shorter periods) in spreadsheet format. The term "locality" is similar to "neighborhood" and its boundaries are defined by ConEd, who supplies electric power to Manhattan.

It is noted that the spatial unit of "locality" is smaller than "parish" or "county" and the majority of the power lines in Manhattan are located underground. Figure 4.4 illustrates the ratio of peak customer outages to the total number of customers X_{max} per locality in Manhattan of the City of New York. The outage data were mostly zero or 100% for this data set. As with the Isaac data, the X_{max} data were geo-coded and then overlaid with hazard data using the ArcGIS software. Although outage data, rainfall and wind speed data were available for 32 localities in Manhattan, only 24 were affected by storm surge. Therefore, the data set for the fragilities focused on the 24 localities affected by all hazards. Figure 4.5 shows the localities of lower Manhattan that lost power during Hurricane Sandy. Also shown for reference is the location of ConEd's East 13th Street complex (including two transmission substations) near the intersection of East 13th Street and Avenue C.

4.3.2 Model analysis

4.3.2.1 Fitting methods

Classical fitting techniques for logistic regression are based on an odds ratio [124]; that is, for this case, the variable X_{max} would only take on values of zero and unity, rather than the fractional values derived from the outage data. The model fitting investigation showed that the fractional values provided a superior fit to those for the binary X_{max} variable. The software environment *R* [125] and 'arm' package [126] were used to fit the models.

The Maximum Likelihood Estimation (MLE) approach was used to estimate fragility model parameters by maximizing the likelihood function in equation 4.8, where Θ^{OPT} are the optimal estimated parameters that maximize the likelihood function, $f(i)$ is the probability density function of variables with parameters θ, and $\prod_{i=1}^{n} f(y_i, X_i; \theta)$ is the likelihood function. The Akaike Information Criterion (AIC) was used to select the best fitted model. AIC provides an indication of the goodness of fit for the statistical model to the observed data. The AIC (equation 4.9) adjusts the log-likelihood function (equation 4.10) for the affected number of parameters (K), where $\prod_{i=1}^{n} f(y_i, X_i; \theta)$ is the likelihood function, and

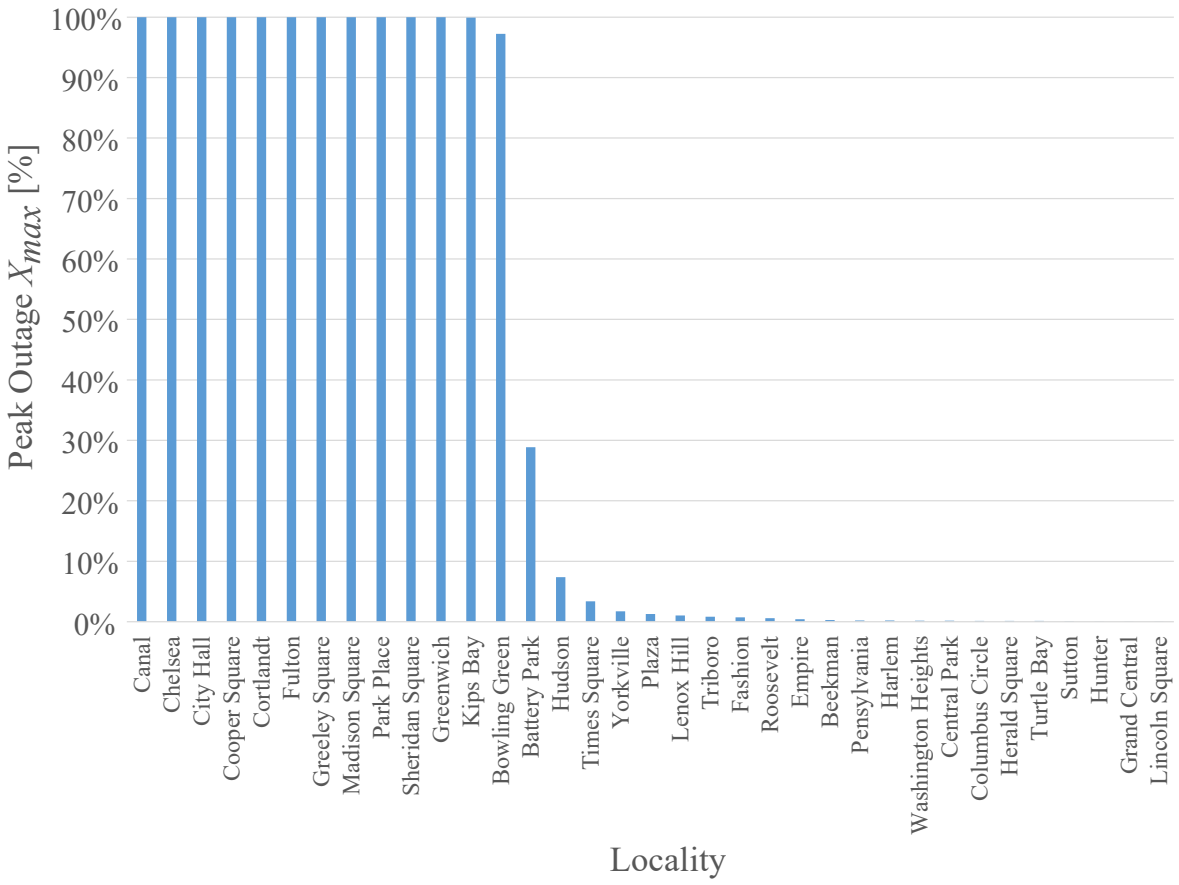

Figure 4.4: Peak outages X_{max} in percent per locality in Manhattan of the City of New York for Hurricane Sandy.

$f(i)$ is the probability density function of variables with parameters θ.

$$\Theta^{\mathrm{OPT}} = \arg\max \left[\prod_{i=1}^{n} f\left(y_i, X_i; \theta\right) \right] \tag{4.8}$$

$$\mathrm{AIC} = -2\left(\mathcal{L}\left(\theta|x\right)\right) + 2K \tag{4.9}$$

$$\mathcal{L}\left(\theta|x\right) = \log\left(\prod_{i=1}^{n} f\left(y_i, X_i; \theta\right) \right) \tag{4.10}$$

Figure 4.5: Locality map for lower Manhattan of the City of New York (Source of Imagery Basemap: Esri, DigitalGlobe, GeoEye, Earthstar Geographics, CNES/Airbus DS, USDA, USGS, AEX, Getmapping, Aerogrid, IGN, IGP, swisstopo, and the GIS User Community).

The best fitted model of a group of models fit to the same data set should have the smallest AIC value. The symbol Δ_i is defined as "the difference of AIC value between the ith model and the best fitted model"[127]. The strategy developed by Burnham and Anderson [127] was used to compare the goodness of fit of multiple models of a given sample set (Table 4.3). The larger the Δ_i, the less plausible it is that the fitted model is the best model. As seen in Table 4.3, models with $\Delta_i > 10$ are considered inappropriate.

Table 4.3: Interpretation of AIC difference Δ_i [127].

Δ_i	Level of Empirical Support of Model i
$0 \sim 2$	Substantial
$4 \sim 7$	Considerably less
> 10	Essentially none

4.3.2.2 Results

The logistic regression results for Hurricane Isaac using the peak outage X_{max} as a direct response variable are summarized in Table 4.4 for the sample size of $N = 20$ data points as described in section 4.3.1.1.

Table 4.4 contains the fitted model parameters for the single hazard linear models, two hazard linear models, a three hazard linear model, two hazard models with interactions and finally, a three hazard model with multiple interactions. The significance of the fitted coefficients is provided through the p-values. The probability value (p-value) of a hypothesis test is the probability of obtaining a value of the test statistic as extreme, or more extreme, than the one observed, if the null hypothesis is true. The models are ranked in each category by the smallest to largest AIC values. Although the three hazard model with multiple interactions provides the overall lowest AIC value of 374.91, not all of the coefficients are significant. The two hazard linear model with rainfall and wind speed (AIC = 398.40) is su-

perior to models for either rainfall or wind speed alone (AIC = 428.49, 462.68, respectively). Figure 4.6 shows the 3-D surface for this particular model. The equation of the 3-D surface has the form as in equation 4.11:

$$F\left(X_{max}|H_1, H_2\right) = \frac{\exp(-5.024 + 0.005H_1 + 0.158H_2)}{1 + \exp(-5.024 + 0.005H_1 + 0.158H_2)} \tag{4.11}$$

where H_1 and H_2 denote the rainfall [mm] and wind speed [m/s] hazard variables respectively.

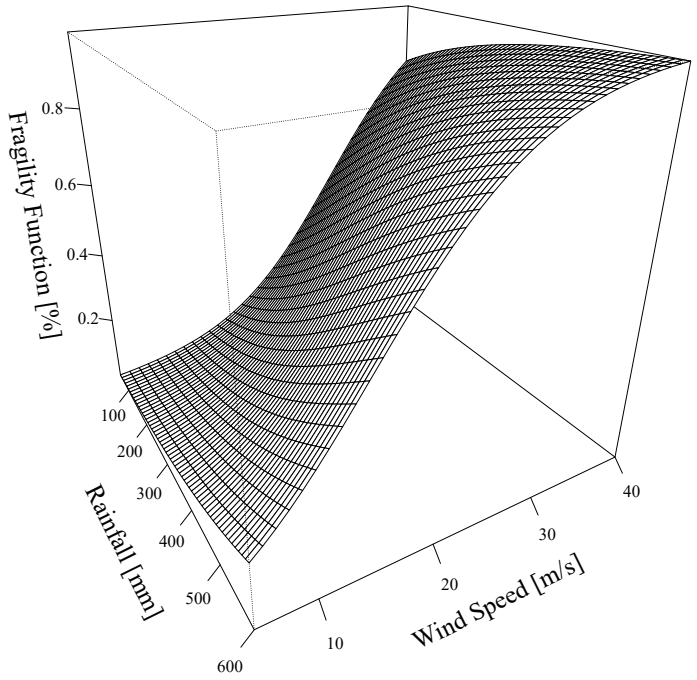

Figure 4.6: 3D surface for two hazard linear model with rainfall and wind speed for Isaac.

Table 4.4: Hurricane Isaac Fragility Fit Results

‡ Significance code for the p-value Column: between 0 ∼ 0.01 ***; 0.01 ∼ 0.05 **; 0.05 ∼ 0.1 *					
Model Variables	**Coefficients**	**Estimate**	**Standard Error**	**‡p-value**	**AIC**
Single Hazard Linear Model Results *listed in order of lowest AIC*					
$X_{max} \sim$ Wind [m/s]	Intercept β_0	-5.748	0.267	<2e-16***	428.49
	Wind [m/s]	0.248	0.011	<2e-16***	
$X_{max} \sim$ Rainfall [mm]	Intercept β_0	-3.206	0.159	<2e-16***	462.68
	Rainfall [mm]	0.011	0.0004	<2e-16***	
$X_{max} \sim$ Inundation [m]	Intercept β_0	-2.165	0.121	<2e-16***	477.38
	Inundation [m]	1.119	0.049	<2e-16***	
Two Hazard Linear Model Results *listed in order of lowest AIC*					
$X_{max} \sim$ Rainfall [mm] + Wind [m/s]	Intercept β_0	-5.024	0.291	<2e-16***	398.40
	Rainfall [mm]	0.005	0.001	1.69e-07***	
	Wind [m/s]	0.158	0.019	3.31e-16***	
$X_{max} \sim$ Inundation [m] + Wind [m/s]	Intercept β_0	-4.681	0.356	<2e-16***	413.06
	Inundation [m]	0.399	0.096	3.07e-15***	
	Wind [m/s]	0.168	0.021	3.05e-15***	
$X_{max} \sim$ Inundation [m] + Rainfall [mm]	Intercept β_0	-2.796	0.186	<2e-16***	452.99

	Inundation [m]	0.520	0.133	9.26e-05***	
	Rainfall [mm]	0.006	0.001	3.11e-06***	
Three Hazard Linear Model Result					
$X_{max} \sim$ Inundation [m]+Rainfall [mm]+Wind [m/s]	Intercept β_0	-4.956	0.371	<2e-16***	400.71
	Inundation [m]	0.043	0.146	0.767	
	Rainfall [mm]	0.004	0.001	0.001***	
	Wind [m/s]	0.156	0.022	6.31e-13***	
Two Hazard Model with Interactions Results *listed in order of lowest AIC*					
$X_{max} \sim$ Rainfall [mm] + Wind [m/s] + (Rainfall × Wind)	Intercept β_0	-5.526	0.707	5.40e-15***	398.54
	Rainfall [mm]	0.007	0.003	0.0093***	
	Wind [m/s]	0.179	0.033	9.33e-08***	
	Rainfall × Wind	-7.75e-05	9.42e-05	0.4111	
$X_{max} \sim$ Inundation [m] + Wind [m/s] + (Inundation × Wind)	Intercept β_0	-5.018	0.520	<2e-16***	412.78
	Inundation [m]	0.682	0.284	0.0162***	
	Wind [m/s]	0.179	0.026	2.38e-12***	
	Inundation × Wind	-0.009	0.009	0.310	
$X_{max} \sim$ Inundation [m] + Rainfall [mm] + (Inundation × Rainfall)	Intercept β_0	-3.359	0.296	<2e-16***	447.82
	Inundation [m]	0.976	0.216	6.33e-06***	
	Rainfall [mm]	0.008	0.001	2.04e-07***	

	Inundation × Rainfall	-0.001	0.000	0.00926***	
Three Hazard Model with Multiple Interactions Result					
$X_{max} \sim$ Inundation [m] + Rainfall [mm] + Wind [m/s] + (Inundation × Rainfall) + (Inundation × Wind) + (Rainfall × Wind) + (Inundation × Rainfall × Wind)	Intercept β_0	-11.140	1.430	6.84e-15***	374.91
	Inundation [m]	0.040	0.423	0.925	
	Rainfall [mm]	0.042	0.009	2.55e-06***	
	Wind [m/s]	0.413	0.065	2.32e-10***	
	Inundation × Rainfall	-0.006	0.002	0.0061***	
	Inundation × Wind	-0.004	0.014	0.7942	
	Rainfall × Wind	-0.001	3.16e-04	3.85e-06***	
	Inundation × Rainfall × Wind	2.44e-04	6.81e-05	0.0003***	

Adding an interaction term to the two hazard linear model with rainfall and wind speed does not significantly decrease the AIC value (398.40 versus 398.54). The three hazard linear model with AIC of 400.71, which is close to 398.40, does not have a storm surge inundation coefficient value that is significant. In summary, the results suggest that the multiple hazard fragilities are better than the single hazard fragility representation, which confirms anecdotal observations regarding combined wind plus rain and surge damage, versus each alone. The lack of significance for the coefficients of the three hazard models with interactions may be due in part to the small data set.

In order to test the logistic model for an electric power delivery fragility in another region of the country, the Sandy data for the localities of Manhattan in the City of New York were used. As noted previously, the spatial resolution for this storm was much smaller than for Isaac. Because the majority of the power infrastructure was located underground, the three hazard model including wind speed was not a good fit.

The maximum storm surge and rainfall variables are reported here for Sandy, as shown in Table 4.5. The two hazard model results were superior to the single hazard models, which confirms the importance of multiple hazards on lifeline fragility. The interaction term did not appear to add much to the model fit and the coefficients were not as significant. In summary, the fragility based on combined storm surge inundation and rainfall hazards was the best model for Manhattan. Figure 4.7 illustrates this fragility model. The equation of the 3-D surface has the form as in equation 4.12:

$$F\left(X_{max}|H_1, H_3\right) = \frac{\exp(-51.372 + 1.399H_1 + 1.394H_3)}{1 + \exp(-51.372 + 1.399H_1 + 1.394H_3)} \tag{4.12}$$

where H_1 and H_3 denote the rainfall [mm] and storm surge inundation [m] hazard variables respectively.

This result confirms observations that the bulk of the power grid in lower Manhattan is underground, with the exception of two power substations near the East River at East 13$^{\text{th}}$ Street. Post-event surveys showed that wind speed effects were significant in Westchester County where overhead lines were more prominent.

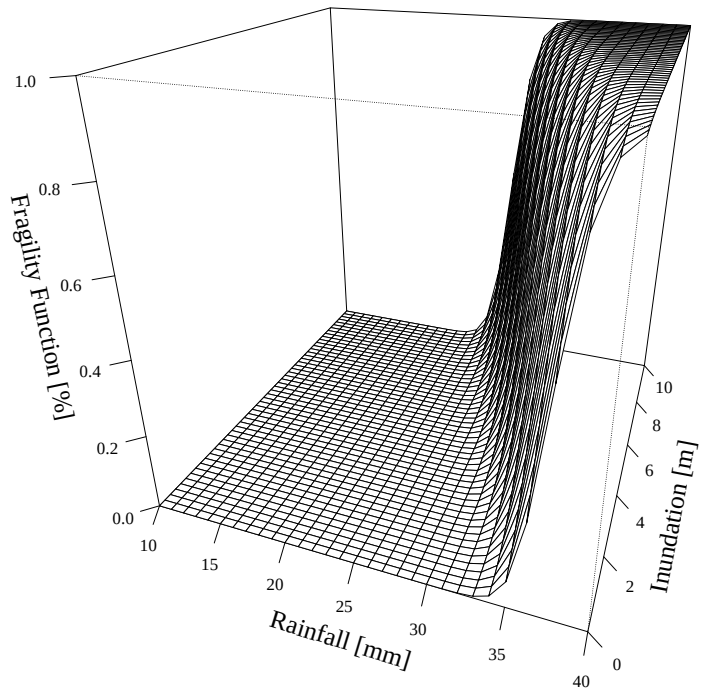

Figure 4.7: 3D surface for two hazard linear model with rainfall and storm surge for Sandy.

Table 4.5: Hurricane Sandy Fragility Fit Results for Manhattan Localities Only

‡ Significance code for the p-value Column: between 0 ∼ 0.01 ***; 0.01 ∼ 0.05 **; 0.05 ∼ 0.1 *					
Model Variables	**Coefficients**	**Estimate**	**Standard Error**	**‡p-value**	**AIC**
Single Hazard Linear Model Results *listed in order of lowest AIC*					
$X_{max} \sim$ Rainfall [mm]	Intercept β_0	-45.346	2.504	<2e-16***	1693.30
	Rainfall [mm]	1.410	0.0770	<2e-16***	
$X_{max} \sim$ Inundation [m]	Intercept β_0	-8.770	0.417	<2e-16***	2438.40
	Inundation [m]	1.880	0.088	<2e-16***	
Two Hazard Linear Model Results: With and Without Interaction					
$X_{max} \sim$ Inundation [m] + Rainfall [mm]	Intercept β_0	-51.372	2.667	<2e-16***	1353.10
	Inundation [m]	1.394	0.096	<2e-16***	
	Rainfall [mm]	1.399	0.079	<2e-16***	
$X_{max} \sim$ Inundation [m] + Rainfall [mm] + Inundation × Rainfall	Intercept β_0	-42.982	7.244	<2.96e-09***	1357.30
	Inundation [m]	-0.251	1.378	0.855	
	Rainfall [mm]	1.138	0.224	3.84e-07***	
	Inundation × Rainfall	0.051	0.043	0.232	

4.3.3 Discussion

The characterization of lifeline fragilities using multiple hazards, including hazard interactions, is an attractive alternative to lognormal single hazard models. The degree to which this additional characterization is useful may only be apparent after the damage due to multiple storms has been analyzed. However, the fragility function is only one facet of the performance-based design process [8, 98]. Ultimately, in order to evaluate the performance of the delivery system for storm hazards, the multivariate probability density of the hazards is required. The theory of total probability indicates that an integration of the product of the conditional probability $F(X_{max}|H = h)$ and marginal $f(h)$ or multivariate densities $f(h_i, h_j, \ldots)$ will yield a probability function. That is, the cumulative distribution function $F(X_{max})$ may be determined from the following integration if a multivariate model for n hazards is used,

$$F(X_{max}) = \iiint_{h_1,\ldots,h_n} F(X_{max}|h_1, \ldots, h_n)\, f(h_1, \ldots, h_n)\, dh_1 \ldots dh_n. \tag{4.13}$$

The representation of joint probability distributions for wind speed and storm surge data has been investigated recently, e.g. [128–130]. Pei et al. [128, 129] considered the joint occurrence of both hazards in a loss estimation scheme for Charleston County, South Carolina. They created a simulation approach that utilized over 50,000 years of synthetic hurricane data to model joint distributions numerically. Phan et al. [130] implemented a proof of concept investigation using bivariate Normal distributions. According to Johnson and Kotz [131] even if two variables are not Normal, their joint distribution may be Normal. However, one of the challenges in fitting the bivariate distribution of any type is the restriction of satisfying stability conditions for the functional form even if the marginal distributions do not completely specify the joint distribution, e.g.[131]. For a two hazard logit fragility model, the joint hazard distribution would be sufficient. For more complex three hazard fragilities, the multivariate hazard distribution would be required. For hurricane hazards, a form of a logistic hazard distribution $P_{H_1H_2H_3}$ is suggested as follows:

$$P_{H_1H_2H_3}(h_1, h_2, h_3) = \frac{1}{1 + e^{-\lambda_1 h_1} + e^{-\lambda_2 h_2} + e^{-\lambda_3 h_3} + \sum_{i,j,i\neq j}^{3} e^{-\lambda_{ij} h_i h_j}} \tag{4.14}$$

where H_1, H_2, and H_3 are defined as three random hazard variables; λ_1, λ_2, and λ_3 are coefficients.

It is noted that correlations among the hazard variables would need to be characterized for these distributions. However, a multivariate approach has yet to be fully explored for storm hazards. Whether the complexity of this model will provide the appropriate characterization remains to be seen.

In addition, the collection of data sets for modeling hazard and related damage will be essential. It is anticipated that predictive models of collected weather hazards will become available in the future from atmospheric scientists at the space and time scales necessary for engineering models.

4.3.4 Summary

The methodology developed in this section is useful to researchers, system owners, government agencies, insurance companies, and others who have access to large data sets describing system functionality during extreme events to facilitate generation of multi-hazard system-level fragility functions. The results of the case studies will be useful to practitioners evaluating system-level performance in Louisiana and New York. Most importantly, the methodology and results generated will be useful for multiple users who rely on loss functions for downstream analysis, including comparative risk assessment, overall system reliability and catastrophe models (e.g. used in the insurance industry).

In summary, logistic regression models have been used successfully to characterize fragilities for electric power delivery subject to hurricane hazards, where fragility is defined here as a conditional probability function. The system-level fragility models, while representing only single event scenarios, are based on geo-coded post-event in-situ hurricane weather hazard and power delivery system damage data rather than numerical simulations. Multiple simul-

taneous hazards of wind speed, rainfall and storm surge were used for the fragility model fits. This multi-hazard characterization property of the logit models is a distinct advantage over lognormal models. However, extensive GIS data are required for fitting the models. It is anticipated that continued investigations into the models presented here for other storms in the same geographical region will yield not only predictive capabilities, but also needed insight into the hurricane damage process. The characterization of the multivariate distributions of the simultaneous weather hazards will also improve damage predictions for hurricane prone regions.

Chapter 5

INTERDEPENDENCY AND INPUT-OUTPUT MODELS

5.1 General formulation

An advantageous property of the functional form of $X(t)$, as opposed to $Q(t)$, is its ability to be used in input-output models directly. Reed et al. [10] extended the input-output modeling work of Haimes and Jiang [66] to hurricane data in order to derive a proof-of-concept approach to determining interdependency metrics using physical damage data rather than economic data. The following model is used for the column vector $\mathbf{X}$ of n interdependent infrastructure systems as described in Figure 1.3 for a given hazard:

$$\mathbf{X} = \begin{bmatrix} X_1 \\ X_2 \\ X_3 \\ \vdots \\ X_n \end{bmatrix} = \mathbf{AX} + \mathbf{F}, \tag{5.1}$$

or

$$\mathbf{X} = [\mathbf{I} - \mathbf{A}]^{-1}\mathbf{F}, \tag{5.2}$$

where $\mathbf{I}$ is the identity matrix; $[\bullet]^{-1}$ is the inverse of the matrix; $\mathbf{A} = \begin{bmatrix} a_{11} & \cdots & a_{1n} \\ \vdots & \ddots & \vdots \\ a_{n1} & \cdots & a_{nn} \end{bmatrix}$ is the interdependency matrix with elements a_{ij} equals to the influence of lifeline j inoperability $[X_j(t)]$ on lifeline i inoperability $[X_i(t)]$. It is noted that elements a_{nn} are assumed to be

zeros, and elements a_{ij} are positive. The fragility vector $\mathbf{F}$ is given by

$$\mathbf{F} = \begin{bmatrix} f_1 \\ \vdots \\ f_n \end{bmatrix}, \tag{5.3}$$

where f_i is the fragility for subsystem or lifeline i.

For a two lifeline system, the interdependency representation is as follows:

$$\begin{aligned} \begin{bmatrix} X_1 \\ X_2 \end{bmatrix} &= \begin{bmatrix} a_{11} & a_{12} \\ a_{21} & a_{22} \end{bmatrix} \begin{bmatrix} X_1 \\ X_2 \end{bmatrix} + \begin{bmatrix} f_1 \\ f_2 \end{bmatrix} \\ &= \begin{bmatrix} 0 & a_{12} \\ a_{21} & 0 \end{bmatrix} \begin{bmatrix} X_1 \\ X_2 \end{bmatrix} + \begin{bmatrix} f_1 \\ f_2 \end{bmatrix}, \end{aligned} \tag{5.4}$$

which reduces to

$$X_1 = a_{12}X_2 + f_1, \tag{5.5}$$

and

$$X_2 = a_{21}X_1 + f_2. \tag{5.6}$$

In this model, coefficient a_{21} represents the influence of lifeline 1 inoperability upon lifeline 2 inoperability. It takes value from range $[0, 1]$. System-based fragilities may be determined as noted earlier.

5.2 Application to hurricane data

The characterization of the coefficients a_{ij} may be determined through linear regression. For example, if X_1 represents power delivery inoperability and X_2 represents telecommunications inoperability, respectively, then regression relationships between X_1 and X_2 will yield a_{21} if the recovery of power outages occurs prior to telecommunications, and it typically does for storms. Usually neither X_1 nor X_2 is linear, and the regression fit will not provide a high goodness of fit R^2 value because it only characterizes some of the fit to the recovery data; that is, only the recovery of X_2 dependent upon X_1 recovery is captured. Limited results

of the evaluation of the parameters of the **A** matrix derived from recovery data are given in Table 5.1. Figure 5.1 shows scatter plots of the electric power and telecommunication outage data with regression lines. Telecommunications data are the easiest to obtain for interdependency analysis. Preliminary results indicate that the interdependency is above 0.2 for telecommunications with power.

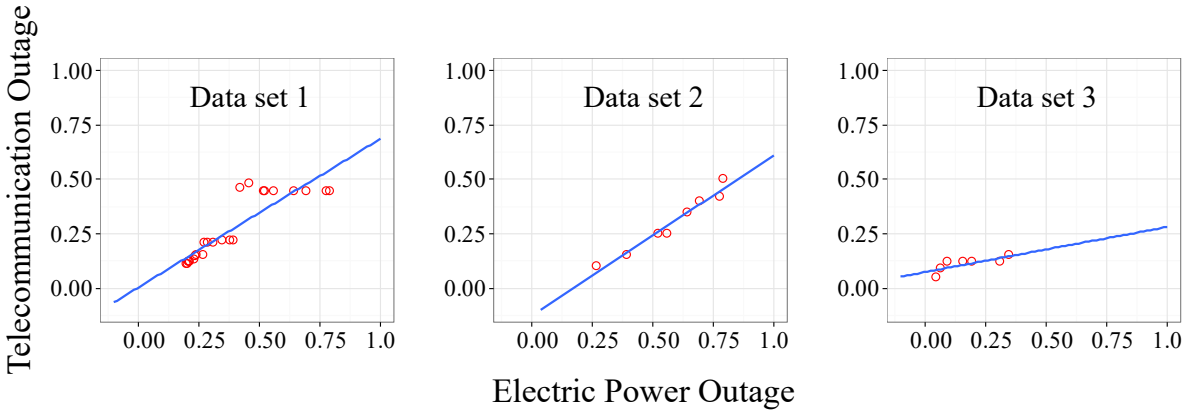

Figure 5.1: Scatter plots and linear regression lines for electric power and telecommunication outages using data sets presented in Table 5.1.

This approach to derive interdependency coefficients as part of a larger model framework differs significantly from the approach of Duenas-Osorio and Kwasinski [41] and others who apply correlation analyses to random variables describing recovery. Using the approach of Duenas-Osorio and Kwasinski, for the Hurricane Katrina data, it was found that at 7 time lags (in days), the correlation coefficient was 0.722 as shown in Figure 5.2. Although this approach provides the relative correlation between one system (power delivery) and another (telecommunications), it does not include enough information for predictive purposes, as does the input-output approach of Equations 5.1 to 5.4.

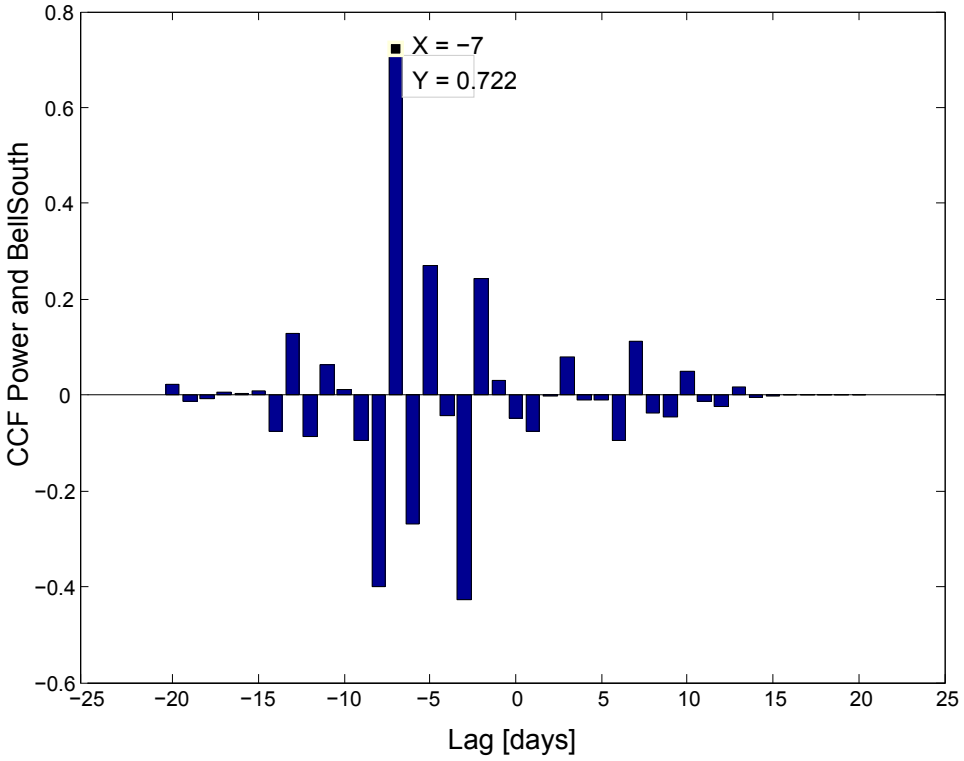

Figure 5.2: CCF function results for Hurricane Katrina for Louisiana.

Table 5.1: Elements of the **A** matrix for specific storms.

Data set	System 1	System 2	a_{21}	R^2
1. Hurricane Katrina: Louisiana outage data for power and telecommunication from LPSC	Power	Telecommunication (wired)	0.685	0.774
2. Hurricane Katrina: power outage data from LPSC and telecommunication data from O'Reilly et al. [132] for BellSouth for Louisiana, Alabama, and Mississippi	Power	Telecommunication (wired and wireless)	0.738	0.957
3. Hurricane Wilma: power outage data for Florida from the Department of Energy [85] and telecommunication data from O'Reilly et al. [132]	Power	Telecommunication (wired and wireless)	0.208	0.517

5.3 Application to earthquake data

Electric power and water supply outage data were obtained for the 2011 Japan Earthquake as previously discussed in Section 3.2.1.2. From Figures 3.9 and 3.10, it can be seen that water supply system sustained longer outage period than electric power system for most of the affected prefectures. The scatter plots of the electric power and water supply outage data with regression lines are shown in Figure 5.3. The regression results are presented in Table 5.2. The a_{21} values for most prefectures show weak interdependencies, which are below 0.1.

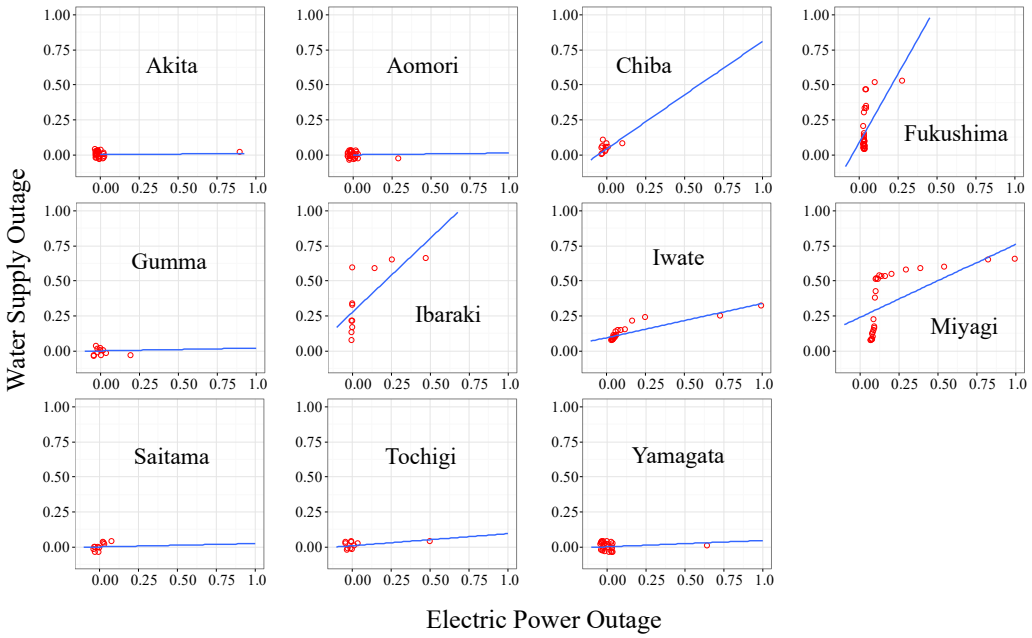

Figure 5.3: Scatter plots and linear regression lines for electric power and water supply outages after 2011 Japan Earthquake.

Table 5.2: Elements of the **A** matrix for power delivery and water supply system for 2011 Japan Earthquake.

Prefecture	a_{21}	R^2
Akita	0.004	0.015
Aomori	0.013	0.965
Chiba	0.771	0.177
Fukushima	1.964	0.319
Gumma	0.020	0.389
Ibaraki	1.052	0.477
Iwate	0.245	0.765
Miyagi	0.523	0.396
Saitama	0.024	0.389
Tochigi	0.087	0.634
Yamagata	0.045	0.645

Electric power and telecommunication (mobile and fixed phones) outage data were obtained for the 2010 Chile Earthquake as shown in Figures 3.12 and 3.13. Compared to the electric power and water supply data from 2011 Japan Earthquake, the electric power and telecommunication systems in Chile Region VII and VIII show stronger correlations. The scatter plots of the power, mobile phone and fixed phone system outages are shown in Figure 5.4 and the regression results are listed in Table 5.3.

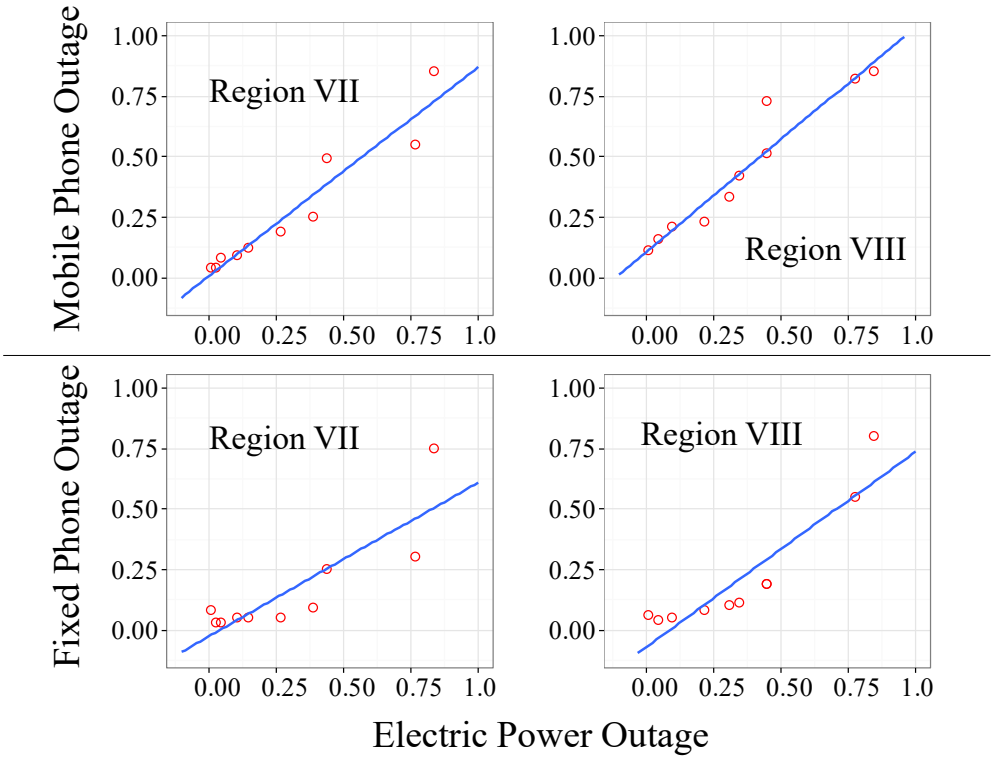

Figure 5.4: Scatter plots and linear regression lines for electric power and telecommunication (mobile and fixed phones) outages after 2010 Chile Earthquake.

5.4 Combined evaluation

Emergency managers often request metrics describing the recovery or response status of the entire infrastructure (a system of eleven systems) at a given point in time. The use of a

Table 5.3: Elements of the **A** matrix for power delivery and telecommunication system for 2010 Chile Earthquake.

Region	System 1	System 2	a_{21}	R^2
Region VII	Power	Mobile Phones	0.866	0.911
Region VII	Power	Fixed Phones	0.637	0.694
Region VIII	Power	Mobile Phones	0.931	0.910
Region VIII	Power	Fixed Phones	0.810	0.817

radial plot as given in Figure 5.5 is suggested for a visual metric. Here the value of $X(t)$ for each system is provided at a single point in time. A fully functional system would have all values of $X(t)$ equal to zero; that is, zero inoperability. This type of plot might also be used to assess the approximate interdependency of the systems during the response and recovery phases at certain post-event intervals. That is, if the $X(t)$ values rise and fall at the same time, interdependency may play a role, and managers may find this information useful in scheduling recovery activities.

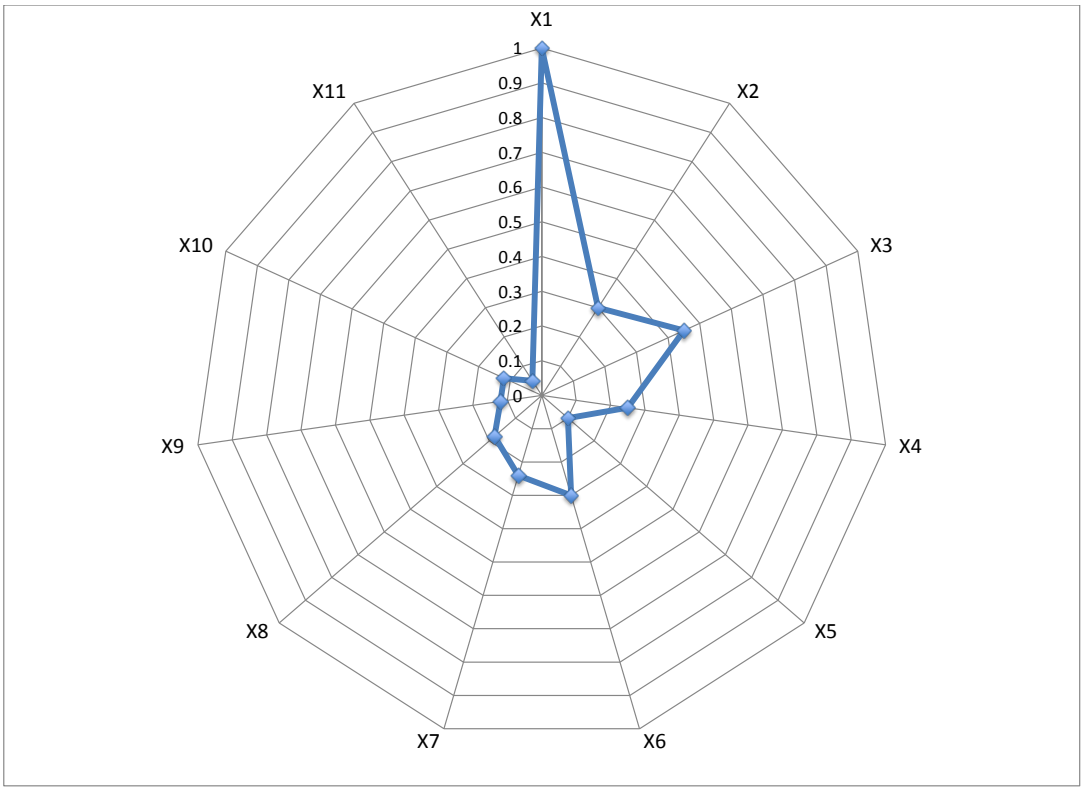

Figure 5.5: Example of using a radial plot for evaluating $X(t)$ for eleven networks at a single time t post-landfall.

Chapter 6

PREDICTIVE METHODS WITH COMBINED FRAGILITY AND RESILIENCE MODELS

The importance of the infrastructure models presented in this thesis is illustrated in Figure 6.1 [72]. The derived predictive framework enables emergency managers and community leaders to estimate the expected effect and duration of certain hazards such as hurricanes and earthquakes. The framework is built on fragility, resilience and interdependency models as discussed throughout this thesis.

The steps of applying this model framework are listed below:

1. Predict extreme weather or seismic event parameters. Extreme weather parameters, such as wind speed V, rainfall R, and storm surge W are usually available from weather related government agencies, such as NOAA and FEMA; seismic event parameters, such as peak ground acceleration (PGA) or peak ground velocity (PGV) are usually available from USGS.

2. Estimate initial damage value X_0 using fragility models. For single hazard H, the fragility F is given by

$$F = \frac{e^{\beta_0+\beta_1 H}}{1+e^{\beta_0+\beta_1 H}}; \tag{6.1}$$

for two hazards, e.g. wind V and storm surge W, the fragility F is given by

$$F = \frac{e^{\beta_0+\beta_1 V+\beta_2 W}}{1+e^{\beta_0+\beta_1 V+\beta_2 W}}; \tag{6.2}$$

for three hazards, e.g. wind V, storm surge W and rainfall R, the fragility F is given by

$$F = \frac{e^{\beta_0+\beta_1 V+\beta_2 R+\beta_3 W}}{1+e^{\beta_0+\beta_1 V+\beta_2 R+\beta_3 W}}. \tag{6.3}$$

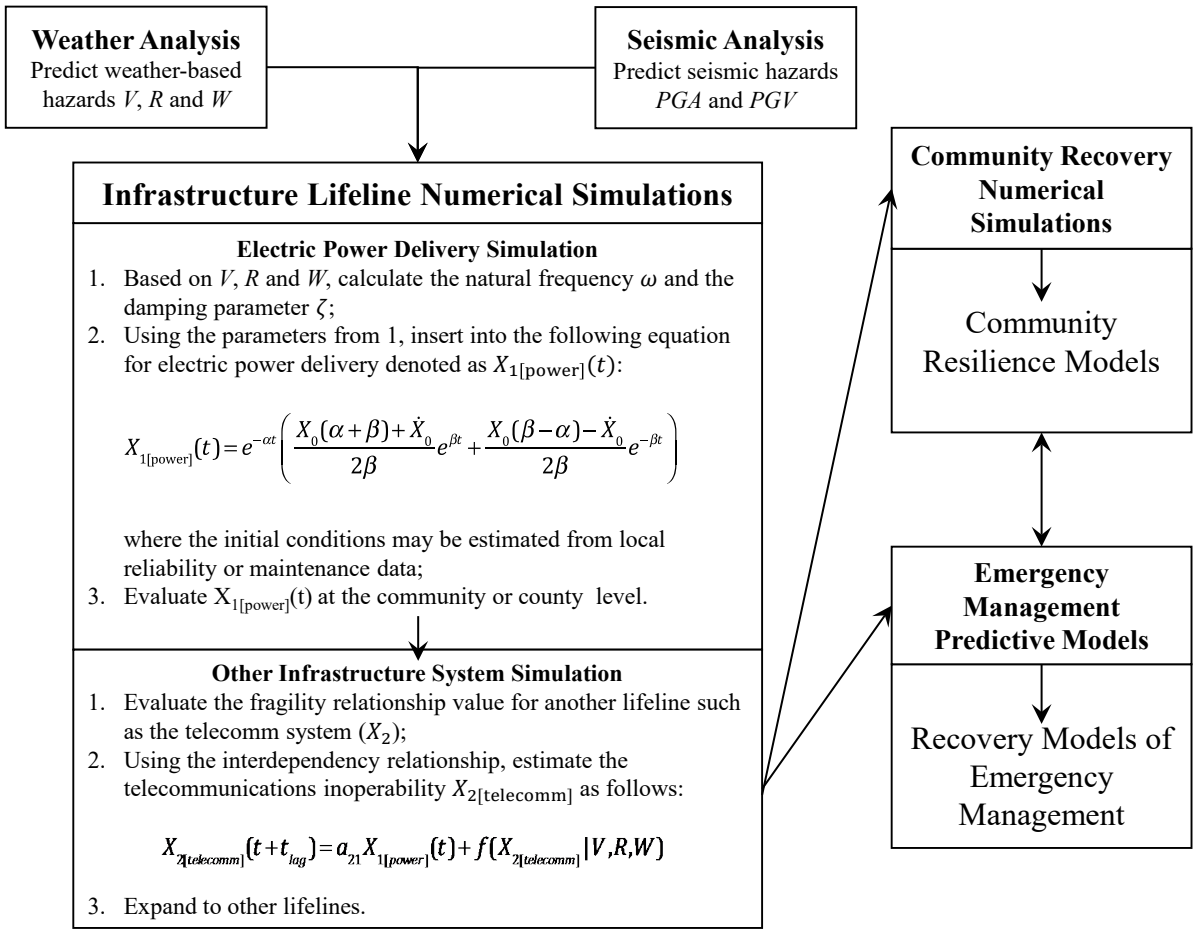

Figure 6.1: Prediction of damage using fragility and inoperability input-output models for storm hazards.

Values of these coefficients are available for certain localities in regions such as Louisiana, but may be derived for any locality from records of past storms using GIS. Logit transformation derivation of seismic fragilities has been undertaken using PGA as the hazard variable. However, the use of substation fragility may be appropriate.

3. Calculate parameters ω and ζ for the locality or region as follows:

$$\omega = d_\omega H, \tag{6.4}$$

and

$$\zeta = d_\zeta H, \tag{6.5}$$

where H can be any given hazard. Initial estimates suggest the following values for wind hazard:

$$\omega = 0.015 V_{\text{sustained}}[\text{m/s}], \tag{6.6}$$

and

$$\zeta = 0.034 V_{\text{sustained}}[\text{m/s}]. \tag{6.7}$$

4. Plug the ω and ζ values into the $X(t)$ equation derived from the SDOF model as follows:

$$X(t) = \frac{(\alpha+\beta)X_0 + \dot{X}_0}{2\beta} e^{-(\alpha-\beta)t} + \frac{(\beta-\alpha)X_0 - \dot{X}_0}{2\beta} e^{-(\alpha+\beta)t}, \tag{6.8}$$

where $\alpha = \omega\zeta$, $\beta = \omega\sqrt{\zeta^2 - 1}$, $X(t=0) = X_0$ and $\dot{X}(t=0) = \dot{X}_0$. The initial value X_0 is obtained of Step 2.

5. After the locality power delivery function is simulated for the time scale of interest, the interdependent $X(t)$ functions may be simulated as follows:

$$\mathbf{X} = \begin{bmatrix} X_1 \\ X_2 \\ X_3 \\ \vdots \\ X_n \end{bmatrix} = \mathbf{AX} + \mathbf{F}, \tag{6.9}$$

where $\mathbf{I}$ is the identity matrix; $[\bullet]^{-1}$ is the inverse of the matrix; $\mathbf{A} = \begin{bmatrix} a_{11} & \cdots & a_{1n} \\ \vdots & \ddots & \vdots \\ a_{n1} & \cdots & a_{nn} \end{bmatrix}$ is the interdependency matrix with elements a_{ij} equals to the influence of lifeline j inoperability $[X_j(t)]$ on lifeline i inoperability $[X_i(t)]$. The fragility vector $\mathbf{F}$ is given

by

$$\mathbf{F} = \begin{bmatrix} f_1 \\ \vdots \\ f_n \end{bmatrix}, \tag{6.10}$$

where f_i is the fragility for subsystem or lifeline i. Here X_1 is the power delivery system $X(t)$. It is necessary to derive the "A" matrix values in-situ.

Chapter 7

SUMMARY AND FUTURE WORK

Models of reliability, robustness and resilience were reviewed and significantly expanded in this thesis. Extensive data sets were obtained and used to verify and calibrate the derived formulations. It has been shown that combining aspects of all three metrics provide a complete formulation of the performance of infrastructure systems subject to hazards and other disruptive events. The framework derived here provides a model to be used by urban planners and civil engineers for enhancing community resilience.

To a certain extent, the space-time scales selected for use in representation of the infrastructure inoperability drive the modeling process. The approach here seeks to simplify complex networks in order to more easily understand the underlying physical phenomena. The results of this approach may be helpful to those researchers with more precise network models for calibration of their predictive models. Mechanical analog models were implemented and correlated with weather and seismic parameters. The model provides predictive capabilities for typical US power distribution and transmission systems, and the simplicity of the model and its use of commonly recorded data by utilities and public service commissions make it ideal for implementation in public policy matters. Logistic regression models have been used successfully to characterize fragilities for electric power delivery and other lifelines subject to hurricane hazards, where fragility is defined as a conditional probability function. The system-level fragility models, while representing only single event scenarios, are based on geo-coded post-event in-situ hurricane hazard and power delivery system damage data rather than numerical simulations. Multiple simultaneous hazards of wind speed, storm surge and rainfall were used for the fragility model fits. This multi-hazard characterization property of the logit models is a distinct advantage over lognormal models.

Extensive hazard GIS and lifeline damage data are required for calibrating the SDOF and fragility models. It is anticipated that future investigations into the models presented here for other storms in the same geographical region will yield not only predictive capabilities, but also needed insight into the hurricane damage process. The characterization of the multivariate distributions of the simultaneous weather hazards will also improve damage predictions for hurricane prone regions.

BIBLIOGRAPHY

[1] ASCE. *Infrastructure Report Card*. American Society of Civil Engineers, Reston, VA, 2017.

[2] National Consortium for the Study of Terrorism and Responses to Terrorism (START). *Global Terrorism Database [Data file]*, 2016. https://www.start.umd.edu/gtd.

[3] D. Guha-Sapir, R. Below, and Ph. Hoyois. *EM-DAT: International Disaster Database*. Universite Catholique de Louvain, Brussels, Belgium. http://www.emdat.be.

[4] Harold C Aikens. *Quality inspired management: The key to sustainability*. Prentice Hall, 2011.

[5] Alessandro Birolini. *Reliability Engineering: Theory and Practice*. Berlin; New York: Springer, 1999.

[6] David A Garvin. Competing on the eight dimensions of quality. *IEEE Engineering Management Review*, 24(1):15–23, 1996.

[7] DC Montgomery. *Statistical quality control: a modern introduction*. Hoboken, NJ: Wiley, 2009.

[8] F. Petrini, M. Ciampoli, and G. Augusti. A probabilistic framework for performance-based wind engineering. In *Proceedings of the 5th European and African Conference on Wind Engineering (EACWE 5)*, Florence, Italy, 2009.

[9] Timothy McDaniels, Stephanie Chang, Darren Cole, Joseph Mikawoz, and Holly Longstaff. Fostering resilience to extreme events within infrastructure systems: Charac-

terizing decision contexts for mitigation and adaptation. *Global Environmental Change*, 18(2):310–318, may 2008.

[10] Dorothy A. Reed, Kailash C. Kapur, and Richard D. Christie. Methodology for assessing the resilience of networked infrastructure. *IEEE Systems Journal*, 3(2):174–180, 2009.

[11] Genichi Taguchi, Subir Chowdhury, and Shin Taguchi. *Robust engineering*. McGraw-Hill Professional, 2000.

[12] Stephanie E. Chang, Timothy L. McDaniels, and Dorothy Reed. Mitigation of extreme event risks: electric power outage and infrastructure failure interactions. In Harry W. Richardson, Peter Gordon, and James E. Moore II, editors, *The Economic Impacts of Terrorist Attacks*, chapter 5. Edward Elgar Publishing, Inc., 2005.

[13] S.M. Rinaldi, J.P. Peerenboom, and T.K. Kelly. Identifying, understanding, and analyzing critical infrastructure interdependencies. *IEEE Control Systems Magazine*, 21(6):11–25, 2001.

[14] Environmental Systems Research Institute, Inc. *ArcGIS Desktop*. Redlands, CA, 2017. http://desktop.arcgis.com/en/.

[15] Google Inc. *Google Earth*. Mountain View, CA, 2017. https://www.google.com/intl/es-419/earth/.

[16] Seattle City Light. *Distribution system reliability*. City of Seattle, Seattle, WA, 2002.

[17] Subcommittee on Fiber-Reinforced Composite Structures for Overhead Lines of the American Society of Civil Engineers. *Recommended practice for fiber-reinforced polymer products for overhead utility line structures (ASCE manuals and reports on engineering practice No. 104)*. American Society of Civil Engineers, Reston, Va., 2003.

[18] Subcommittee on Guyed Transmission Structures of the American Society of Civil Engineers. *Design of guyed electrical transmission structures (ASCE manuals and reports on engineering practice No. 91)*. American Society of Civil Engineers, New York, N.Y., 1997.

[19] Michael D Miller, C. Jerry Wong, and Task Committee on Structural Loadings of the American Society of Civil Engineers. *Guidelines for electrical transmission line structural loading (ASCE manuals and reports on engineering practice No. 74)*. American Society of Civil Engineer, Reston, Va., 2010.

[20] Wesley J Oliphant, Douglas C Sherman, and Task Committee on Concrete Pole Structures of the Structural Engineering Institute. *Prestressed concrete transmission pole structures : recommended practice for design and installation (ASCE manuals and reports on engineering practice No. 123)*. American Society of Civil Engineers, Reston, Va., 2012.

[21] Dale R. Patrick and Stephen W. Fardo. *Electrical Distribution Systems*. Fairmont Press, 2nd edition, 2009.

[22] B. S. Dhillon. *Design Reliability: Fundamentals and Applications*. Boca Raton, FL: CRC Press, 1999.

[23] Patrick D. T. O'Connor, David Newton, and Richard Bromley. *Practical reliability engineering*. John Wiley & Sons, Ltd, 4th edition, 2002.

[24] K.C. Kapur and L.R. Lamberson. *Reliability in engineering design*. Wiley, 1977.

[25] Alfred M. Freudenthal. The safety of structures. *Transactions of the American Society of Civil Engineers*, 112(1):125–159, 1947.

[26] Bruce Ellingwood, Theodore V. Galambos, James G. MacGregor, and C. Allin Cornell. *Development of a Probability-Based Load Criterion for American National Standard*

A58, volume NBS Special Publication. National Bureau of Standards, Washington, DC, 1980.

[27] Bruce Ellingwood, C. Allin Cornell, James G. MacGregor, and Theodore V. Galambos. A probability-based load criterion for structural design. *Civil Engineering –ASCE*, 51(7):74–76, 1981.

[28] American Wood Council. *ASD/LRFD Manual for Engineered Wood Construction*. American Wood Council, 2012 edition, 2012.

[29] IEEE. *IEEE Guide for Electric Power Distribution Reliability Indices*. Institute of Electrical and Electronics Engineers, 2012.

[30] The City of New York. *A Stronger, More Resilient New York*, 2013. http://www.nyc.gov/html/sirr/html/report/report.shtml.

[31] R.E. Brown, S. Gupta, R.D. Christie, S.S. Venkata, and R. Fletcher. Distribution system reliability assessment: momentary interruptions and storms. *IEEE Transactions on Power Delivery*, 12(4):1569–1575, 1997.

[32] Dorothy A. Reed, Mark D. Powell, and Julie M. Westerman. Energy infrastructure damage analysis for hurricane rita. *Natural Hazards Review*, 11(3):102–109, aug 2010.

[33] Dorothy Reed and Carolyn Cook. Multi-hazard analysis of utility lifeline systems. *Technical Council on Lifeline Earthquake Engineering Monograph*, (16):940–949, August 1999.

[34] Jaewook Park, Nobuoto Nojima, and Dorothy A Reed. Nisqually earthquake electric utility analysis. *Earthquake spectra*, 22(2):491–509, 2006.

[35] Dorothy A. Reed. Electric utility distribution analysis for extreme winds. *Journal of Wind Engineering and Industrial Aerodynamics*, 96(1):123–140, jan 2008.

[36] Rachel A. Davidson, Haibin Liu, Isaac K. Sarpong, Peter Sparks, and David V. Rosowsky. Electric Power Distribution System Performance in Carolina Hurricanes. *Natural Hazards Review*, 4(1):36–45, feb 2003.

[37] M. Le Du, B. Rassineux, and P. Cochet. The french power network facing the 1999 storms. In *Power Systems and Communication Infrastructures for the Future: Proceedings of the CRIS Conference*, September 2002.

[38] Applied Technology Council. Seismic vulnerability and impact of disruption of lifelines in the conterminous united states. Technical Report ATC-25, Applied Technology Council, Redwood City, CA, 1991.

[39] Anshel J. Schiff. *Hyogoken-Nanbu (Kobe) Earthquake of January 17, 1995: Lifeline Performance (Technical Council on Lifeline Earthquake Engineering Monograph Number 14, September 1998)*. American Society of Civil Engineers, 1998.

[40] Stuart D. Werner and Craig E. Taylor. Component vulnerability modeling issues for analysis of seismic risks to transportation lifeline systems. In *Acceptable Risk Processes: Lifelines and Natural Hazards*. American Society of Civil Engineers, 2002.

[41] Leonardo Dueñas-Osorio and Alexis Kwasinski. Quantification of Lifeline System Interdependencies after the 27 February 2010 Mw 8.8 Offshore Maule, Chile, Earthquake. *Earthquake Spectra*, 28(S1):S581–S603, jun 2012.

[42] Madhav Shridhar Phadke. *Quality Engineering Using Robust Design*. Prentice-Hall International editions. Prentice Hall, 1989.

[43] Yuin Wu and Alan Wu. *Taguchi methods for robust design*. American Society of Mechanical Engineers, 2000.

[44] Torben Hasenkamp, Martin Arvidsson, and Ida Gremyr. A review of practices for robust design methodology. *Journal of Engineering Design*, 20(6):645–657, 2009.

[45] Martin Arvidsson and Ida Gremyr. Principles of robust design methodology. *Quality and Reliability Engineering International*, 24(1):23–35, 2008.

[46] R.W. Hertzberg. *Deformation and fracture mechanics of engineering materials*. John Wiley & Sons Canada, Limited, 1983.

[47] Crawford S Holling. Resilience and stability of ecological systems. *Annual review of ecology and systematics*, pages 1–23, 1973.

[48] Erik Hollnagel. How Resilient Is Your Organisation? An Introduction to the Resilience Analysis Grid (RAG). In *Sustainable Transformation: Building a Resilient Organization*, Toronto, Canada, 2010.

[49] Thomas B Sheridan. Risk, human error, and system resilience: fundamental ideas. *Human Factors: The Journal of the Human Factors and Ergonomics Society*, 50(3):418–426, 2008.

[50] Michel Bruneau, Stephanie E Chang, Ronald T Eguchi, George C Lee, Thomas D O'Rourke, Andrei M Reinhorn, Masanobu Shinozuka, Kathleen Tierney, William A Wallace, and Detlof von Winterfeldt. A framework to quantitatively assess and enhance the seismic resilience of communities. *Earthquake spectra*, 19(4):733–752, 2003.

[51] Dorothy A Reed, Mark D Powell, and Julie M Westerman. Energy supply system performance for Hurricane Katrina. *Journal of Energy Engineering*, 136(4):95–102, 2010.

[52] National Infrastructure Advisory Council. Critical infrastructure resilience: Final report and recommendations. Technical report, U.S. Department of Homeland Security, 2009.

[53] Randy Starr, Jim Newfrock, and Michael Delurey. Enterprise resilience: managing risk in the networked economy. *Strategy and Business*, (30):70–79, 2003.

[54] Richard A Caralli, Julia H Allen, Pamela D Curtis, David W White, and Lisa R Young. CERT® resilience management model, v1. 0: Improving operational resilience processes. Technical Report CMU/SEI-2010-TR-012, Software Engineering Institute, Carnegie Mellon University, Hanscom AFB, MA, 2010.

[55] George Aggelou. *Wireless Mesh Networking*. McGraw-Hill Professional, 2008.

[56] Gill Windle, Kate M Bennett, and Jane Noyes. A methodological review of resilience measurement scales. *Health and quality of life outcomes*, 9(8):1–18, 2011.

[57] Applied Technology Council. Earthquake damage evaluation data for california. Technical Report ATC-13, Applied Technology Council, Redwood City, CA, 1985.

[58] Executive Order, 13010. Critical infrastructure protection. *Federal Register*, 61(138):3747–3750, July 1996.

[59] The President's Commission on Critical Infrastructure Protection. *Critical Foundations: Protecting America's Infrastructures*. Washington, DC, October 1997.

[60] Stephanie E Chang. Infrastructure resilience to disasters. *The Bridge*, 39(4):36–41, 2009.

[61] P. Pederson, D. Dudenhoeffer, S. Hartley, and M. Permann. Critical Infrastructure Interdependency Modeling: A Survey of U.S. and International Research. Technical Report INL/EXT-06-11464, Idaho National Laboratory, Idaho Falls, Idaho, August 2006.

[62] Donald Dudenhoeffer, May Permann, and Milos Manic. CIMS: A framework for infrastructure interdependency modeling and analysis. In *Proceedings of the 2006 Winter Simulation Conference*. IEEE, dec 2006.

[63] Vaidyanathan Krishnamurthy, Alexis Kwasinski, and Leonardo Dueñas-Osorio. Comparison of Power and Telecommunications Dependencies and Interdependencies in

the 2011 Tohoku and 2010 Maule Earthquakes. *Journal of Infrastructure Systems*, 22(3):04016013, sep 2016.

[64] Yacov Y. Haimes, Barry M. Horowitz, James H. Lambert, Joost R. Santos, Chenyang Lian, and Kenneth G. Crowther. Inoperability Input-Output Model for Interdependent Infrastructure Sectors. I: Theory and Methodology. *Journal of Infrastructure Systems*, 11(2):67–79, jun 2005.

[65] Yacov Y. Haimes, Barry M. Horowitz, James H. Lambert, Joost Santos, Kenneth Crowther, and Chenyang Lian. Inoperability Input-Output Model for Interdependent Infrastructure Sectors. II: Case Studies. *Journal of Infrastructure Systems*, 11(2):80–92, jun 2005.

[66] Yacov Y. Haimes and Pu Jiang. Leontief-based model of risk in complex interconnected infrastructures. *Journal of Infrastructure Systems*, 7(1):1–12, mar 2001.

[67] Chenyang Lian, Joost R. Santos, and Yacov Y. Haimes. Extreme risk analysis of interdependent economic and infrastructure sectors. *Risk Analysis*, 27(4):1053–1064, aug 2007.

[68] Wassily Leontief. *Input-Output Economics*. Oxford University Press, 1986.

[69] Wassily Leontief. Input-output economics. *Scientific American*, pages 15–21, October 1951.

[70] Chenyang Lian and Yacov Y. Haimes. Managing the risk of terrorism to interdependent infrastructure systems through the dynamic inoperability input–output model. *Systems Engineering*, 9(3):241–258, 2006.

[71] T. D. O'Rourke. Critical infrastructure, interdependencies, and resilience. *The Bridge*, 37(1):22–29, 2007.

[72] Dorothy Reed, Shuoqi Wang, Kailash Kapur, and Cheng Zheng. Systems-based approach to interdependent electric power delivery and telecommunications infrastructure resilience subject to weather-related hazards. *Journal of Structural Engineering*, 142(8):C4015011–1–12, 2016.

[73] Stephanie E. Chang. Direct economic impacts. In M. Shinozuka, A. Rose, and R. T. Eguchi, editors, *Engineering and Socioeconomic Impacts of Earthquakes*, chapter 6, pages 75–94. Multidisciplinary Center for Earthquake Engineering Research, 1998.

[74] Federal Emergency Management Agency (FEMA). *HAZUS-MH Earthquake Model*. Washington, D.C., 2015.

[75] Gian Paolo Cimellaro, Andrei M Reinhorn, and Michel Bruneau. Framework for analytical quantification of disaster resilience. *Engineering Structures*, 32(11):3639–3649, 2010.

[76] Christopher W. Zobel. Representing perceived tradeoffs in defining disaster resilience. *Decision Support Systems*, 50(2):394–403, 2011.

[77] Rae Zimmerman, Carol J. Friedland, and Dorothy A. Reed. Rapid collaborative research: Collection of perishable hurricane sandy data on weather-related damage to urban power and transit infrastructure. In *S&T Innovations in Hurricane Sandy Research Workshop held under the auspices of DIMACS and CCICADA*, New Brunswick, NJ, 2013.

[78] Igor Griva, Stephen G. Nash, and Ariela Sofer. *Linear and Nonlinear Optimization*. Society for Industrial and Applied Mathematics, 2nd edition, 2009.

[79] Kenneth Levenberg. A method for the solution of certain non-linear problems in least squares. *Quarterly of Applied Mathematics*, 2(2):164–168, 1944.

[80] Donald W. Marquardt. An algorithm for least-squares estimation of nonlinear parameters. *Journal of the Society for Industrial and Applied Mathematics*, 11(2):431–441, 1963.

[81] Henri P. Gavin. *The Levenberg-Marquardt method for nonlinear least squares curve-fitting problems*. Department of Civil and Environmental Engineering, Duke University, March 2017.

[82] Bruce H. Karnopp and Francis E. Fisher. On the vibrations of overdamped systems. *Journal of the Franklin Institute*, 327(4):601–609, 1990.

[83] National Hurricane Center. *Tropical Cyclone Reports*. National Oceanic and Atmospheric Administration, Miami, FL. http://www.nhc.noaa.gov/data/tcr/.

[84] Office of Electricity Delivery and Energy Reliability. *Electric Emergency Incident and Disturbance Report*. U.S. Department of Energy, Washington, DC, 2014. https://www.oe.netl.doe.gov/docs/OE417_Instructions_03312018.pdf.

[85] Office of Electricity Delivery & Energy Reliability. *Emergency Situation Reports*. U.S. Department of Energy, Washington, DC. https://www.oe.netl.doe.gov/emergency_sit_rpt.aspx.

[86] Shuoqi Wang. *Hurricane Sandy Database*. University of Washington, Seattle, WA. http://depts.washington.edu/hursandy/index.html.

[87] Shuoqi Wang. *Hurricane Isaac Database*. University of Washington, Seattle, WA. http://depts.washington.edu/hurisaac/.

[88] Louisiana Public Service Commission (LPSC). *Electric Utilities Outage Report - Hurricanes Gustav & Ike*. Baton Rouge, LA, 2008.

[89] John Eidinger, Craig Davis, Alex Tang, and Leon Kempner. *M 9.0 Tohoku Earthquake*

March 11 2011 Performance of Water and Power Systems. G&E Engineering Systems Inc., Oakland, CA, June 2012.

[90] Earthquake Hazards Program Office. *M9.1 - near the east coast of Honshu, Japan*. U.S. Geological Survey, Reston, VA, 2017.

[91] Nobuoto Nojima and Hiroki Kato. Modification and validation of an assessment model of post-earthquake lifeline serviceability based on the great east japan earthquake disaster. *Journal of Disaster Research*, 9(2):108–120, mar 2014.

[92] Earthquake Hazards Program Office. *M8.8 - offshore Bio-Bio, Chile*. U.S. Geological Survey, Reston, VA, 2017.

[93] Paolo Gardoni, Armen Der Kiureghian, and Khalid M. Mosalam. Probabilistic models and fragility estimates for bridge components and systems. Technical report, Pacific Earthquake Engineering Research Center, 2002.

[94] Amir M Kaynia, Fabio Taucer, Ufuk Hancilar, and Iunio Iervolino. Guidelines for deriving seismic fragility functions of elements at risk: Buildings, lifelines, transportation networks and critical facilities. Technical Report SYNER-G Reference Report 4, Joint Research Centre, European Commission, 2013.

[95] Masanobu Shinozuka, M. Q. Feng, Jongheon Lee, and Toshihiko Naganuma. Statistical analysis of fragility curves. *Journal of Engineering Mechanics*, 126(12):1224–1231, dec 2000.

[96] Bruce R. Ellingwood, David V. Rosowsky, Yue Li, and Jun Hee Kim. Fragility assessment of light-frame wood construction subjected to wind and earthquake hazards. *Journal of Structural Engineering*, 130(12):1921–1930, dec 2004.

[97] John W. van de Lindt and Thang N. Dao. Performance-based wind engineering for wood-frame buildings. *Journal of Structural Engineering*, 135(2):169–177, feb 2009.

[98] Keith A. Porter. An overview of peer's performance-based earthquake engineering methodology. In *Ninth International Conference on Applications of Statistics and Probability in Civil Engineering (ICASP9)*, San Francisco, CA, July 2003.

[99] Mark D. Powell and Timothy A. Reinhold. Tropical cyclone destructive potential by integrated kinetic energy. *Bulletin of the American Meteorological Society*, 88(4):513–526, apr 2007.

[100] RMS HWind. *RMS HWIND LEGACY ARCHIVE*. Risk Management Solutions, Inc., Silicon Valley, CA. http://www.rms.com/perils/hwind/.

[101] Jayadipta Ghosh, Keivan Rokneddin, Jamie E. Padgett, and Leonardo Dueñas-Osorio. Seismic Reliability Assessment of Aging Highway Bridge Networks with Field Instrumentation Data and Correlated Failures, I: Methodology. *Earthquake Spectra*, 30(2):795–817, may 2014.

[102] P.S. Koutsourelakis. Assessing structural vulnerability against earthquakes using multi-dimensional fragility surfaces: A bayesian framework. *Probabilistic Engineering Mechanics*, 25(1):49–60, jan 2010.

[103] Nobuoto Nojima and Masata Sugito. Development of a probabilistic assessment model for post-earthquake residual capacity of utility lifeline systems. In *Advancing Mitigation Technologies and Disaster Response for Lifeline Systems*. American Society of Civil Engineers, jul 2003.

[104] D.A. Reed, C.J. Friedland, S. Wang, and C.C. Massarra. Multi-hazard system-level logit fragility functions. *Engineering Structures*, 122:14–23, sep 2016.

[105] Kazi R Karim and Fumio Yamazaki. Effect of earthquake ground motions on fragility curves of highway bridge piers based on numerical simulation. *Earthquake engineering & structural dynamics*, 30(12):1839–1856, 2001.

[106] M. Shinozuka, M.Q. Feng, H. Kim, T. Uzawa, and T. Ueda. Statistical analysis of fragility curves. Technical Report MCEER-03-0002, Multidisciplinary Center for Earthquake Engineering Research (MCEER), 2001.

[107] David Lallemant, Anne Kiremidjian, and Henry Burton. Statistical procedures for developing earthquake damage fragility curves. *Earthquake Engineering & Structural Dynamics*, 44(9):1373–1389, jan 2015.

[108] Warner Marzocchi, Alexander Garcia-Aristizabal, Paolo Gasparini, Maria Laura Mastellone, and Angela Di Ruocco. Basic principles of multi-risk assessment: a case study in italy. *Natural Hazards*, 62(2):551–573, jan 2012.

[109] Megan C. McCullough, Ahsan Kareem, Aaron S. Donahue, and Joannes J. Westerink. Structural damage under multiple hazards in coastal environments. *Journal of Disaster Research*, 8(6):1042–1051, dec 2013.

[110] M.S. Kappes, M. Papathoma-Köhle, and M. Keiler. Assessing physical vulnerability for multi-hazards using an indicator-based methodology. *Applied Geography*, 32(2):577–590, mar 2012.

[111] Melanie S. Kappes, Margreth Keiler, Kirsten von Elverfeldt, and Thomas Glade. Challenges of analyzing multi-hazard risk: a review. *Natural Hazards*, 64(2):1925–1958, jul 2012.

[112] Pierre Gehl, Darius M. Seyedi, and John Douglas. Vector-valued fragility functions for seismic risk evaluation. *Bulletin of Earthquake Engineering*, 11(2):365–384, nov 2012.

[113] Sabarethinam Kameshwar and Jamie E. Padgett. Multi-hazard risk assessment of highway bridges subjected to earthquake and hurricane hazards. *Engineering Structures*, 78:154–166, nov 2014.

[114] Keivan Rokneddin, Jayadipta Ghosh, Leonardo Dueñas-Osorio, and Jamie E. Padgett. Seismic reliability assessment of aging highway bridge networks with field instrumentation data and correlated failures, II: Application. *Earthquake Spectra*, 30(2):819–843, may 2014.

[115] Maryam Mardfekri and Paolo Gardoni. Multi-hazard reliability assessment of offshore wind turbines. *Wind Energy*, 18(8):1433–1450, may 2014.

[116] Habib Joseph. Dagher and Reliability-Based Design Committee of the Structural Engineering Institute. *Reliability-based Design of Utility Pole Structures (ASCE manuals and reports on engineering practice No. 111)*. American Society of Civil Engineers, Reston, VA, 2006.

[117] The Special Initiative for Rebuilding and Resiliency (SIRR). *A Stronger, More Resilient New York*. The City of New York, New York, NY, June 2013.

[118] Robbie Berg. Tropical Cyclone Report Hurricane Isaac (AL092012). Technical report, National Hurricane Center of National Oceanic and Atmospheric Administration/National Weather Service, January 2013.

[119] The Coastal Emergency Risks Assessment (CERA) Group. Cera - coastal emergency risks assessment. online, July 2015.

[120] National Weather Service. Advanced hydrologic prediction service. online, July 2015.

[121] Louisiana Public Service Commission (LPSC). *Emergency operations center: daily service outage report (Excel spreadsheets for each day summarizing electric and phone outage)*. Baton Rouge, LA, 2012.

[122] Eric S Blake, Todd B Kimberlain, Robert J Berg, JP Cangialosi, and John L Beven II. Tropical cyclone report: Hurricane sandy tcr-al182012. Technical report, National Hurricane Center, 2013.

[123] FEMA Modeling Task Force (MOTF). *FEMA MOTF Hurricane Sandy Impact Analysis*, July 2015.

[124] Douglas C. Montgomery and George C. Runger. *Applied statistics and probability for engineers*. Wiley, Hoboken, NJ, 5th ed. edition, 2011.

[125] R Core Team. *R: A Language and Environment for Statistical Computing*. R Foundation for Statistical Computing, Vienna, Austria, 2017.

[126] Andrew Gelman, Yu-Sung Su, Masanao Yajima, Jennifer Hill, Maria Grazia Pittau, Jouni Kerman, Tian Zheng, and Vicent Dorie. Data analysis using regression and multilevel/hierarchical models. r package version 1.8-6, July 2015.

[127] Kenneth P Burnham and David R Anderson. *Model selection and multimodel inference: a practical information-theoretic approach*. Springer Science & Business Media, 2002.

[128] Bin Pei, Weichiang Pang, Firat Testik, and Nadarajah Ravichandran. *Joint Distributions of Hurricane Wind and Storm Surge for the City of Charleston in South Carolina*, pages 703–714. American Society of Civil Engineers, 2013.

[129] Bin Pei, Weichiang Pang, Firat Y Testik, Nadarajah Ravichandran, and Fangqian Liu. Mapping joint hurricane wind and surge hazards for charleston, south carolina. *Natural Hazards*, 74(2):375–403, 2014.

[130] LT Phan, E Simiu, MA McInerney, AA Taylor, B Glahn, and MD Powell. *NIST Technical Note 1482, Methodology for development of design criteria for joint hurricane wind speed and storm surge events: Proof of concept*. Department of Commerce, U.S. Government, Gaithersburg, M.D., April 2007.

[131] Norman Lloyd. Johnson and Samuel Kotz. *Continuous multivariate distributions*. New York, Wiley, 1972.

[132] Gerard O'Reilly, Ahmad Jrad, Ramesh Nagarajan, Theresa Brown, and Stephen Conrad. Critical infrastructure analysis of telecom for natural disasters. In *Networks 2006. 12th International Telecommunications Network Strategy and Planning Symposium*. IEEE, 2006.